9-12-2014

Soil Moisture Measurements and Modeling at a Geomorphically Reclaimed Coal Mine in New Mexico

Shahedur Rahman

Shahedur Rahman
Candidate

Civil Engineering
Department

This thesis is approved, and it is acceptable in quality and form for publication:

Approved by the Thesis Committee:

Dr. John Stormont, Chairperson

Dr. Mark Stone

Dr. Marcy Litvak

SOIL MOISTURE MEASUREMENTS AND MODELING AT A GEOMORPHICALLY RECLAIMED COAL MINE IN NEW MEXICO

by

SHAHEDUR RAHMAN

BACHELOR OF SCIENCE IN CIVIL ENGINEERING

THESIS

Submitted in Partial Fulfillment of the
Requirements for the Degree of

Master of Science
Civil Engineering

The University of New Mexico
Albuquerque, New Mexico

July, 2014

DEDICATION

This thesis is dedicated to my parents. They have provided me encouragement in every aspect to reach my career goal and never gave up on me. Without their dedication and support completion of my university degrees may have become much more of a dream than a reality.

ACKNOWLEDGEMENTS

I would like to acknowledge and express my gratitude for the funding provided by the Office of Graduate Studies for the pursuit of my education, here, at the University of New Mexico. I would like to thank Dr. John Stormont, my advisor and committee chair, for his continued support and inspiration throughout my time at University of New Mexico. His constant guidance and teachings has provided me the knowledge, insight, and experiences necessary to perform the work presented here. I would also like to thank my other committee members, Dr. Mark Stone, and Dr. Marcy Litvak, for their valuable recommendations and helpful guidance through the thesis writing process. I would like to acknowledge Colin Byrne, Rachel Powell and Jeffrey Samson for helping me in field tests and laboratory experiments. BHP Billiton deserves acknowledgement and gratitude for providing us support to pursue this research.

SOIL MOISTURE MEASUREMENTS AND MODELING AT A GEOMORPHICALLY RECLAIMED COAL MINE IN NEW MEXICO

by

Shahedur Rahman

B. Sc., Civil Engineering, Bangladesh University of Engineering & Technology, 2011

M. Sc., Civil Engineering, University of New Mexico, 2014

ABSTRACT

Geomorphic reclamation is a relatively new technique in which landforms are built to be similar to those that eventually form in nature given the particular conditions of a location, making them self-sustaining and functional. The near surface water balance will have a large impact on the establishment and health of vegetation which in turn is important for maintaining a stable landform. This study developed a one-dimensional water balance model for a geomorphically reclaimed site and used the model to investigate seed germination and plant survival for a range of slope aspects and climate conditions. Disturbed and undisturbed samples of reclaimed soil were collected for laboratory tests from the mine site located in northwest New Mexico. Saturated and unsaturated hydraulic properties were determined from falling head tests, hanging column tests, pressure plate tests, and dew point potentiometer measurements. In addition, hydraulic properties were estimated from field tension infiltrometer tests. Laboratory and field tests accounted for the variable soil density in the near surface. Periodic soil moisture measurements at the reclaimed site were made from August 2012 to March 2014. Simulated and measured water contents were compared by statistical analyses to validate the numerical model, and indicated that a reasonable comparison was attained between predicted and observed soil water contents. The water balance simulations revealed that it is necessary to consider near surface variability in soil hydraulic properties to produce reasonable predictions of soil moisture. The numerical model was then used to predict soil water potential and temperature for different climates (one wet year and one dry year) and aspect conditions. A population based hydrothermal time model was used to predict the seed response to environmental condition available at soil surface. Germination potential

of a native plant bottlebrush squirreltail (*Elymus elymoides*), and an invasive species cheatgrass (*Bromus tectorum*) was determined in terms of cumulative progress towards germination (PTG). Survivability of existing plant blue grama grass (*Bouteloua gracilis*) and cheatgrass was also predicted by comparing soil water potential at different depths with the wilting points of the respective plants. The results show that establishment of vegetation in geomorphically reclaimed soil is dependent on climate and aspect conditions. The study of germination potential indicates that for a range of climates studied, cheatgrass has higher germination potential than bottlebrush squirreltail. Germination potential and survivability is greater on the northern aspect than the southern aspect. Wet conditions provide favorable conditions for germination and survival for all species. Potential for invasion by cheatgrass is greater on the northern aspect in dry climate conditions when bottlebrush squirreltail is seeded on reclaimed soil. This study reveals that the method of placement of soil and watershed design followed in geomorphic reclamation provide favorable environment for vegetation during the wet climate conditions. The dependence of plant germination and survivability on climate and aspect in this study suggest that geomorphic reclamation - which results in numerous small watersheds with slopes with varying aspects - may result in a healthier overall ecosystem compared to the larger, more uniform aspects associated with traditional reclamation. Comparing the predictions of seed germination and plant survival with long term field measurements and observation of vegetation cover is suggested to validate the approach described in this study.

TABLE OF CONTENTS

1 INTRODUCTION

New Mexico has numerous coal mine fields with reserves of 4.65 billion tons. Over 23 million tons of coal were produced from New Mexico coal mines in 2010, most of which came from the San Juan Basin (New Mexico Mining and Mineral Division, 2014). Among all the coal mines, most of them have been mined at one time or another since the mid-nineteenth century. Federal and state regulations require coal mines to restore the mine site to a sustainable ecosystem to the degree possible after the completion of mining activities. Traditional reclamation approaches rely on stabilizing existing waste piles with hardened drainage structures and vegetation. A relatively new approach of reclamation has been developed to recreate land surface which mimics the natural landscape. This approach, designated geomorphic reclamation, is based on the hydrology, soil types, topography and climatic condition of the surrounding area. Geomorphic reclamation promotes establishment of a sustainable ecosystem and is more stable than the traditional approach.

The performance of geomorphic reclamation is an active area of research (Bugosh, 2009; Clark, 2009; Golnar et al., 2009). However, there are few studies that focus on the near surface water balance associated with geomorphic reclamation. The soil moisture in the near surface will have a large impact on the establishment and health of vegetation, which, in turn, is important for a stable landform. Soil moisture is expected to vary not only temporally in response to climatic conditions, but also spatially as a result of variable angles and aspects of slopes within the reclaimed site conditions (Burnett et al., 2008; Geroy et al., 2011; Gutierrez-Jurado et al., 2013). In order to account for the range of conditions that may be encountered at a reclaimed site, it is necessary to develop numerical models of the near surface water balance. Results from these models can be used to estimate the favorability of the conditions for germination and/or survivability of vegetation.

A key input for a numerical model of the near surface water balance are the soil hydraulic properties. The saturated and unsaturated hydraulic properties of mine reclaimed soil cannot be predicted accurately from correction factors using particle size analysis or other prediction methods (Milczarek et al., 2006). The placement,

compaction and subsequent tillage change the bulk density of reclaimed soil at the top layers (Indorante et al., 1981). Measurements are therefore required for accurate determination of hydraulic properties.

The objectives of this study were to:

- Investigate the effect of soil layering on hydraulic properties of topdressing.
- Evaluate the impact of soil hydraulic properties, specifically variability in topdressing, on the ability of a numerical model to predict the soil water balance.
- Investigate the relation between near surface water balance and plant germination for different climates and slope aspects using results from numerical model.
- Evaluate geomorphic reclamation in terms of germination and survival of native species and potential for invasion by cheatgrass for a range of potential future climate conditions.

2 BACKGROUND

2.1 Site Description

The La Plata Mine is located twenty six kilometers north of Farmington, in San Juan county New Mexico (Fig. 1). It was opened to provide a supplemental source of coal for the San Juan Mine to generate electricity. Open cut mining method was followed to extract coal. The reclamation of the entire mine, about 836 hectares, began near the end of mineral extraction in 2001. Instead of using traditional reclamation process, geomorphic reclamation was adopted for mine reclamation. Elevations at the mine range from 1,795 m to 1,892 m and the annual precipitation is between 30.5 and 35.6 cm (Bugosh, 2009). The original soils are thin and sandy with bedrock cropping out regularly. The vegetation is sparse, with bunch grasses, some forbs, and stands of pinyon pine and juniper. Together these elements comprise a semi-arid terrain that is highly erosive (Bugosh, 2009).

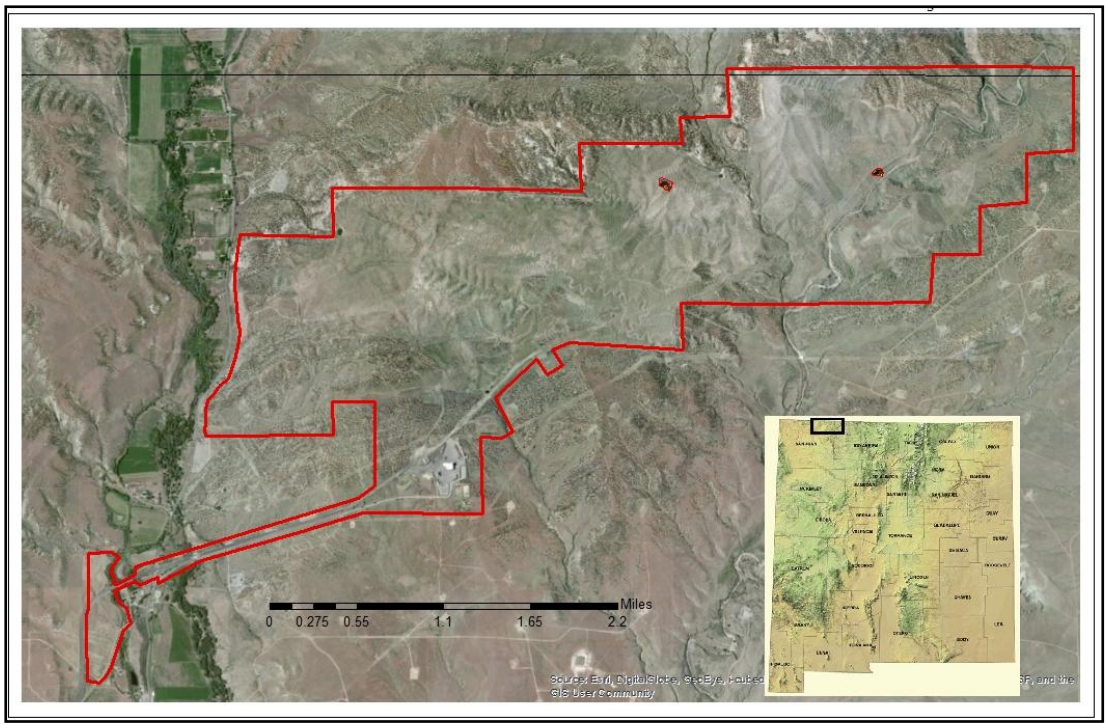

Fig. 1: La Plata Mine Area

2.1.1 Placement of Soil

Reclaimed materials consist of spoil and topdressing materials. The spoil materials consist primarily of broken sandstone fragments and fines that come from strata near the surface of the pit. The final surface cover was achieved by laying the topdressing on top of heavily compacted spoil materials. The thickness of topdressing is based on the revegetation community (i.e., grassland and shrubland). Topdressing was placed at an average thickness of 35 cm in the grassland areas, and 15 cm in the shrubland areas. A v-ripper or chisel was used after the placement of topdressing to alleviate compaction and disrupt the surface soil/spoil interface (La Plata Mine Permit, 2001).

2.1.2 Revegetation Technique

The goal of all revegetation activities is to establish a diverse, effective, and permanent vegetation cover that is capable of stabilizing the soil and is compatible with post mine land use. All seeding, mulching, and crimping were done during the months of July and August and/or October through April. Four vegetation communities were planned (La Plata Mine Permit, 2001):

(1) Upland shrub, southern exposures: This shrub community was targeted on strongly sloping areas (>6% slopes) with southern and western exposures. Topdressing materials were placed over these areas at an average thickness of 15 cm.

The reclamation species selected for this community are adapted to the more arid conditions associated with these exposures.

(2) Upland shrub, northern exposures: This shrub community was targeted on strongly sloping areas (>6% slopes) with northern and eastern exposures. Topdressing materials were placed over these areas at an average thickness of 15 cm. The reclamation species selected for this community are adapted to semi-arid conditions associated with northern exposures.

(3) Grassland: This community was targeted on nearly level and gently sloping areas (<6% slopes). Topdressing materials were placed in these areas at an average thickness of 35 cm.

(4) Drainage: This grassland type community was targeted for areas adjacent to major drainages (approximately 4 m on each side of drainage bottom) constructed within reclamation areas. The bottoms of the drainages, which vary in width according to design standards, may or may not be topdressed or seeded depending on the size of the channel. The areas adjacent to the drainage bottoms were topdressed with soil at a thickness comparable to the adjacent reclamation community (i.e., upland shrub or grassland) and seeded using the drainage seed mix. The reclamation species selected for this community are adapted to areas with higher quantities of available water.

2.2 Geomorphic Reclamation

Geomorphic reclamation is a new technique of landform reconstruction. It was developed in 2000 by Nicholas Bugosh (Eckels et al., 2010). This reclamation method was developed to create post mining landform in an efficient and cost effective way. In traditional reclamation the waste material is dump as flat topped pyramid shape with constant gradient. The design of traditional waste dump is based on minimization of "footprint" of waste dump, optimization in movement of soil material, and meeting the environmental regulations related to erosion. Rock drains, concrete channels, and contour banks are constructed in order to prevent erosions from running water. Side slopes are planted with local vegetation for stabilization. It has been found that the traditional approach of reclamation fails to maintain stability of the slopes. Rainfall events lead to the significant erosion of surface soil by the development of incised gullies and water channel on the dump, and at times, slope failures (Eckels et al.,

2010). The erosion from soil dumps affects the environment by increasing turbidity, salinity, and mineral content at downstream channels. The mine therefore is required to undertake constant maintenance of water routing structures of the dump to satisfy regulatory requirements. Geomorphic reclamation was introduced to address the problems related to waste dump by traditional approach. Landscapes in geomorphic reclamation are built in the same way they would naturally form, making them self-sustaining and functional. The design of Final Surface Configuration (FSC) is based on stable drainages by using fluvial geomorphic principles to create channels that are appropriate for post-mining slope, aspect, earth materials, vegetation, and land use (Bugosh, 2009). The drainage patterns, longitudinal profile of ridge lines are designed from hydrological concept based on climatic condition, geology and soils. The resulting landscapes are stable, aesthetically pleasing and promote biodiversity of native vegetation.

2.3 Factors Affecting Vegetation

A coal mining permit in New Mexico requires that the reclamation will reconstruct the pre-mining landscape and ecosystem as much as possible. Through effective mine reclamation, the long-term environmental effect of mining is minimized. To evaluate the effectiveness of mine reclamation in terms of restoration of ecology it is important to study plant growth and vegetation. Soil water potential and temperature are important regulators of plant germination success. Plants will not survive if the water potential of the soil goes below wilting point for prolonged period of times. In arid and semi-arid environments, where rainfall is limited for extended periods and depth to groundwater typically limits availability to plants, water stored in the soil profile can be the primary bio-available reservoir (Geroy et al., 2011). The storage capacity of a soil profile depends on soil depth and the capacity of the soil to retain water under stresses imposed by gravitational drainage and evapotranspiration. The soil holds some of the moisture during periods of precipitation, allows some back to the surface during evaporative periods, and rejects the remainder to the water table more or less continuously (Eagleson, 1978).

The topdressing should be such that it is compatible for plant growth. The constructed topdressing of a reclaimed surface is normally composed of material different from the underlying backfill material. The physical and hydraulic properties of topdressing and spoil materials are different from each other. A study by Indorante et al., (1981)

shows that backfilling, compaction operation, and subsequent tillage affect the bulk density for top 15 cm of reclaimed mine soil. The distinct properties of these soils influence the water movement and the resulting water balance in the soil profile.

The influence of slope aspect on soil moisture and temperature for the semi-arid climate of northeastern Arizona was studied by Burnett et al. (2008). Southwest facing slopes were found to have higher average temperatures relative to the other aspects. Soil moisture data from different aspects showed that only the northwest facing slope retained moisture from winter through most of the summer. Geroy et al. (2011) conducted a statistical analysis on soil water retention data from opposing slopes. The results show that the north facing slopes retain more water than the south facing slopes. Gutierrez-Jurado et al. (2013) showed the microclimate related influence of slope aspect on the vegetation condition. South facing slopes lose more moisture by evapotranspiration than north facing slopes. The higher potential evapotranspiration of south facing slopes is due to higher solar radiation in the Northern hemisphere.

In water limited ecosystems, the existing native or non-native vegetation may not effectively utilize the moisture resources from the upper portion of the soil. Due to the high potential evaporation the rate of recession of water from soil surface is very high. Failure to utilize the soil moisture resources leaves the system vulnerable to establishment by other plants, either native or exotic. Studies on the germination potential of cheatgrass, an annual invasive species, show that it can germinate at low temperature and low water potential (Bauer et al., 1998; Roundy et al., 2007). Invasion by cheatgrass in already degraded ecosystems has become a large concern. The potential of invasion by cheatgrass is higher when it has more favorable conditions for germination and survival than the native species (Ducas et al., 2010). In an area of reclamation where new ecosystem is being created the invasion of cheatgrass will affect the establishment of native species.

2.4 Plant Germination and Survival

2.4.1 Plant Germination

Seed germination refers to the initiation of embryo growth. The process is completed by penetration of the embryo through the covering tissue. In a physiological sense, the time to germination, is the time from imbibition of the seed or from the end of

dormancy breaking treatment until the end of visible emergence of embryonic tissue from seed (Bradford, 2002). Temperature and water potential of the soil regulate the germination process. Understanding the interaction between these parameters and time to germination is essential for developing a model for effective establishment of plants. Population-based threshold model provides a useful framework for this purpose (Finch-Savage, 2004). Within this model, the rate of development, such as progress toward germination, increases above a base (threshold) value for a given factor e.g., temperature, water potential, hormone concentration, etc. Below the base value, the development stops. An appropriate mathematical function is used to describe the effect of the factors on the rate of development above the base value. According to this germination model, a number g is assigned (e.g., g_{10}, g_{50}, and g_{90}) which is the fraction of the population which germinate. The percentage of seeds that will germinate as well as germination time within the seed population are all greatly influenced by temperature and water potential (Finch-Savage, 2004).

Seeds can germinate over a wide range of temperatures. Three cardinal temperatures generally characterize the germination response to temperature: the minimum, optimum and maximum. Germination will not occur below the minimum (or base, T_b) and above the maximum (or ceiling, T_c) temperatures. Germination is most rapid at the optimum temperature (T_{opt}). In many cases germination response to temperature is described by linear relationships where the base and ceiling temperatures are defined by the intercepts on the temperature axis where the rate tends to zero. According to Bradford (2002) this can be formulated in a thermal time model as:

$$\theta_T(g) = (T - T_b)t_g \qquad (1)$$

Here $\theta_T(g)$ is the thermal time to germination of a fraction or percentage g, T is the germination temperature, T_b is the base temperature and t_g is the time to germination for a fraction g. According to this equation, the time to completion of germination for a given seed fraction g, is a constant at all sub-optimal temperatures when expressed on a thermal time basis. The germination rate which is the inverse of time to germination will increase linearly above T_b with a slope of $1/\theta_T(g)$. If GR_g is the germination rate, then:

$$GR_g = 1/t_g = (T - T_b)/\theta_T(g) \qquad (2)$$

As with temperature, water potential is essential for seed germination and its availability is a key factor affecting time to germination. Gummerson (1986) was the first to propose the hydrotime concept, a scale analogous to thermal time that describes the relationship of germination time with different water potentials. The hydrotime (θ_H) approach considers germination rate as a function the extent to which seed water potential (ψ) exceeds a base water potential (ψ_b) below which germination will not occur (Bradford, 2002).

$$\theta_H = \left(\psi - \psi_b(g)\right) t_g \qquad (3)$$

$$GR_g = 1/t_g = \left(\psi - \psi_b(g)\right)/\theta_H \qquad (4)$$

Here θ_H is the hydrotime constant, ψ is the seed water potential, and $\psi_b(g)$ is the base or threshold water potential for a specific germination fraction g. The total hydrotime required for germination for a specific fraction of population is constant. So, the more ψ exceeds the ψ_b value of a given seed, the more rapid is its progress towards germination. For a small difference between ψ and ψ_b, the t_g will be large and germination will be slow.

Gummerson (1986) developed a combined description of response of temperature and water potential in the theory of hydrothermal time. The effect of sub-optimal temperatures is included in the hydro time model by joining equation (2) and (4) to develop hydrothermal time model θ_{HT}.

$$\theta_{HT} = \left(\psi - \psi_b(g)\right)(T - T_b)t_g \qquad (5)$$

$$GR_g = 1/t_g = \left(\psi - \psi_b(g)\right)(T - T_b)/\theta_{HT} \qquad (6)$$

2.4.2 Plant Survival

Survivability of plants depends on the water potential of soil within the root zone. The ability to intake water from soil by roots of plants is described in terms of wilting point of the respective plant. Wilting point is the water content expressed in percentage that is held so tightly by the soil matrix that roots of plant cannot absorb the water. The negative pressure at which water is held by the soil matrix depends on the soil texture, compaction, and stratification. So the wilting point is also defined in terms of soil water potential. If the soil water potential goes below a certain value then

roots of plant can no longer extract water from soil and wilts (Philip, 1957; Gardner, 1960).

2.5 Water Balance and Hydraulic Properties of Soil

The water balance is simply a statement of the law of conservation of matter. In its simplest form, the water balance equation states that, changes in volumetric water content of a soil over a period of time are equal to the difference between the amount of water added W_{in} and amount of water withdrawn W_{out} during the same period (Lascano, 1991).

$$\Delta W = W_{in} - W_{out} \qquad (7)$$

The amount of water added may be in the form of precipitation or irrigation or both. The loss of water may be due to the process of runoff, drainage, soil evaporation and transpiration.

Infiltration of water into the soil from precipitation or irrigation causes the soil to become wetter with time. Water moves into the soil under the influence of matric potential gradients as well as gravity. Several infiltration models developed by Horton, Green and Ampt, Philip describe the wetting process during infiltration (Jury et al., 2004). Runoff will occur when the rate of infiltration of soil is lower than the rate of precipitation. Water continues to move from higher water potential to lower water potential in the system. The movement of water in unsaturated steady state condition is described by Buckingham-Darcy flux law. Richard modified the Buckingham-Darcy equation for one-dimensional vertical flow of water through unsaturated soil (Jury et al., 2004).

$$\frac{\partial \theta}{\partial t} = \frac{\partial}{\partial z}\left[K(h)\left(\frac{\partial h}{\partial z} + 1\right)\right] \qquad (8)$$

Here h is the water pressure head [L], θ is the volumetric water content [L^3/L^3], t is time [T], z is the spatial coordinate [L], $K(h)$ is the unsaturated hydraulic conductivity corresponding to pressure h [L/T].

The unsaturated hydraulic properties of soil $\theta(h)$ and $K(h)$ are highly nonlinear functions of pressure head h. The van Ganuchten (1980) model is used to describe the unsaturated hydraulic functions in terms of soil water retention parameters. The expressions of van Ganuchten model are given by:

$$\theta(h) = \frac{\theta_s - \theta_r}{[1+(-\alpha h)^n]^m} + \theta_r \qquad (9)$$

$$K(h) = K_{sat}\, S_e^l \left[1 - (1 - S_e^{\frac{1}{m}})^m\right]^2 \qquad (10)$$

$$S_e = \frac{\theta - \theta_r}{\theta_s - \theta_r} \qquad (11)$$

Here $\theta(h)$ is the volumetric water content corresponding to negative pressure head h [L^3/L^3], θ_r is the residual volumetric water content [L^3/L^3], θ_s is the saturated volumetric water content [L^3/L^3], α is a curve fitting parameter representing inverse of air-entry suction [1/L], h is negative pressure head [L], n is curve fitting parameter (dimensionless), and $m = 1\text{-}1/n$ (dimensionless), $K(h)$ is unsaturated hydraulic conductivity [L/T], K_{sat} is the saturated hydraulic conductivity [L/T], and l is the pore connectivity parameter (dimensioless).

Evapotranspiration from soil can be calculated using Penman-Monteith combination equation that considers both radiation and aerodynamic term (Simunek et al., 2013).

$$ET_o = ET_{rad} + ET_{aero} = \frac{1}{\lambda}\left[\frac{\Delta(R_n - G)}{\Delta+\gamma(1+r_c/r_a)} + \frac{\rho c_p (e_a - e_d)/r_a}{\Delta+\gamma(1+r_c/r_a)}\right] \qquad (12)$$

Here ET_o is the evapotranspiration rate (mm/day), ET_{rad} is the radiation term (mm/day), ET_{aero} is the aerodynamic term (mm/day), λ is the latent heat of vaporization (MJ/kg), R_n is the net radiation at surface (MJ/m^2/day), G is the soil heat flux (MJ/m^2/day), ρ is the atmospheric density (kg/m^3), c_p is the specific heat of moist air (i.e., 1.013 KJ/kg/^{o}C), $(e_a\text{-}e_d)$ is the vapor pressure deficit (KPa), e_a is the saturation vapor pressure at temperature T (KPa), e_d is the actual vapor pressure (KPa), r_c is the crop canopy resistance (s/m), and r_a is the aerodynamic resistance (s/m). The slope of the vapor pressure curve, Δ (KPa/^{o}C), and the psychrometric constant, λ (KPa/^{o}C) are defined as follows:

$$\Delta = \frac{4098 e_a}{(T+237.3)^2} \qquad (13)$$

$$\gamma = \frac{c_p P}{\varepsilon\lambda} * 10^{-3} = 0.00163\frac{P}{\lambda} \qquad (14)$$

where T is the average air temperature (^{o}C), P is the atmospheric pressure (KPa), ε is the ratio of the molecular weights of water vapor and dry air (i.e., 0.622), and λ is the latent heat (MJ/kg).

2.6 Numerical Modeling

The one dimensional numerical model HYDRUS-1D is used to simulate coupled liquid water, water vapor, and heat flow in variably saturated soil (Simunek et al., 2013). HYDRUS 1D can model both upward and downward flow of water through a soil column at varying angles of surface inclination. The extended version of Richards' equation, modified to include temperature and pressure head gradients, is used to model interactions between liquid water, thermal (temperature driven) vapor, isothermal (pressure head driven) vapor, and heat flow.

$$\frac{\partial \theta}{\partial t} = -\frac{\partial q_L}{\partial z} - \frac{\partial q_v}{\partial z} - S \qquad (15)$$

Here θ is the total volumetric water content (liquid and vapor) ([L^3/L^3]; q_L and q_V are volumetric fluxes of liquid water and water vapor [L/T] (upward positive), respectively; t is time [T]; z is the spatial coordinate [L]; and S is a sink term representing root water uptake [1/T]. The flux of liquid water, separated into isothermal, q_{Lh}; and thermal, q_{LT} liquid fluxes is:

$$q_L = q_{Lh} + q_{LT} = -K_{Lh}\left(\frac{\partial h}{\partial z} + 1\right) - K_{LT}\frac{\partial T}{\partial z} \qquad (16)$$

where K_{Lh} [L/T] and K_{LT} [L^2/K/T] are the isothermal and thermal liquid hydraulic conductivities, respectively; h is pressure head [L]; and T is temperature [K]. The flux of water vapor, separated into isothermal q_{vh}, and thermal, q_{vT}, vapor fluxes is:

$$q_v = q_{vh} + q_{vT} = -K_{vh}\frac{\partial h}{\partial z} - K_{vT}\frac{\partial T}{\partial z} \qquad (17)$$

where K_{vh} [L/T] and K_{vT} [L^2/K/T] are the isothermal and thermal vapor hydraulic conductivities, respectively (Simunek et al., 2013). Heat transport by convection-dispersion for variably saturated media is:

$$\frac{\partial C_p T}{\partial t} + L_o\frac{\partial \theta_v}{\partial t} = \frac{\partial}{\partial z}\left[\lambda(\theta)\frac{\partial T}{\partial z}\right] - C_w\frac{\partial q_L T}{\partial z} - C_v\frac{\partial q_v T}{\partial z} - L_o\frac{\partial q_v}{\partial z} - C_w S T \qquad (18)$$

where $\lambda(\theta)$ is the apparent thermal conductivity of the soil [J/L/T/K]; C_p, C_w, and C_v are volumetric heat capacities [J/L^3/K] of the moist soil, liquid phase, and vapor phase, respectively; and L_o is the volumetric latent heat of vaporization of liquid water [J/L^3]. The governing equations are solved numerically using Galerkin-type linear finite element schemes (Simunek et al., 2013).

3 MATERIALS AND METHODS

3.1 Laboratory Measurements

3.1.1 Soil Sampling

Two reclaimed watersheds were selected for this study. They were named according to the vegetation condition that existed during study period: the well-vegetated site and the moderately-vegetated site. The distance between well-vegetated site and moderately-vegetated site is around 2 kilometers. The area of each watershed is approximately 1 acre. Locations of study areas are shown in Fig. 2. Twelve locations were selected from each watershed for soil sampling. First, the whole watershed area was divided into four quadrants. This was done by visual inspection of whole watershed area. Basically border lines between the quadrants were selected by following the ridge lines or changes in aspects of slopes in the watershed. Next, coordinates of three sampling locations were determined for each quadrant by random number generators. Soil sampling and measurement locations were marked in field log book in sketch and also GPS coordinates were recorded.

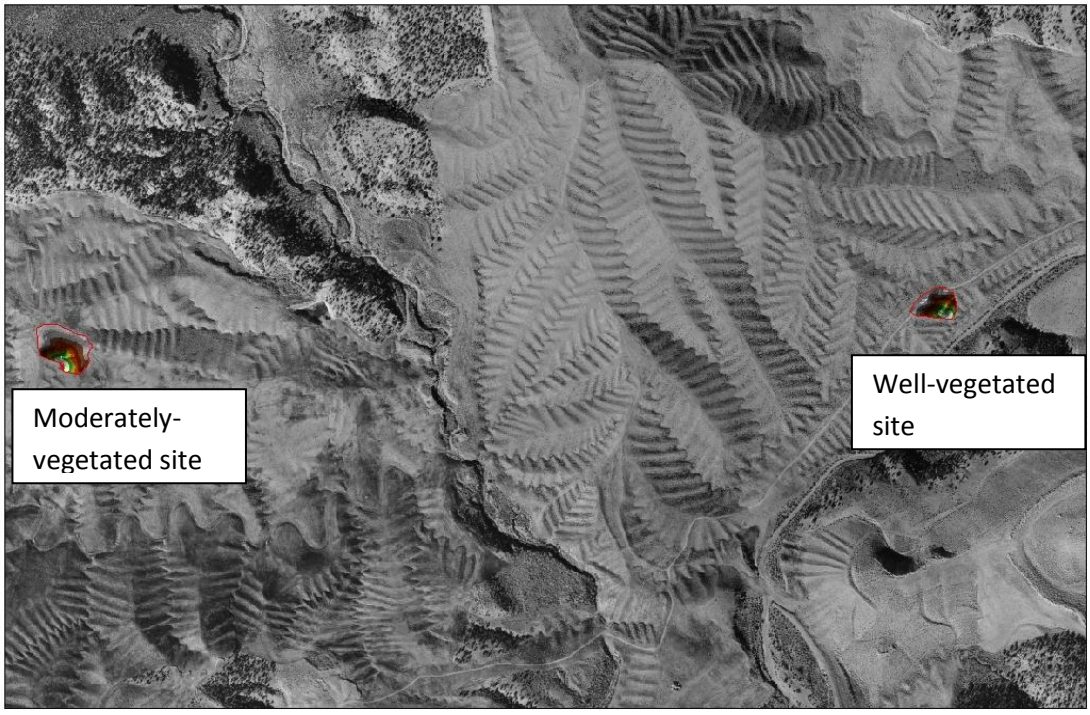

Fig. 2: Locations of study areas

Disturbed and undisturbed soil samples were collected to determine physical and hydraulic properties of the soils. Undisturbed samples were collected from one location of each quadrant of a watershed. A split spoon sampler with a diameter of 5 cm and a height of 15 cm was used to collect undisturbed samples from top of soil surface. Disturbed samples were collected from two different depths. Top samples were collected within depth of 15 cm from surface. Bottom samples were collected from 15 cm to 30 cm depth of soil. Two undisturbed samples were collected from the top of the reclaimed channel to determine properties of the spoil materials. Method B and C of ASTM standard D4220 were followed for transportation and preservation of samples. Samples were labeled according to the name of watershed and sampling location in watershed. This was done by using the initial of the name of watershed followed by a digit to mark the quadrant number and a digit to mark sampling number of that quadrant. Positions of samples were also marked as "T" for top samples and "B" for bottom samples.

3.1.2 Determination of Physical Properties

Grain size distributions of the disturbed samples were determined following the method of ASTM D422. Approximately 500 g of dry samples were taken and washed through #200 sieve. Sieve analysis was conducted for the materials retained on #200

sieve. Hydrometer analysis was conducted for approximately 50 g of soil samples passing through #200 sieve.

Specific gravity tests were conducted according to the method described by ASTM D854. Two specific gravity tests were conducted for each sample. Approximately 50 g of sample was taken and de-aired using vacuum suction for 2 hours to determine specific gravity.

Method B and C of ASTM standard D2974 were followed to determine organic content of the soils. Approximately 50 g of oven-dried samples were ignited at 440°C in a muffle furnace to determine the organic contents.

Laboratory experiments were conducted to determine soil density of the undisturbed samples collected by split spoon sampler. ASTM standard D2937 was followed to measure density of undisturbed samples. The density values measured from "Top" samples, represented cumulative average densities for top 15 cm of soils where the values from "Bottom" samples represented cumulative average densities for 15-30 cm depths of soils

Moisture contents were determined for the undisturbed samples collected from each location following ASTM D2216.

Cation Exchange Capacity (CEC) of soil samples were determined by ASTM standard D7503. Twelve samples were selected with varying percentage of clay size particles to conduct CEC test.

3.1.3 Determination of Hydraulic Properties

Falling head permeability tests were conducted for the measurement of saturated hydraulic conductivities of undisturbed samples collected from different locations of the study area. Method B of ASTM standard D5084 was followed for maintaining constant tailwater pressure. Falling head permeability tests were also conducted on remolded samples with varying densities. The samples were prepared from the disturbed soils. Each compacted sample measured 12 cm in height and 7.5 cm in diameter. A total of 5 different samples were prepared to determine the effect of soil density on the saturated hydraulic conductivity of soil.

Unsaturated hydraulic properties can be estimated from the moisture characteristic curve (MCC) of soil sample. MCCs during desorption were developed for the undisturbed samples collected from the study area. The undisturbed samples were first divided into two equal parts and tests for determining data points of MCC were conducted for bottom halves of the samples. Testing methods to collect data for MCCs include hanging column test, pressure plate test, and chilled mirror hygrometer test.

Hanging column tests were conducted according to the method A of ASTM D6836. Saturated samples were placed directly into saturated Buchner funnels connected to reservoirs by flexible tubing. A thin layer of diatomaceous earth was spread on each porous plate to improve the hydraulic contact with the sample. Samples were allowed to equilibrate at 6 different negative pressure heads ranging from 0 cm to 150 cm of water. Our test method differed from the ASTM standard in application of negative pressure and determination of equilibrium point. In ASTM standard suction is imposed by air filled tubing connected to two water reservoirs at different elevations. In our experiment the pressure was applied by relative elevation of a water reservoir and the Buchner funnel holding the sample connected by water filled tubing. Instead of measuring outflow in capillary tube, the equilibrium point was determined by weighing the samples at regular intervals. When the difference in weight of sample was less than 0.05 g for subsequent measurements then it was considered to reach the equilibration point. The final mass of sample at each pressure head point was taken to the nearest 0.01 g and subsequently used to determine volumetric water content. It took about 10 days to 30 days to reach the equilibrium point after imposing each negative pressure in hanging column test.

After the final measurement in the hanging column, the samples were moved to pressure plate apparatus. Method C of ASTM standard D6836 was followed to apply pressure heads of -500, -1000, and -3000 cm of water. The pressure was applied by compressed air. A thin layer of diatomaceous earth was spread on the plate to improve the hydraulic contact with the samples. ASTM standard requires measurement of expelled water for determination of equilibrium point. For our experiment the equilibrium point and corresponding volumetric water content was determined by the same method as followed for hanging column test. Equilibration at each pressure, determined by water ceasing to move out from the sample, took 15 to 30 days.

A chilled mirror hygrometer was used to collect data for MCC at negative pressure heads ranging from $1x10^4$ cm to $6x10^5$ cm of water. Method E of ASTM standard D6836 was followed for this experiment. A WP4 dew point potentiometer from Decagon Device, Inc. was used as testing apparatus. Dew point potentiometer tests were conducted for the fraction passing #10 sieve only. Before conducting the test the device was calibrated using standard KCl solution. Water potential of the sample was read and the sample was weighed immediately following the reading to obtain gravimetric water content. Gravimetric water contents and water potentials were converted to volumetric water contents and negative pressure heads in water.

3.2 Field Testing

Periodic soil moisture content measurements were conducted using a TDR (Time Domain Reflectometer). A TDR measures the volumetric water content of soil by calculating the dielectric constant of soil. ASTM standard D6565 was followed for calibration and measurement of volumetric water content by TDR. Twelve random locations were selected in each watershed by the method previously mentioned to take TDR readings. At each location cumulative average volumetric water contents were measured for the heights of 7.5 cm and 20 cm from the surface by TDR.

To capture the variation in densities with depth, field density tests were conducted at different depths and locations of the study area. Sand cone tests were conducted at different locations according to ASTM D1556 to measure density for the top 7.5 cm of soil. Small hand borers were also used to collect undisturbed samples and measure density at various depths. The diameter of the borers ranged from 0.375 cm to 1.15 cm and the length of the borers were 10.3 cm. Borers were inserted horizontally inside the soil to measure densities at depths of 4, 12, and 23 cm from the surface.

A field test was conducted to determine unsaturated hydraulic properties of the topdressing and spoil material. Tension infiltrometer tests (Ankeny et al., 1991) were conducted at seven random locations of the reclaimed soil surface. Three tests were conducted at depths of 7.5, 15, and 30 cm from soil surface. Three additional tests were conducted on the surface of the reclaimed channel to determine unsaturated hydraulic properties of the spoil material. A 20 cm diameter tension disc infiltrometer was used for our study. The experiments were carried out for three different pressure heads ranging from -20 to -4 cm of water at each location. A thin (≈ 0.3 cm) layer of

sand was placed between the disc membrane and the soil surface to improve hydraulic contact (Reynolds et al., 1996). Correction of pressure head was applied to get actual pressure head on the soil surface due to the use of contact sand (Reynolds et al., 2006). No corrections were required in conducting the test in sloping surface, because the slope of the soil surface in study area was less than 20% (Bodhinayake et al., 2004). The infiltration test was carried out until a steady state flow is reached for any supply pressure head. Cumulative flow of water at different time intervals was recorded. Disturbed samples were collected before and after the infiltration experiments to determine the initial and final gravimetric water contents. Soil densities measured from the previous experiments were used to convert gravimetric water contents into volumetric water contents.

4 RESULTS OF SOIL PROPERTIES

4.1 Physical Properties

Textural classifications of soil samples were made using grain size distribution data. The soils were classified according to the texture classification system developed by U.S. Department of Agriculture (USDA). USDA texture classification system is based on the particle size limits and the soils are named according to the principle component of the soil (Das, 2010). Average percentage of various soil components are presented in Table 1. Figure 3 shows the frequency distribution of soil types based on USDA classification for 12 samples collected from each location. From Fig. 3 it is observed that the soil used for reclamation purpose is mostly loam or sandy clay loam.

Table 1: Average percentages of soil components according to USDA

Sampling Location	Average percentage			
	Gravel	Sand	Silt	Clay
W top	11.15	41.10	27.70	20.05
W bottom	11.10	41.98	29.25	17.67
M top	6.05	38.11	35.38	20.46
M bottom	4.77	36.73	32.83	25.67

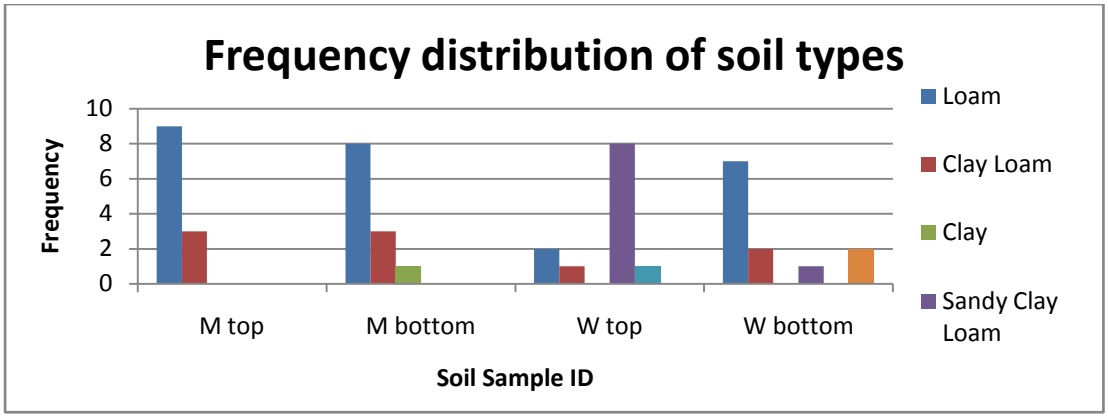

Fig. 3: Frequency distribution of soil types

Results of organic content tests and specific gravity tests are presented graphically using boxplot in Fig. 4 and 5. Summary of the test results are presented by average values in Table 2. The results show that the average specific gravity values fall within the range of specific gravity values for silty or clayey soils, which is 2.6 to 2.9 (Das, 2010). The average organic content values of the reclaimed soil ranged from 3.8% to 5.7%. The organic content values can be compared with the typical values of the surface soils in Arizona-Nevada where the yearly rainfall is analogous to the rainfall of our study area (30 cm). Typical organic content of loamy coarse sand is 0.60% and for fine sandy loam it is 1.64% (Gardiner, 2008); thus, the organic content values of the reclaimed soils are higher than the typical values. Seed mixes and grass mulch carried out following the seeding work (La Plata Mine Permit, 2001) may have contributed to the higher organic content results for the reclaimed soils.

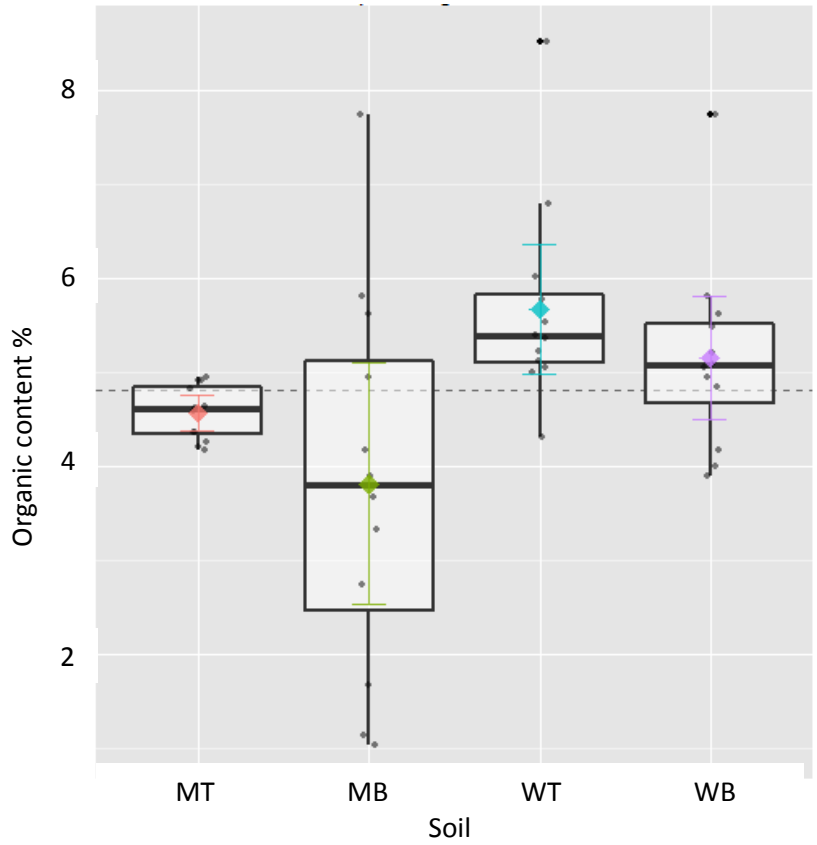

Fig. 4: Organic content test results for samples from different locations

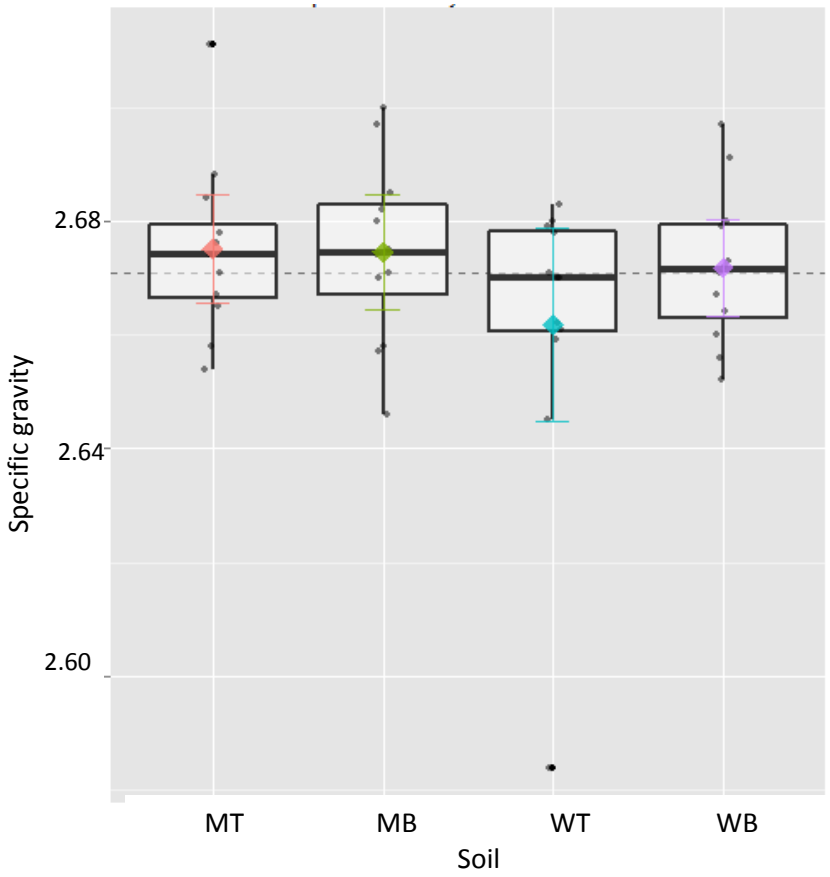

Fig. 5: Specific gravity test results for samples from different locations

Table 2: Summary of specific gravity and organic content test of soil sample

Soil	No of samples	Average specific gravity	Average organic content %
W top	12	2.68	5.67
W bottom	12	2.66	5.16
M top	12	2.68	4.57
M bottom	12	2.67	3.82

The result of the CEC tests for soils with varying percentages of clay size materials is presented graphically in Fig. 6. No significant relation was found between the CEC and clay size particles of the soil. This result suggests that not all of the clay size particles were clay materials.

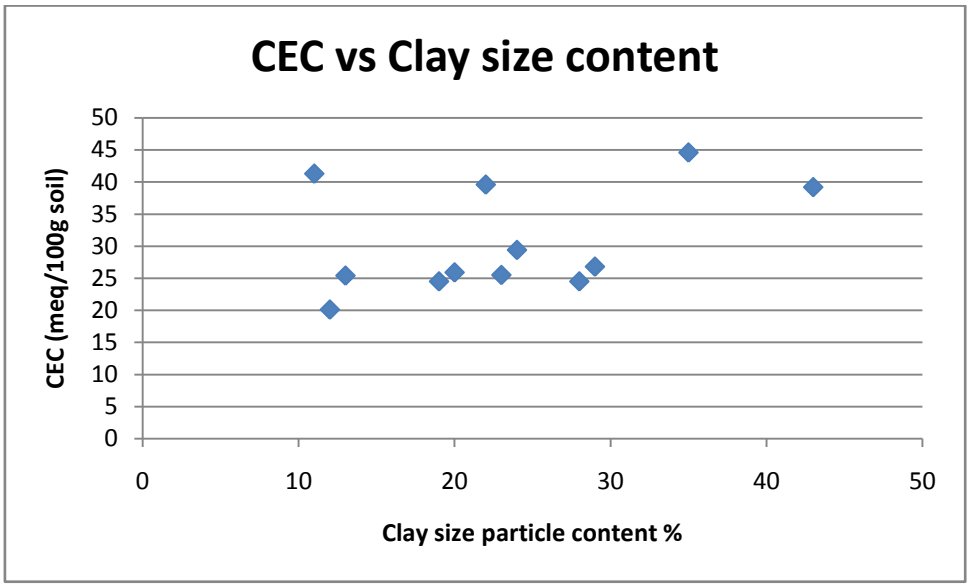

Fig. 6: CEC vs. clay size particle contents

Three different measurement techniques were followed to determine soil density: density test of undisturbed samples; density test using sand cone apparatus; and density test of samples collected by hand borer. Results of density measurement from undisturbed samples are presented in Table 3. The volume of the each sample collected in tube was 260.15 cm^3. Table 4 shows the results of sand cone density measurements at three locations of reclaimed soil surface. Results of horizontal density measurements at different depths by hand borer are presented in Table 5. The results show density values varied at different depths. The surface soil up to depth of 7.5 cm from surface has the lowest density as determined by sand cone test and the average density is 1.06 g/cm^3. Density measurement from undisturbed sample

represents cumulative average density for top 15 cm of soil. The values are within the range of 1.50 to 1.77 g/cm^3. The density values from undisturbed samples are higher than the density values measured from hand borer within the collection depth of undisturbed sample. This is because the hand borer has a very small diameter compared to the diameter of large and heavy size particles present in the soil. The hand borer measures the density of soils for particles smaller than its diameter. The density test by hand borer indicates that there is an increase in density with depth from surface (Fig. 7). This result is consistent with the method of preparation of reclaimed soil surface: after reclamation work the final surface grade was ripped or disked to loosen the top foot to improve the movement of water, air, and roots in the root zone (La Plata Mine Permit, 2001).

Table 3: Soil density from undisturbed samples

Sample ID	Mass of soil (g)	Bulk density (g/cm^3)	Gravimetric water content %	Dry density (g/cm^3)
spoil 1	388.82	1.49	6.76	1.40
spoil 2	364.16	1.40	6.76	1.31
W11 T	417.33	1.60	2.29	1.57
W21 T	469.02	1.80	2.14	1.77
W31 T	398.13	1.53	3.27	1.48
W41 T	435.73	1.67	2.84	1.63
M11 T	435.02	1.67	4.61	1.60
M21 T	438.63	1.69	3.68	1.63
M31 T	438.44	1.69	3.45	1.63
M42 T	407.32	1.57	4.50	1.50
M31 B	433.33	1.67	4.12	1.60

Table 4: Sand cone density test results at soil surface

Test no	Volume of soil (cm^3)	Weight of moist soil (g)	Bulk density of soil (g/cm^3)	Average bulk density of soil (g/cm^3)	Moisture content of soil %	Dry density of soil (g/cm^3)	Average dry density of soil (g/cm^3)
1	459.39	515.26	1.13		4.40	1.07	
2	502.56	515.28	1.03	1.10	5.83	0.97	1.06
3	383.30	445.92	1.17		3.22	1.13	

Table 5: Results of horizontal density measurements by hand borer at different depths

Location from surface (cm)	Volume of sample (cm^3)	Weight of sample (g)	Bulk density of sample (g/cm^3)	Gravimetric water content %	Dry density of sample (g/cm^3)
4	2.34	3.04	1.3	19.73	1.09
4	2.44	3.08	1.26	17.75	1.07
12	2.39	3.48	1.46	18.25	1.23
12	4.96	7.95	1.6	17.78	1.36
23	2.25	3.76	1.67	16.03	1.44
23	9.03	14.67	1.62	15	1.41

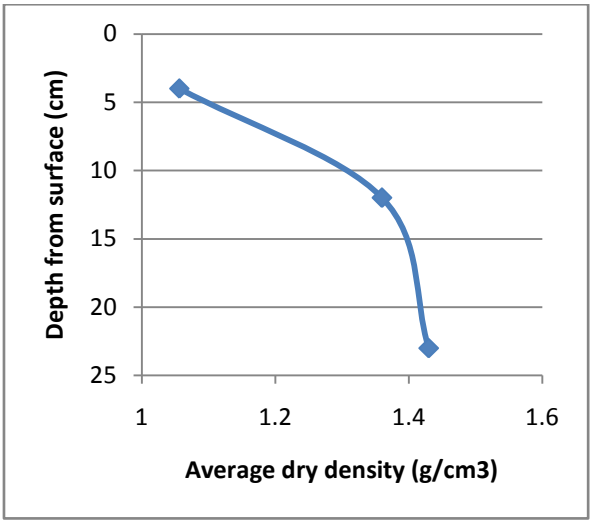

Fig. 7: Density profile as determined by hand borer

4.2 Hydraulic Properties

Results from falling head saturated hydraulic conductivity tests for undisturbed samples are presented in Table 6. For each sample three tests were conducted and averaged. The results show that the highest and lowest average saturated hydraulic conductivity (K_{sat}) measured for reclaimed soil was 1.46×10^{-4} cm/sec and 3.60×10^{-6} cm/sec, respectively. The spoil material has average K_{sat} of 2.61×10^{-4} cm/sec. The results of falling head saturated hydraulic conductivity tests of remolded samples for varying soil densities are presented in Table 7. Remolded samples yielded K_{sat} values ranging from 10^{-5} to 10^{-6} cm/sec depending upon the density of the samples. The lowest dry density achieved after saturation was 1.32 g/cm^3. The measured K_{sat} corresponding to lowest density was 6.25×10^{-5} cm/sec. The K_{sat} value corresponding to soil density of 1.58 g/cm^3 was measured as 4.62×10^{-6} cm/sec.

Table 6: Falling head saturated hydraulic conductivity test results for undisturbed samples

Sample ID	Test 1 K_{sat} (cm/sec)	Test 2 K_{sat} (cm/sec)	Test 3 K_{sat} (cm/sec)	Average K_{sat} (cm/sec)
M11 T	3.11E-05	3.14E-05	3.17E-05	3.14E-05
M21 T	5.95E-05	5.73E-05	5.82E-05	5.83E-05
M31 T	1.64E-04	1.38E-04	1.37E-04	1.46E-04
M42 T	1.86E-05	2.14E-05	2.46E-05	2.45E-05
W11 T	1.87E-05	1.88E-05	1.57E-05	1.77E-05
W21 T	3.60E-06	3.60E-06	3.61E-06	3.60E-06
W31 T	7.01E-05	7.15E-05	6.65E-05	6.94E-05
W41 T	2.56E-05	2.84E-05	2.54E-05	2.84E-05
M31 B	1.84E-05	1.54E-05	1.55E-05	1.64E-05
Spoil 1	2.57E-04	2.54E-04	2.53E-04	2.55E-04
Spoil 2	2.19E-04	2.47E-04	2.29E-04	2.68E-04

Table 7: Falling head saturated hydraulic conductivity test results of remolded samples with varying soil densities

Sample no	Weight of sample (g)	Volume of sample (cm^3)	Bulk density of sample (g/cm^3)	Gravimetric water content %	Dry density (g/cm^3)	Average Ksat (cm/sec)
1	678.11	474.04	1.43	8.28	1.32	6.25E-04
2	846.41	566.57	1.49	8.17	1.38	2.91E-04
3	810.33	537.85	1.51	8.84	1.38	1.90E-04
4	931.49	577.51	1.61	5.62	1.53	3.44E-05
5	772.73	463.55	1.67	5.63	1.58	4.62E-06

Laboratory test results of volumetric water contents corresponding to negative pressure heads were fitted to van Ganuchten model (1980) for MCC. The Retention Curve Program (RETC) for unsaturated soils (van Ganuchten et al., 1997) was used to fit the data. Figure 8, 9 and 10 show the MCCs for different soil types as developed by RETC program. RETC program follows the non-linear least square parameter optimization method for quantifying the soil water retention parameters. Non-linear optimization was done for the van Ganuchten parameters of $\theta_r, \theta_s, \alpha,$ and n while keeping the K_{sat} value constant found from laboratory measurement. The value of parameter l was fixed at 0.5 according to Mualem (Simunek et al., 2013). Results of the van Ganuchten model parameters from RETC program is summarized in Table 8.

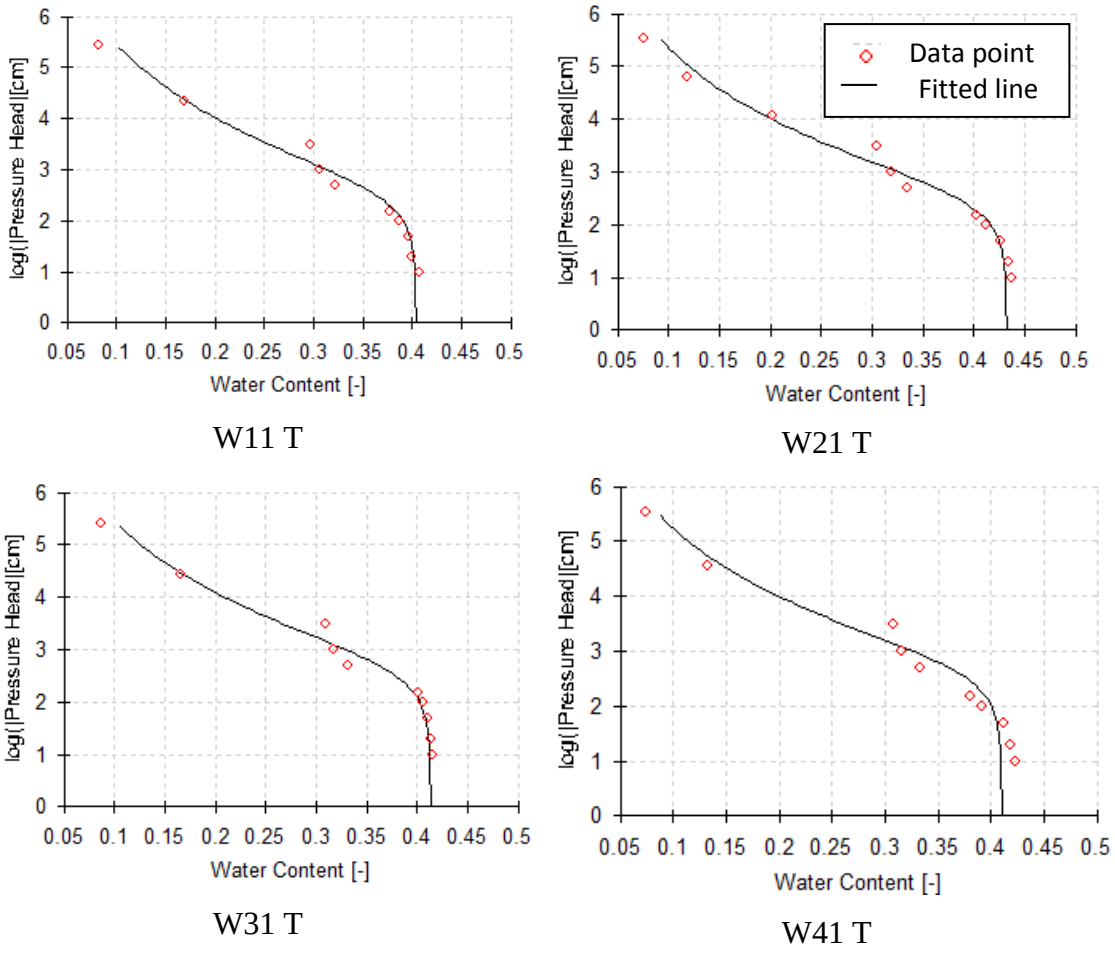

Fig. 8: MCCs for of undisturbed samples collected from well-vegetated site as developed by RETC program

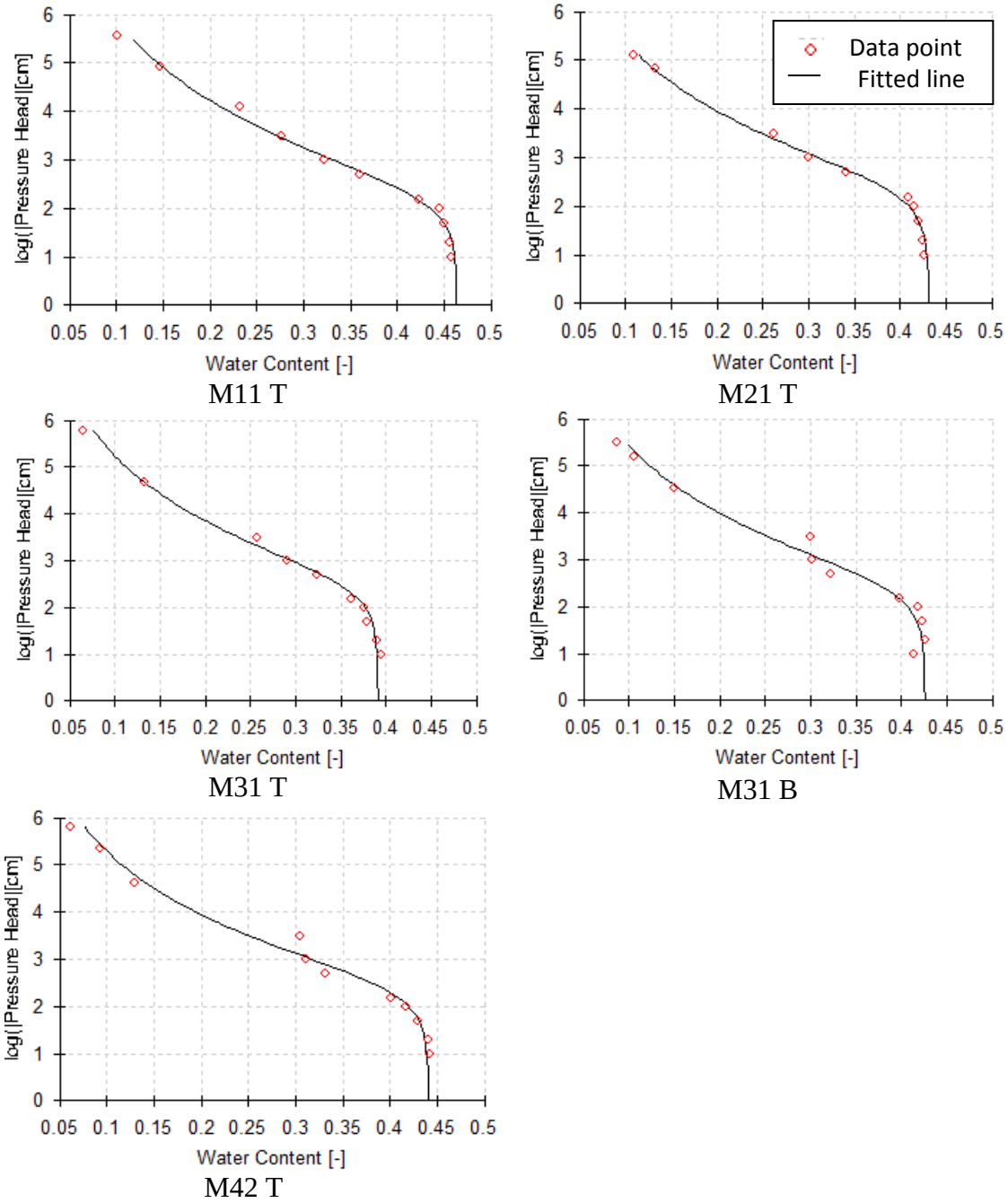

Fig. 9: MCCs for of undisturbed samples collected from moderately-vegetated site as developed by RETC program

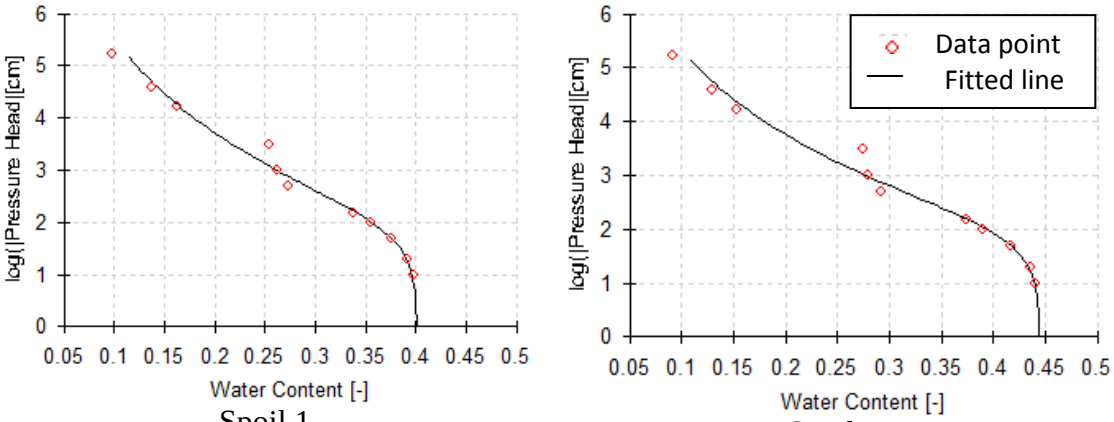

Fig. 10: MCCs for of undisturbed samples collected from channel as developed by RETC program

Table 8: van Ganuchten model parameters for undisturbed samples

Sample ID	θ_r (cm^3/cm^3)	θ_s (cm^3/cm^3)	α (cm^{-1})	n	K_{sat} (cm/s)
M11 T	0.002	0.464	0.0086	1.18	3.14E-05
M21 T	0.003	0.431	0.0056	1.21	5.83E-05
M31 B	0.006	0.426	0.0075	1.21	1.64E-05
M31 T	0.006	0.391	0.0044	1.22	1.46E-04
M42 T	0.002	0.440	0.0069	1.23	2.45E-05
W11 T	0.007	0.404	0.0054	1.21	1.77E-05
W21 T	0.003	0.432	0.0055	1.23	3.60E-06
W31 T	0.005	0.413	0.0045	1.22	6.94E-05
W41 T	0.006	0.410	0.0041	1.24	2.84E-05
Spoil 1	0.006	0.401	0.0125	1.16	2.55E-04
Spoil 2	0.004	0.445	0.0113	1.19	2.68E-04

The field tension infiltrometer data were analyzed in two ways to determine hydraulic properties of the soil. One of the methods was analytical solution of steady-state flow rate and the other method was numerical solution by inverse simulation of time dependent cumulative flow data.

In analytical method, saturated hydraulic conductivity of soil was determined by solving Wooding's (1968) equation for steady-state flow rates at multiple negative pressure heads (Hussen et al., 1995). Steady state flow rate (Q) from tension infiltrometer device is presented as:

$$Q = K_{sat} \exp\left(\frac{h}{\lambda_c}\right)\left[1 + \frac{4\lambda_c}{\pi r_o}\right] \qquad (19)$$

where r_o is the radius of the disc infiltrometer [L], h is the supply negative pressure head [L], and λ_c is the macropore capillary length [L]. Measurement of steady-state flow rate for multiple tensions at the same site solves for λ_c.

$$\lambda_c = \frac{|h_2 - h_1|}{|\ln Q_2/Q_1|} \qquad (20)$$

Here Q_1 and Q_2 are steady-state flow rates at two different supply negative pressure heads h_1 and h_2. The value of K_{sat} is found by substituting λ_c into equation 19. A correction was made to the supply pressure head because of using contact sand on top of soil surface. The offset (Δh) between the pressure head set on bubble tower (h_o) and the pressure head applied to the soil surface (h_s) is determined from Reynolds (2006) equation.

$$\Delta h = (h_s - h_o) = \left[\frac{K_{cs}T_{cs} - q(h_o)T_{cs}}{K_{cs}}\right] \qquad (21)$$

Here K_{cs} is the saturated hydraulic conductivity of the contact sand [L/T], T_{cs} is the average thickness of the contact sand layer over the infiltration surface [L], and $q(h_o)$ [L/T] is the steady-state flow rate corresponding to pressure head h_o.

A summary of the results of analytical solution of infiltration tests conducted at the reclaimed soil surface, reclaimed channel surface, and at different depths from reclaimed soil surface are given in Table 9, 10 and 11.

Table 9: Analytical solution of saturated hydraulic conductivity determined from tension infiltrometer test data at reclaimed soil surface

Measurement location	Pressure head applied to soil surface, h_s (cm)	Steady state flow rate from disc, Q (cm/sec)	λ_c (cm)	Saturated hydraulic conductivity, K_{sat} (cm/sec)
W1	-23.60 -10.20 -4.81	1.20E-04 2.50E-04 4.95E-04	18.29 7.91	1.31E-04 4.53E-04
W1	-20.71 -10.21 -4.72	3.49E-04 5.16E-04 1.13E-03	26.82 7.05	1.71E-04 1.16E-03
W3	-20.20 -10.11 -4.72	2.06E-04 6.51E-04 1.46E-03	8.78 6.73	9.71E-04 1.58E-03
W4	-20.20 -9.71 -4.73	2.81E-04 9.90E-04 1.90E-03	8.34 7.65	1.54E-03 1.79E-03
M1	-15.90 -9.70 -4.71	1.77E-04 2.98E-04 4.13E-04	11.86 15.41	2.69E-04 1.89E-04
M2	-14.41 -9.41 -4.01	3.75E-04 5.50E-04 9.90E-04	13.06 9.19	4.25E-04 7.06E-04
M3	-15.80 -9.30 -4.41	1.54E-04 2.75E-04 5.38E-04	11.18 7.3	2.61E-04 5.10E-04

Table 10: Analytical solution of saturated hydraulic conductivity determined from tension infiltrometer test data at reclaimed channel

Test no	Pressure head applied to soil surface, h_s (cm)	Steady state flow rate from disc, Q (cm/sec)	λ_c (cm)	Saturated hydraulic conductivity, K_{sat} (cm/sec)
1	-9.71 -4.72	6.19E-04 1.41E-03	6.05	1.74E-03
2	-9.71 -4.71	3.96E-04 5.50E-04	15.22	2.55E-04
3	-8.06 -4.72	1.24E-03 1.65E-03	11.61	9.99E-04

Table 11: Analytical solution of saturated hydraulic conductivity determined from tension infiltrometer test data at depths from reclaimed soil surface

Depth from surface	Pressure head applied to soil surface, h_s (cm)	Steady state flow rate from disc, Q (cm/sec)	λ_c (cm)	Saturated hydraulic conductivity, K_{sat} (cm/sec)
7.5 cm	-15.71 -9.51 -4.71	4.67E-04 6.69E-04 9.90E-04	17.25 12.24	3.63E-04 5.68E-04
15 cm	-14.81 -4.71 -2.11	5.50E-04 7.50E-04 8.25E-04	32.56 27.28	1.68E-04 1.99E-04
30 cm	-9.70 -2.10	4.95E-05 8.84E-05	13.11	3.89E-05

Inverse simulation by HYDRUS 2D program was used to estimate soil hydraulic properties from data obtained during tension infiltrometer test. The inverse procedure combined the Levenberg-Marquardt nonlinear parameter optimization method with a numerical solution of the axisymmetric variably-saturated flow equation (Simunek et al., 1996). The objective function was defined in terms of the cumulative infiltration and the final moisture content measured directly below the tension-disc infiltrometer at the end of the experiment. This final water content was assumed to correspond to the final supply pressure head. The initial condition was defined in terms of the water content measured before the test. The residual water content value, θ_r was fixed at zero during optimization of the other hydraulic properties. Table 12, 13 and 14 summarizes the results of soil hydraulic properties estimated from inverse simulation of tension infiltrometer test data at reclaimed surface, reclaimed channel and at depths of reclaimed soil.

Table 12: Hydraulic properties of reclaimed soil at the surface determined from inverse simulation of tension infiltrometer test data

Sample ID	θ_s (cm^3/cm^3)	α (cm^{-1})	n	K_{sat} (cm/s)
W1	0.377	0.0055	1.25	8.77E-04
W1	0.351	0.0373	1.40	6.41E-05
W2	0.311	0.0114	1.50	1.61E-04
W4	0.349	0.0120	1.39	3.24E-03
M1	0.319	0.0084	1.20	8.27E-04
M2	0.312	0.0077	1.38	8.14E-04
M3	0.351	0.0089	1.30	2.90E-04

Table 13: Hydraulic properties of soil at reclaimed channel determined from inverse simulation of tension infiltrometer test data

Test no	θ_s (cm^3/cm^3)	α (cm^{-1})	n	K_{sat} (cm/s)
1	0.407	0.0467	1.99	1.42E-04
2	0.500	0.0731	2.00	1.14E-04
3	0.354	0.0391	1.14	2.72E-03

Table 14: Hydraulic properties of reclaimed soil at different depths from surface determined from inverse simulation of tension infiltrometer test data

Depth from surface	θ_s (cm^3/cm^3)	α (cm^{-1})	n	K_{sat} (cm/s)
7.5 cm	0.350	0.0100	1.21	1.42E-04
15 cm	0.350	0.0100	1.45	9.73E-05
30 cm	0.382	0.0861	1.75	1.54E-04

Saturated hydraulic conductivity values obtained from undisturbed samples, tension infiltrometer test data and laboratory prepared samples varied in magnitude. The tests were conducted on soils at different depths. Texture properties of reclaimed soil shows that there are no significant differences between soils collected from different depths. The principal difference which exists among the soils at different depths is density. With the increase in soil density the saturated hydraulic conductivity is decreased as the pore spaces between the particles are decreased (Das, 2001). Measured saturated hydraulic conductivity values were plotted against the dry density of the respective soil samples (Fig. 11). For surface soil (0-7.5 cm from top) the dry

density was assumed to be 1.32 g/cm^3 which is the dry density of loose sample after saturation as measured from remolded sample. It is observed that the variation in saturated hydraulic conductivity for different depths is due to the variation in soil density and as the density of soil is increased the saturated hydraulic conductivity is decreased.

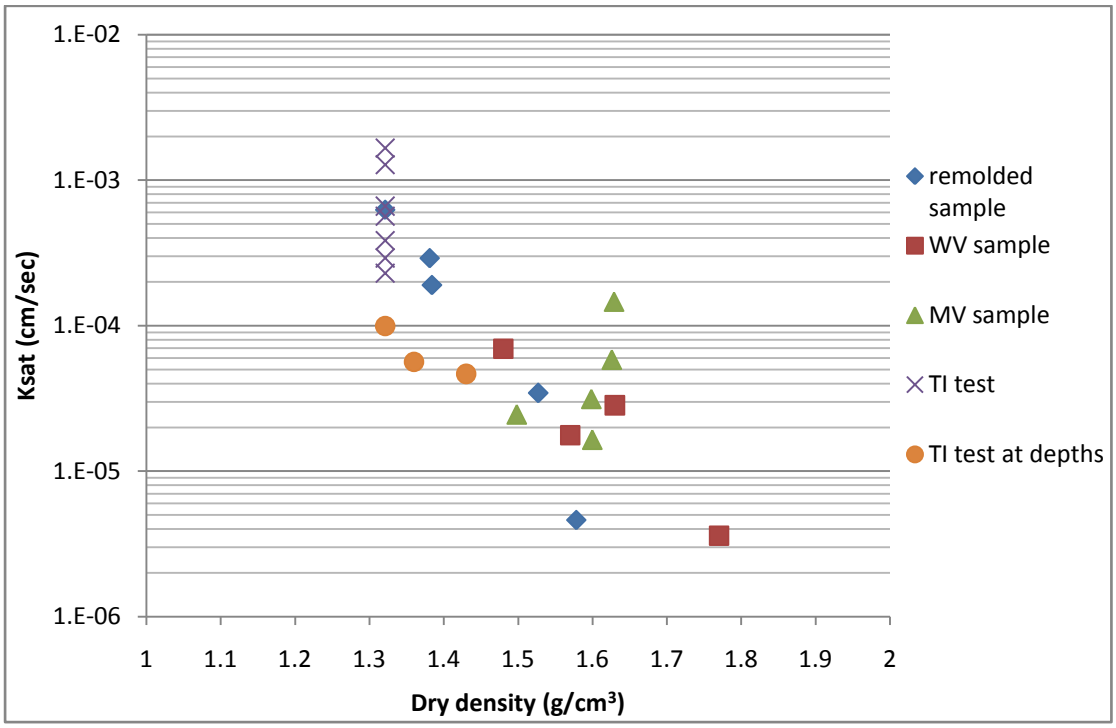

Fig. 11: K_{sat} vs density of soil at different depths and locations

Instead of considering one uniform layer of soil, the average hydraulic properties of the soil were determined for three separate layers, e.g., surface layer, middle layer, and sub-surface layer or spoil layer. The surface layer was assumed to extend from the surface to 7.5 cm of depth and has the least density as measured by sand cone test. The hydraulic properties of this layer were estimated from the average results of tension infiltrometer tests conducted at the top of the soil surface. The middle layer was considered from 7.5 to 30 cm of depth from surface. The middle layer has the density higher than that of surface layer. The hydraulic properties of middle layer were estimated from the average results of laboratory tests of undisturbed samples and tension infiltrometer test results at depths of 7.5 cm and 15 cm from surface. The hydraulic properties of the sub-surface layer, or the spoil material, were estimated from the average results of tension infiltrometer tests conducted at the reclaimed channel surface, at 30 cm depth from reclaimed soil surface, and laboratory test data

of undisturbed spoil materials. The residual water content (θ_r) for all layers were estimated from average values of laboratory test results of undisturbed samples. Table 15 summarizes the hydraulic properties of different layers of soil as obtained from field tests and laboratory experiments.

Table 15: Hydraulic properties of soil layers

Depth	Material	θ_r (Cm^3/cm^3)	θ_s (cm^3/cm^3)	α (1/cm)	n	K_{sat} (cm/day)
0-7.5 cm	Surface	0.005	0.339	0.01	1.3	67.56
7.5-30 cm	Middle	0.005	0.3745	0.007	1.28	5
Below 30 cm	Sub-surface	0.005	0.41	0.06	1.54	20.22

5 ONE DIMENSIONAL MODEL FOR WATER BALANCE SIMULATION

5.1 Profile Development

One dimensional model profile was created for a 13 m depth to minimize boundary effects on numerical simulation following Garcia et al. (2011). The profile was discretized into 1001 nodes with increased spacing with depth from surface. The spacing between the top nodes was 0.4333 cm where the spacing was 2.17 cm between the bottom nodes. To represent actual sloping condition of the watershed, the one dimensional profile was created with an inclination of 12° with the horizontal. In HYDRUS-1D the inclination is specified in terms of the cosine of the angle between the vertical axis and the axis of the soil profile.

The profile was divided into three separate soil layers based on measured physical and hydraulic properties. The depth of surface layer was taken as 7.5 cm. The middle layer was from 7.5 cm to 30 cm depth. The remainder of the domain was defined as sub-surface soil layer.

5.2 Boundary Conditions

The soil surface water-flow boundary was controlled by a time variable atmospheric boundary condition including solar radiation, air temperature, wind speed, and precipitation. Input values were based on hourly data collected from the La Plata

meteorological station. The water flow boundary condition at the bottom was assumed to be controlled by gravity and was assigned a unit hydraulic gradient. The time variable air temperature and constant bottom temperature of 21.7°C were used for the upper and lower heat flow boundaries, respectively (Fischer, 1992).

The absolute value of minimum allowed pressure head at the surface was determined from the following equation.

$$H_\gamma = exp\left[\frac{hM_g}{RT}\right] \qquad (22)$$

where H_γ is the relative humidity, g is the gravitational acceleration [L/T^2] (=9.81 m s^{-2}), M is the molecular weight of water [M/mol^1] (=0.018015 kg mol^{-1}), R is the universal gas constant [$J/mol^1/K^1$, $ML^2/T^2/mol^1/K^1$] (=8.314 J $mol^{-1}K^{-1}$), T is the absolute temperature [K], and h is the pressure head [L] (Simunek et al., 2013). Runoff was assumed negligible in these simulations.

5.3 Root Water Uptake

The root water uptake for water balance model was adopted from Meyer et al. (2012), who investigated the effect of vegetation on calcite accumulation with root water uptake by blue grama grass (*Bouteloua gracilis)* in New Mexico. The plant root distribution at each of the nodes was determined using a function described by Jackson et al. (1996):

$$\gamma = 1 - \beta^d \qquad (23)$$

where γ is the cumulative root fraction at depth d, β is a coefficient value (0-1) designated to describe specific biome, and d is the depth of interest. The β value used in this study (β=0.972) represents a semi-arid grassland (Jackson et al., 1996) composed of blue grama grass. Root water uptake was not considered below 41 cm depth as blue grama grass typically exhibits a maximum rooting depth of near 40 cm (Meyer et al., 2012).

The HYDRUS 1D model was also used to determine survivability of an invasive species. Cheatgrass (*Bromus tectorum)* was selected for modeling as an invasive species because it is common and well studied for semi-arid condition similar to that at the study site. The root water uptake of cheatgrass was considered up to 30 cm

depth and the root distribution was defined as described by Kemp et al. (1997) for annual species.

Root water uptake is calculated by HYDRUS 1D using Feddes equation (Feddes et al., 1978). Constant values for root water uptake are calculated at each node by multiplying plant potential transpiration by the normalized root distribution at each node. Feddes parameters for root water uptake by blue grama grass (Meyer, 2012) and cheatgrass (Ducas et al., 2011) are presented in Table 16.

Table 16: Root water uptake parameters for use in HYDRUS 1D

Model parameter	Blue grama grass	Cheatgrass
Po (cm)	-10	-15
Popt (cm)	-25	-546
P2H (cm)	-200	-920
P2L (cm)	-800	-3783
P3 (cm)	-90000	-9100
r2H (cm/day)	0.37	0.7
r2L (cm/day)	0.01	0.1

5.4 Material Properties

Hydraulic properties of the surface, middle and sub-surface soil layers were obtained from measured laboratory and field values. A summary of the hydraulic properties of different layers are given in Table 15. Soil moisture simulations were also conducted considering uniform soil density at the topdressing. In case of uniform topdressing, laboratory measured soil hydraulic properties were used from top to 30 cm depth. Hydraulic properties of the spoil materials were used at the sub-surface layer starting from 30 cm depth.

Heat transport parameters of the soil were used as determined by Chung et al. (1987). Heat transport parameter for loam type soil was used as the laboratory experiments on soils showed that the reclaimed soils were mostly loam type.

5.5 Meteorological Parameters

Global solar radiation was measured using a LI-200 Pyranometer at the La Plata weather station. The global radiation data was used to calculate incoming shortwave radiation on any sloping surface. According to Tian et al. (2000), incoming shortwave radiation SW_{in} of a sloping surface can be calculated from

$$SW_{in} = Q_r + D_r + A_r \qquad (24)$$

where Q_r is the irradiance received by the surface directly from the solar beam, D_r is the amount of diffuse radiation reaching the ground and emitted isotropically from all sky directions, and A_r is the radiation received on the surface by reflection from blocking terrain. The terms in equation 24 are calculated as:

$$Q_r = G_m . R_d . (1 - K_r) \qquad (25)$$

$$D_r = G_m . f_\beta . K_r \qquad (26)$$

$$A_r = G_m . alb. (1 - f_\beta) \qquad (27)$$

here G_m is the global incoming radiation measured on a horizontal surface and R_d is the ratio of direct radiation on the slope to direct radiation on a horizontal surface. According to Revfeim (1978), for any declination the value of R_d at any hour of the day can be expressed as:

$$R_d = \frac{\cos z^*}{\cos z} \qquad (28)$$

here z is the zenith angle and z^* is the zenith angle relative to slope.

$$\cos z = \cos \delta . \cos\Lambda . \cos(\omega . t_d) + \sin\delta . \sin \Lambda \qquad (29)$$

$$\cos z^* = \cos \delta . \cos\Lambda^* . \cos(\omega . t_d - g) + \sin\delta . \sin \Lambda^* \qquad (30)$$

$$\Lambda^* = \sin^{-1}(\sin\Lambda . \cos \beta - \cos\Lambda . \sin \beta . \cos b) \qquad (31)$$

$$g = \sin^{-1}(\sin \beta . \sin b . \sec \Lambda^*) \qquad (32)$$

δ is the declination angle (degrees) that incorporates the effect of the angle between horizontal plane on the earth and the solar beam and is computed according to Iqbal (1983).

$$\delta = \left(\frac{180}{\pi}\right) . [0.006918 - 0.399912 . \cos \Gamma + 0.070257 . \sin \Gamma - 0.006758 . \cos(2 . \Gamma) + 0.000907 . \sin(2 . \Gamma) - 0.002697 . \cos(3 . \Gamma) + 0.000148 . \sin(3 . \Gamma)] \qquad (33)$$

Here Γ is day angle (radian) calculated from the Julian day of the year (J).

$$\Gamma = \frac{2.\pi.(J-1)}{365} \qquad (34)$$

Λ is the latitude (degrees); ω is the angular velocity of the earth's rotation (15 hr^{-1}); and t_d is the time before or after the solar noon (S_h) in hours and is calculated as:

$$t_d = S_h - t \qquad (35)$$

where t is time in hour (0 to 24). S_h is computed from equation of time (E_{rc}) and longitude of the plane (Ω).

$$S_h = 12 - E_{rc} - \left(\frac{105-\Omega}{15}\right) \qquad (36)$$

The equation of time (E_{rc}) is calculated according to Campbell et al. (2000) in hours.

$$E_{rc} = \frac{-104.7 \sin f + 596.2 \sin 2f + 4.3 \sin 3f - 12.7 \sin 4f - 429.3 \cos f - 2 \cos 2f + 19.3 \cos 3f}{3600} \qquad (37)$$

where $f = 279.575 + .9856J$, in degrees.

Here β is the slope angle of the terrain in degrees, and b is bearing from south of horizontal projection of normal to surface.

K_r is the ratio of diffuse to global radiation; f_β is a slope reduction factor accounting for the portion of the sky hemisphere above the slope surface and alb is the albedo.

$$f_\beta = 1 - \frac{\beta}{180} \qquad (38)$$

The ratio of diffuse to global radiation can be obtained as:

$$K_r = \frac{K_{diff}}{G_m} \qquad (39)$$

here $K_{diff} = 0.5\, \gamma_s\, K_{ETh}$

γ_s is the attenuation of the solar beam due to scattering by water vapor and permanent atmospheric constituents. Adding the effect of dust yields

$$\gamma_s = 1 - \tau_s + \gamma_{dust} \qquad (40)$$

The value of γ_{dust} was estimated as 0.03 for remote station according to Bolsenga (1964). τ_s can be calculated as:

$$\tau_s = \exp(a_s + b_s . M_{opt}) \qquad (41)$$

where M_{opt} is the average daily optical air mass. M_{opt} was calculated using a chart by Bolsenga (1964) based on latitude and declination angle. a_s and b_s are calculated based on precipitable water content (W_p).

$$a_s = -0.0363 - 0.0084\, W_p \qquad (42)$$

$$b_s = -0.0572 - 0.0173\, W_p \qquad (43)$$

W_p is calculated from the empirical relation (Bolsenga, 1964):

$$W_p = 1.12 \exp(0.0614\, T_d) \qquad (44)$$

Here T_d is the surface dew point in ^{o}C and W_p is in cm. T_d is calculated from relative humidity (RH) and vapor pressure (e) as:

$$T_d = \frac{\ln(e)+0.4926}{0.0708-0.00421\ln(e)} \qquad (45)$$

$$RH = \frac{e}{e^*} \qquad (46)$$

e^* is the saturation vapor pressure. It can be calculated from temperature (T) ^{o}C.

$$e^* = 0.611 \exp\left(\frac{17.3\,T}{T+237.3}\right) \qquad (47)$$

The instantaneous direct radiation on a horizontal plane K_{ETh} was calculated following Iqbal (1983) as:

$$K_{ETh} = I_{SC}.E_o[\cos(\delta).\cos(\Lambda).\cos(\omega.t_d) + \sin(\delta).\sin(\Lambda)] \qquad (48)$$

where I_{SC}=1367 W/m^2 is the average radiation flux on a plane perpendicular to the solar beam in the upper atmosphere; E_o is an eccentricity correction factor that accounts for changes in the relative distance between the sun and the earth, calculated daily from day angle (Γ).

$$E_o = 1.00011 + 0.034221.\cos(\Gamma) + 0.00128.\sin(\Gamma) + 0.000719.\cos(2.\Gamma) + 0.000077.\sin(2.\Gamma) \qquad (49)$$

The numerical models for water balance simulation were developed with the meteorological data from January 2012 to April 2014. During this period of time soil moisture measurements were taken at regular intervals to be used for validation of the

models with predicted soil moisture. For the water balance models, we converted the incoming solar radiation data for the southern aspect, because both well-vegetated site and moderately-vegetated site are facing south.

Leaf Area Index (LAI) for calculation of potential evapotranspiration was determined from Surface Cover Fraction (SCF) (Simunek et al., 2013).

$$LAI = -\frac{1}{a_i}\ln(1 - SCF) \qquad (50)$$

Here a_i is the constant for the radiation extinction by canopy (=0.463). The SCF was used as 0.11 for moderately-vegetated site and 0.25 for well-vegetated site as determined from vegetation study at the site (Powell, unpublished data).

6 WATER BALANCE SIMULATION RESULTS

HYDRUS 1D simulations were conducted from the beginning of year 2012 to April 2014 with meteorological data of the corresponding year. During this period of time TDR measurements were taken at several locations of well-vegetated site and moderately-vegetated site which provided cumulative average water contents over depths of 7.5 cm and 20 cm. The measured water contents on a watershed exhibit variability that could be due to local differences in soil properties, proximity to plants, surface characteristics, or other factors. Cumulative average water contents for the depth of 7.5 cm and 20 cm were also simulated by HYDRUS 1D. Figure 12 and 13 show the observed and simulated values for well-vegetated site and moderately-vegetated site respectively. Average water contents over the depths of 7.5 cm and 20 cm were higher for moderately-vegetated site than for well-vegetated site. This may be due to the difference in vegetation condition between the two sites. The existence of higher vegetation coverage at well-vegetated site causes the increase in root water uptake and lowers the water content in soil.

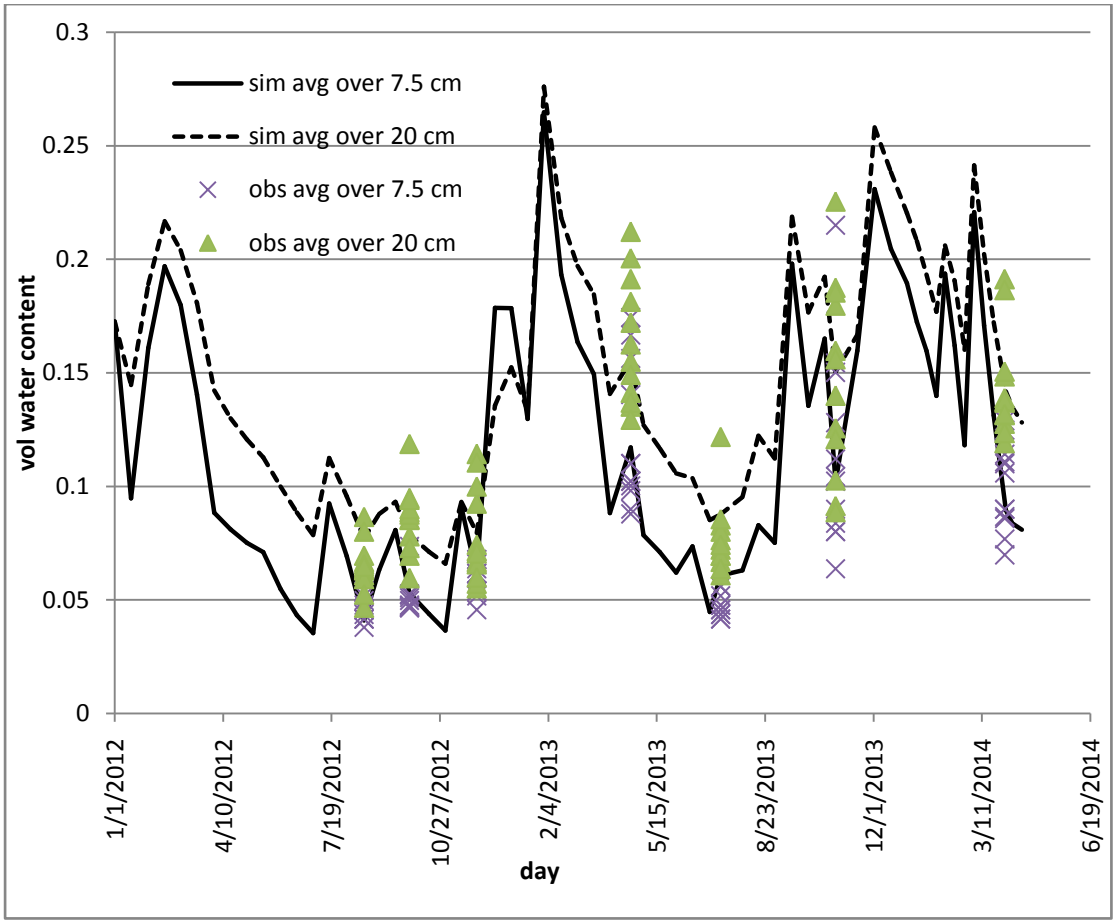

Fig. 12: Comparison of observed volumetric water content with HYDRUS 1D simulated water content from January 2012 to April 2014 at well-vegetated site for non-uniform topdressing

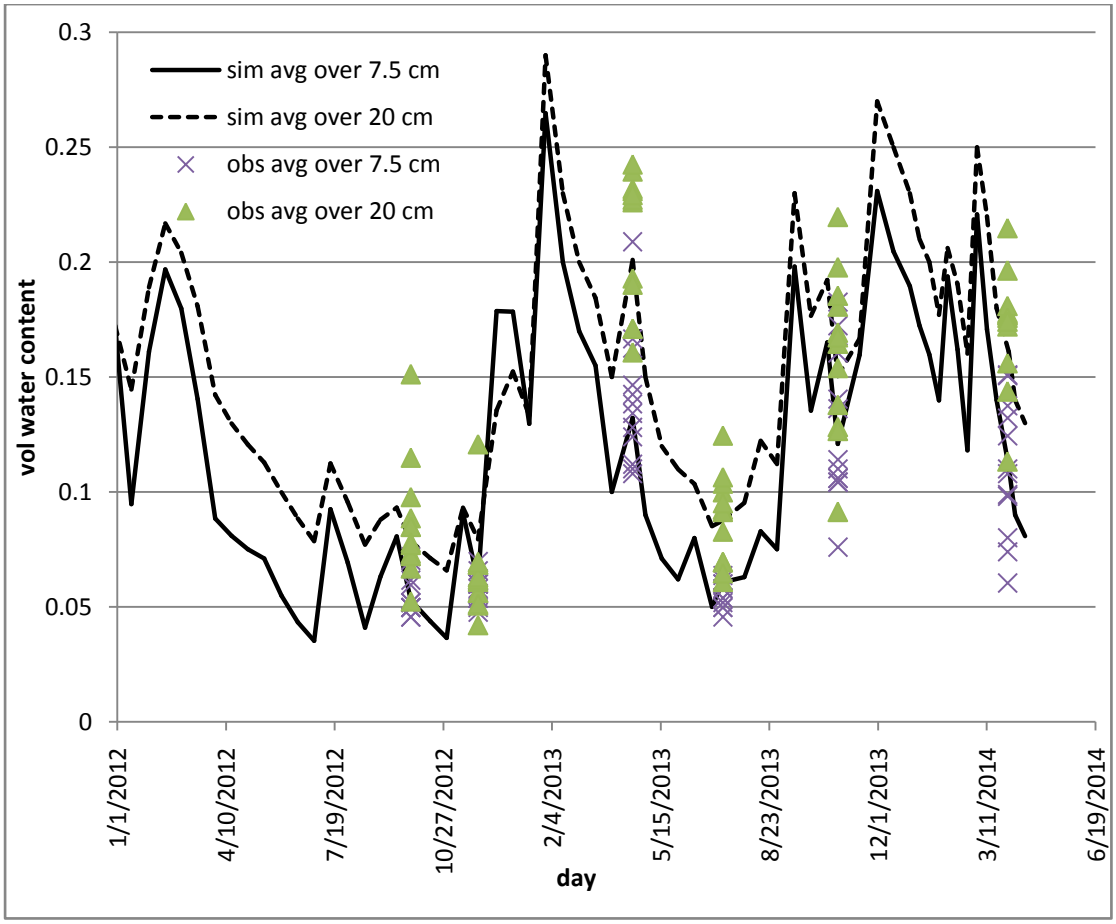

Fig. 13: Comparison of observed volumetric water content with HYDRUS 1D simulated water content from January 2012 to April 2014 at moderately-vegetated site for non-uniform topdressing

A hypothesis test was conducted to compare the simulated average moisture contents and observed average moisture contents over 7.5 cm depth and 20 cm depth. For normal distribution of observed values a two sided hypothesis test was conducted to check whether the mean of observed value was equal to the simulated value at measurement period. Test statistics, t_s was calculated as:

$$t_s = \frac{\hat{Y} - \mu_o}{SE_{\hat{Y}}} \qquad (51)$$

here $\hat{Y}$ is the mean of the observed values, μ_o is the hypothesized value which is the simulated value, and $SE_{\hat{Y}}$ is the standard error calculated as $s/\sqrt{n}$. Here s is the sample standard deviation and n is the number of sample. The value of t_s was compared with t_{crit} for 95% confidence level to determine whether the hypothesis is valid or not. t_{crit} is determined from statistical probability curve for sample size and confidence interval. The hypothesis is rejected when $|t_s| > t_{crit}$ or the measure of

plausibility p-value as determined by the R program is less than 0.05 at 95% confidence level. Two sample t-test was conducted for 12 observed cumulative average water content values at each day. For 12 samples the t_{crit} at 95% confidence level is 2.2.

Table 17: Comparison between observed average water content and simulated water content over 7.5 cm depth at well-vegetated site for non-uniform topdressing

Date	Observed mean value	Simulated result	Difference	t_s	p-value
8/17/2012	0.046	0.044	0.0027	1.79	0.101
9/27/2012	0.051	0.055	0.0035	-1.64	0.129
11/28/2012	0.059	0.063	0.0038	-1.88	0.087
4/19/2013	0.120	0.119	0.0005	0.05	0.957
7/11/2013	0.048	0.063	0.0148	-9.28	1.55E-06
10/25/2013	0.114	0.099	0.0147	1.20	0.257
3/31/2014	0.100	0.090	0.0099	1.81	0.098

Table 18: Comparison between observed average water content and simulated water content over 20 cm depth at well-vegetated site for non-uniform topdressing

Date	Observed mean value	Simulated result	Difference	t_s	p-value
8/17/2012	0.065	0.077	0.0121	-3.91	0.002
9/27/2012	0.085	0.079	0.0067	1.57	0.146
11/28/2012	0.078	0.079	0.0012	-0.21	0.839
4/19/2013	0.164	0.155	0.0085	1.07	0.306
7/11/2013	0.077	0.088	0.0107	-2.31	0.041
10/25/2013	0.147	0.150	0.0036	-0.29	0.778
3/31/2014	0.144	0.142	0.0018	0.28	0.787

Table 19: Comparison between observed average water content and simulated water content over 7.5 cm depth at moderately-vegetated site for non-uniform topdressing

Date	Observed mean value	Simulated result	Difference	t_s	p-value
9/27/2012	0.055	0.053	0.0019	0.72	0.484
11/28/2012	0.057	0.061	0.0035	-1.93	0.080
4/19/2013	0.140	0.132	0.0080	0.96	0.356
7/11/2013	0.056	0.061	0.0052	-3.23	8.05E-03
10/25/2013	0.126	0.121	0.0051	0.55	0.596
3/31/2014	0.110	0.111	0.0005	-0.06	0.953

Table 20: Comparison between observed average water content and simulated water content over 20 cm depth at moderately-vegetated site for non-uniform topdressing

Date	Observed mean value	Simulated result	Difference	t_s	p-value
9/27/2012	0.087	0.079	0.0082	1.11	0.292
11/28/2012	0.064	0.079	0.0153	-2.70	0.021
4/19/2013	0.209	0.201	0.0085	0.98	0.349
7/11/2013	0.088	0.088	0.0008	0.14	0.892
10/25/2013	0.160	0.150	0.0098	0.96	0.357
3/31/2014	0.172	0.161	0.0106	1.45	0.176

Soil moisture simulations were also conducted for two study sites considering uniform density and hydraulic properties at the topdressing found from laboratory experiments of undisturbed samples. Average cumulative water content for 7.5 cm and 20 cm depth were compared with measured values at different times of the study period. The results are presented graphically in Fig. 14 and 15 for well-vegetated site and moderately-vegetated site respectively.

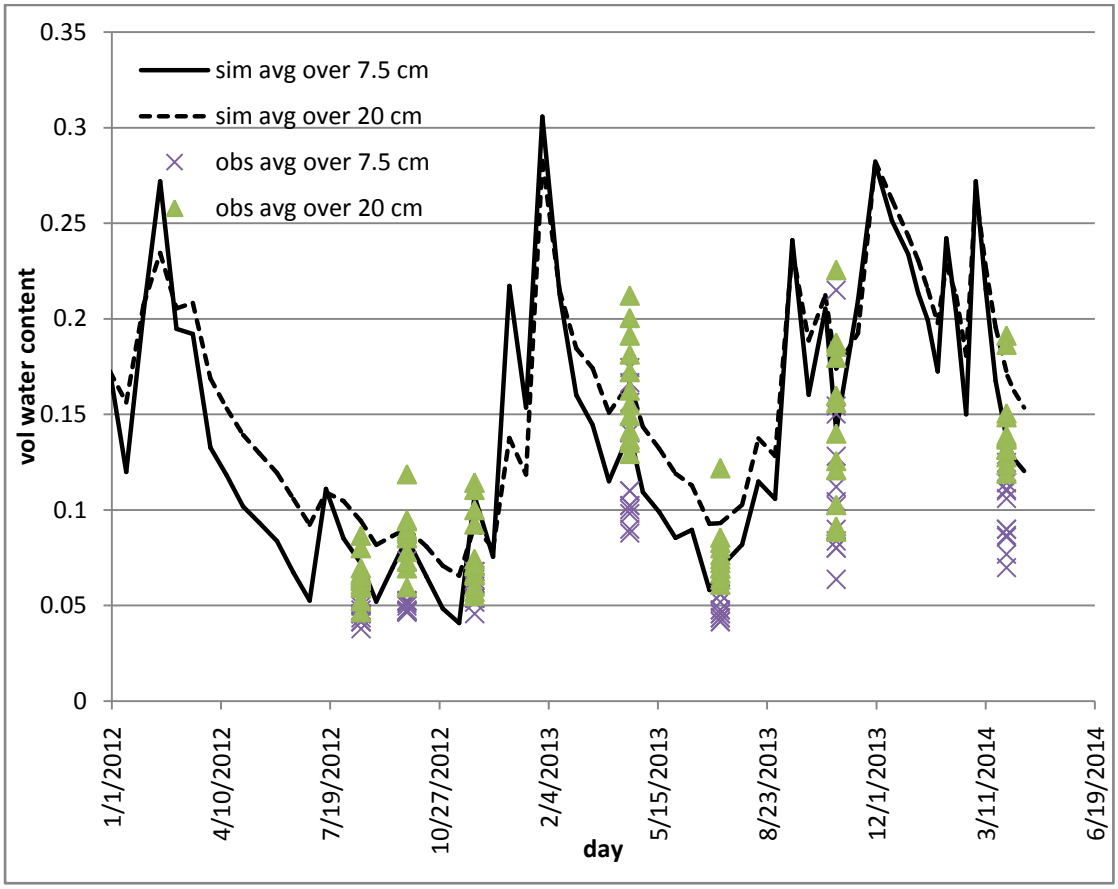

Fig. 14: Comparison of observed volumetric water content with HYDRUS 1D simulated water content from January 2012 to April 2014 at well-vegetated site for uniform topdressing

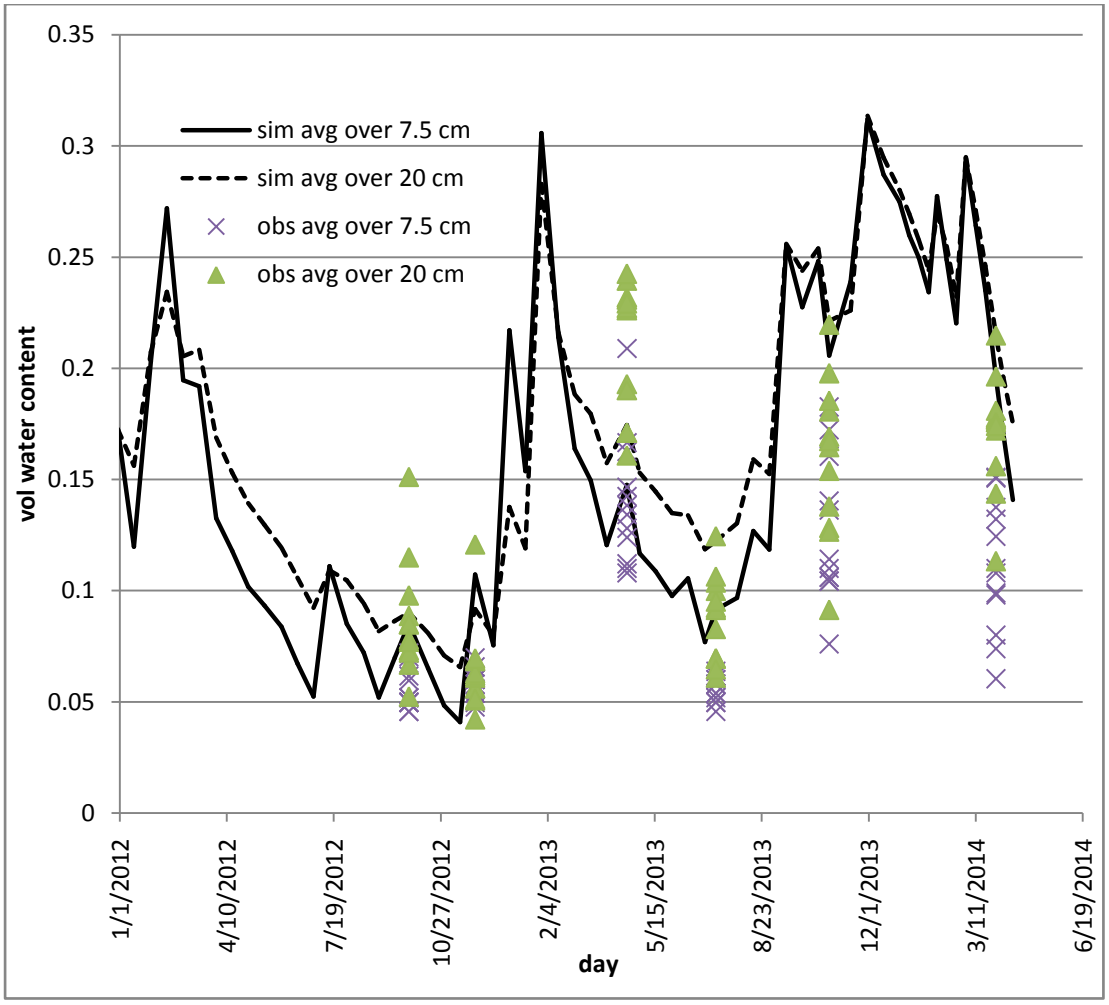

Fig. 15: Comparison of observed volumetric water content with HYDRUS 1D simulated water content from January 2012 to April 2014 at moderately-vegetated site for uniform topdressing

Statistical analyses were conducted to compare the observed and simulated water content for uniform topdressing soil. The results are shown in Table 21, 22, 23 and 24.

Table 21: Comparison between observed average water content and simulated water content over 7.5 cm depth at well-vegetated site for uniform topdressing

Date	Observed mean value	Simulated result	Difference	t_s	p-value
8/17/2012	0.046	0.052	0.006	-3.77	0.003
9/27/2012	0.051	0.065	0.014	-6.49	4.48E-05
11/28/2012	0.059	0.076	0.017	-8.13	5.6E-06
4/19/2013	0.120	0.14	0.02	-2.3	0.042
7/11/2013	0.048	0.07	0.022	-13.68	3.01E-08
10/25/2013	0.114	0.141	0.027	-2.26	0.04
3/31/2014	0.100	0.135	0.035	-6.46	4.697E-05

Table 22: Comparison between observed average water content and simulated water content over 20 cm depth at well-vegetated site for uniform topdressing

Date	Observed mean value	Simulated result	Difference	t_s	p-value
8/17/2012	0.065	0.082	0.017	-5.42	2E-04
9/27/2012	0.085	0.081	0.004	1.057	0.313
11/28/2012	0.078	0.08	0.002	-0.277	0.784
4/19/2013	0.164	0.166	0.002	-0.323	0.323
7/11/2013	0.077	0.093	0.016	-3.51	0.005
10/25/2013	0.147	0.174	0.027	-2.17	0.05
3/31/2014	0.144	0.17	0.026	-3.98	0.002

Table 23: Comparison between observed average water content and simulated water content over 7.5 cm depth at moderately-vegetated site for uniform topdressing

Date	Observed mean value	Simulated result	Difference	t_s	p-value
9/27/2012	0.055	0.065	0.01	-3.98	0.002
11/28/2012	0.057	0.076	0.019	-9.95	7.78E-07
4/19/2013	0.140	0.148	0.008	-0.89	0.393
7/11/2013	0.056	0.091	0.035	-22.37	1.61E-10
10/25/2013	0.126	0.206	0.08	-8.54	3.48E-06
3/31/2014	0.110	0.192	0.082	-9.56	1.16E-06

Table 24: Comparison between observed average water content and simulated water content over 20 cm depth at moderately-vegetated site for uniform topdressing

Date	Observed mean value	Simulated result	Difference	t_s	p-value
9/27/2012	0.087	0.081	0.006	0.811	0.435
11/28/2012	0.064	0.08	0.016	-2.77	0.018
4/19/2013	0.209	0.175	0.034	4.04	0.002
7/11/2013	0.088	0.122	0.034	-6.05	8.27E-05
10/25/2013	0.160	0.2213	0.0613	-6.02	8.63E-05
3/31/2014	0.172	0.212	0.04	-5.52	1.8E-04

7 WATER BALANCE SIMULATION DISCUSSIONS

Statistical analyses on the results of numerical water balance simulation with varying properties of topdressing and measured values show that the model developed by HYDRUS 1D is consistent in representing the existing natural condition. Cumulative

average water contents over the depth of 7.5 cm and 20 cm were taken as parameters for evaluating the numerical model. For well-vegetated site simulated values are similar to the observed values at 95% confidence level for all data collection days except for July 11, 2013. A small deviation from measured value to simulated value was also observed for 20 cm depth on August 17, 2012. In case of moderately-vegetated site water content measured over 7.5 cm on July 11, 2013 differed from the simulated value at 95% confidence level. For all other points of comparison the measured values are consistent with the simulated values.

Graphical and statistical comparison of simulated and measured water content for HYDRUS 1D model with uniform topdressing shows that predicted water content is always higher than the measured water content. In these simulations, results from laboratory tests of undisturbed samples were used to define hydraulic properties of the surface soil layer. Consequently, the hydraulic properties of the very top loose surface were ignored. The lower hydraulic conductivity at the top surface decreases the soil moisture removal by evaporation and increases the soil water content. Soil water modeling based on uniform hydraulic properties at the topdressing fails to simulate actual soil water balance condition.

For most of the data measurement periods and depths, model with uniform topdressing has better prediction in terms of two sample t-test. The distribution of observed values at a particular period and depth was compared with a single water content value predicted by HYDRUS.

The p-value as calculated by the R program shows the result of statistical analysis for 95% confidence level. When the p-value is more than 0.05 then the hypothesis of equality between the predicted and the average of the observed water content is valid for 95% confidence level. Table 17, 18, 19, 20 present the results of statistical analyses for non-uniform topdressing soil. The results show that for most of the data measurement periods and depths, the p-values are more than 0.05. Table 21, 22, 23, 24 present the results of statistical analyses for uniform topdressing soil. For most of the data measurement periods and depths, the results show that the p-values are less than 0.05. The statistical analyses indicate that, the model with non-uniform topdressing has higher prediction accuracy than the model with uniform topdressing. The numerical model with non-uniform topdressing is able to predict the soil water

contents which are closer to the averages of the observed water contents at different locations. The uniform depths of various soil layers and uniform vegetation coverage over the land limit the model in predicting the variation in near surface water contents.

8 DEVELOPMENT OF GERMINATION MODELING

A population based hydrothermal time model was used to observe the seed's response to environmental condition available at the soil surface. The HYDRUS 1D model was used to simulate water and thermal flow through the reclaimed mine soil including blue grama grass as the simulated vegetation. An observation node was placed at 2 cm depth to get the results of temperature and water potential of soil. The observation node was placed at 2 cm depth because seed germination potential depends on the soil condition at 1-3 cm depth (Roundy, et al., 2007). The germination potential was estimated in terms of progress towards germination (PTG) for 50% of seeds of a species (Rawlins et al., 2012).

Time to germination was calculated from hydrothermal time equation with the input of hourly temperature and water potential as simulated by HYDRUS 1D. The hydrothermal time constant for germination of cheatgrass from 50% of total population was determined by Bauer et al. (1998). For a threshold temperature of 0°C and threshold water potential of -1.15 MPa, the hydrothermal time constant was 43 MPa-degree-days for any incubation temperature. Meyer et al. (2000) determined the hydrothermal time constant for 50% germination bottlebrush squirreltail (*Elymus elymoides*). The hydrothermal time constant was determined to be 108.3 MPa-degree-days. The threshold water potential was -1.41 MPa when the incubation temperature was 20°C and -0.88 MPa when the incubation temperature was 30°C. The threshold temperature was considered as 0°C.

To estimate hourly PTG, the rate of germination or inverse of germination time in days was divided by 24 (Rawlins et al., 2012). The hydrothermal time model sums PTG only for hours when the soil water potential and temperature is above given

threshold values. Cumulative PTG was calculated for each month as a convenient means to evaluate the PTG over the course of a year.

One wet and one dry climate conditions were selected to determine germination potential of bottlebrush squirrelatil and cheatgrass. The climate conditions were selected from 20 year weather data of the study area. Year 2005 was selected as wet climate condition with total precipitation of 35 cm and year 2012 was selected as dry climate condition with total precipitation of 14 cm. The total precipitation of 2005 used as the wet climate is similar to the record annual precipitation in nearby Farmington, NM recorded in 1957. The lowest recorded annual precipitation in Farmington, NM was 10 cm in 1956. The hourly precipitation data for the selected years are plotted in Fig. 16. Temperature and water potential results from HYDRUS 1D model were taken for both climate conditions to determine the PTG. The germination potentials were also determined for Northern and Southern aspect of each climate condition. Four HYDRUS 1D models were created with different climate and aspect conditions to determine germination potential of bottlebrush squirreltail and cheatgrass. PTG for cheatgrass was calculated only for the first six months considering it as a winter annual species. Table 25 shows the different climate and aspect conditions for which germination potential was determined.

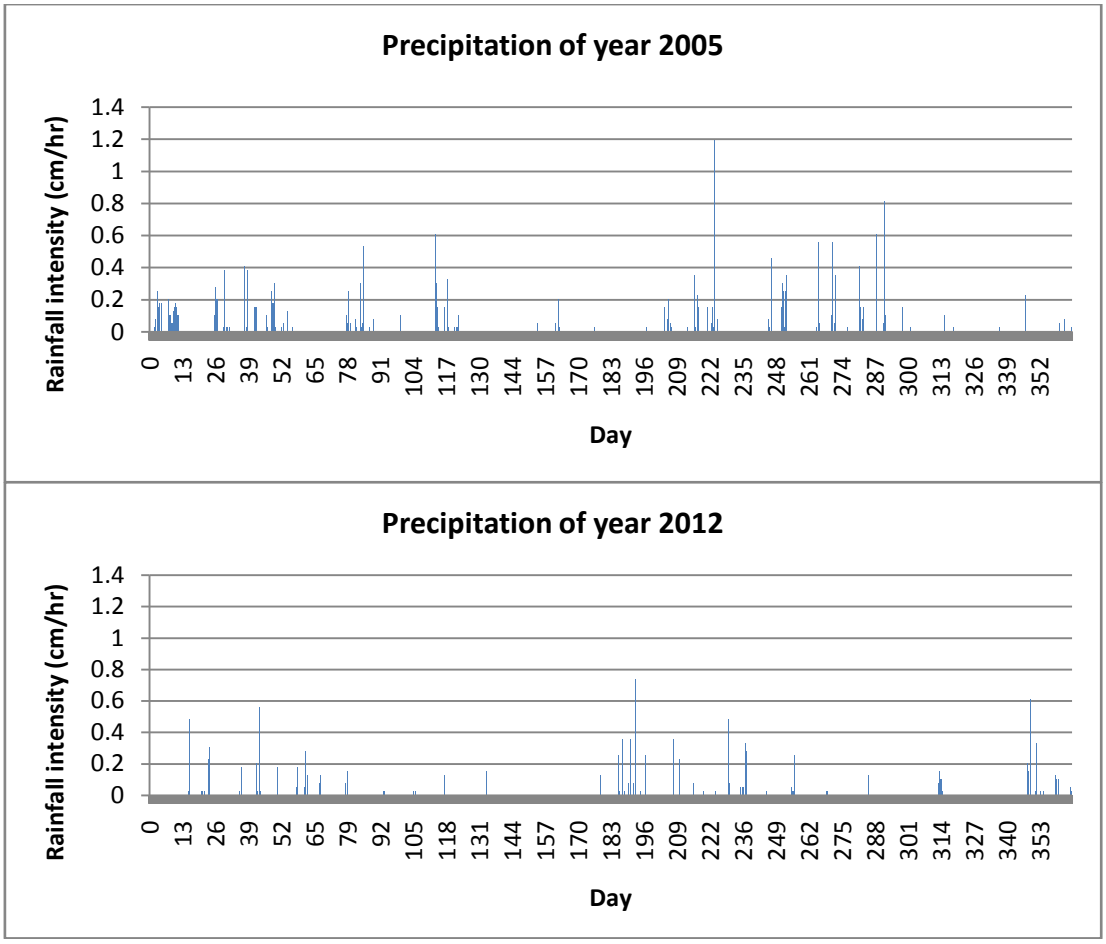

Fig. 16: Precipitation for year 2005 and 2012

Table 25: Different climate and aspect conditions for determining germination potential of bottlebrush squirreltail and cheatgrass

Existing vegetation	Climate condition	Slope aspect
Blue grama	Wet climate (Year 2005)	North
	Wet climate (Year 2005)	South
	Dry climate (Year 2012)	North
	Dry climate (Year 2012)	South

The HYDRUS 1D model was used to estimate availability of water potential at different depths of soil to determine the ability of existing blue grama grass and cheatgrass to survive. Four observation nodes were set to provide water potentials at 5, 10, 20 and 40 cm depth from the soil surface. The water potentials at these locations were compared with the wilting point of respective plants to determine whether the condition is favorable for survival or not. Eight HYDRUS 1D models were created with different climate, aspect and vegetation conditions (Table 26). Blue grama grass was used to model a perennial species (phenology based on C_4 grass) and

cheatgrass as a winter annual species (phenology based on C_3 grass) which dies during summer.

C_3 and C_4 plants have different photosynthetic pathways. In C_3 plants, carbon dioxide is taken out of the atmosphere by the enzyme Rubisco. Rubisco also has an affinity for oxygen, and when oxygen is fixed instead of carbon dioxide (photorespiration), photosynthetic efficiency decreases because carbon is released rather than fixed in plant tissues. Photorespiration increases, and thus, photosynthetic efficiency of C_3 plants decreases, as temperature increases. The problem of photorespiration is overcome in C_4 plants which use the enzyme PEP Carboxylase that has no affinity for oxygen, to take carbon dioxide out of the atmosphere. The carbon dioxide fixed is then shunted to bundle sheath cells that are impermeable to gas diffusion. As a result, C_4 plants not only eliminate photorespiration, but also don't need to open their stomates as often as C3 plants. C_4 plants are more water efficient and can survive in hot dry weather (Furbank et al., 1995).

Table 26: Different climate, aspect and vegetation conditions for determining plant survival

Vegetation	Climate condition	Slope aspect
Blue grama	Wet climate (Year 2005)	North
	Wet climate (Year 2005)	South
	Dry climate (Year 2012)	North
	Dry climate (Year 2012)	South
Cheatgrass	Wet climate (Year 2005)	North
	Wet climate (Year 2005)	South
	Dry climate (Year 2012)	North
	Dry climate (Year 2012)	South

9 RESULTS ON GERMINATION AND PLANT SURVIVAL

9.1 Germination Potential

Progress toward germination (PTG) of the 50% seed subpopulations were estimated for bottlebrush squirreltail and cheatgrass. PTG was calculated every hour as a function of both temperature and soil water potential. Conditions are considered favorable for germination when the cumulative PTG value reaches 1. PTG values of

the two plants were calculated for climate conditions similar to year 2005 and 2012 with blue grama grass as existing vegetation. We compared aspect influence on the PTG for the two climate conditions. Figure 17 shows the effect of climate condition and slope aspect on the germination potential of bottlebrush squirreltail and cheatgrass. The germination potential of cheatgrass is higher than the germination potential of bottlebrush squirreltail at any month. This is because the hydrothermal time constant required for germination of bottlebrush squirreltail is higher than that of cheatgrass.

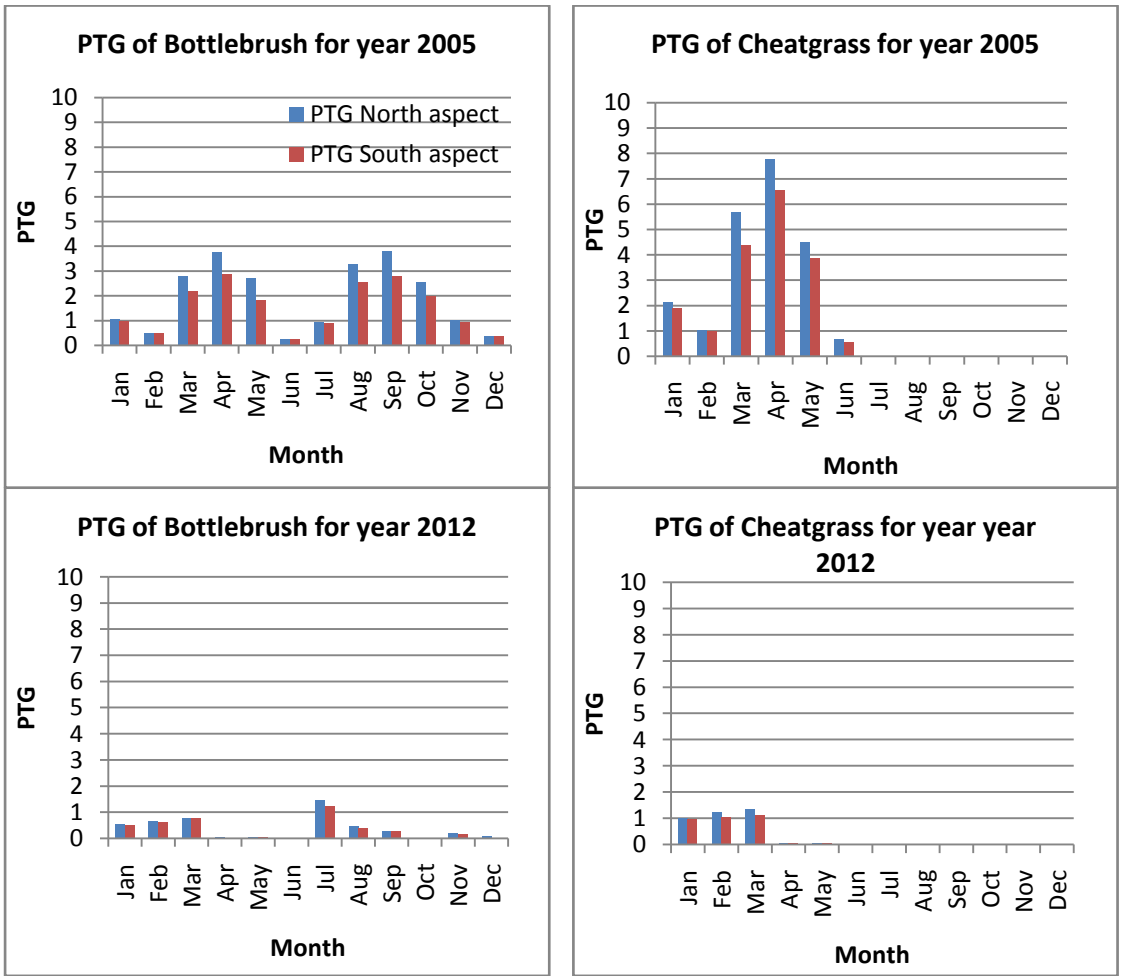

Fig. 17: PTG for bottlebrush squirreltail and cheatgrass for different slope aspects and climate conditions

For the climate condition similar to 2012 the PTG values are lower than the PTG values of year 2005 for any month. The intensity and distribution of rainfall events in 2005 contributed to the creation of favorable condition for germination of the two plants. During 2005 the conditions appear more favorable for germination of bottlebrush squirreltail for the months of March, April, May, August, September, and

October than other months of the year. Cheatgrass has more favorable conditions for germination during January, March, April, and May than February and June for all aspects. Bottlebrish squirreltail has less favorable condition for germination in dry climate conditions than wet climate conditions in all aspects. Cheatgrass has approximately the same conditions for germination during the first three months of the dry climate conditions similar to 2012.

The Northern aspect has a somewhat higher germination potential than the Southern aspect for any month in terms of PTG. We compared matric potentials and temperatures at 2 cm depth for different aspects and climate conditions. Figure 18 shows the daily average matric potentials at two different aspects and climate conditions. From Fig. 18 it is observed that the Southern aspect has lower matric potential than the Northern aspect at any day of the year. Lower matric potential in the Southern aspect decreases the chances of germination in terms of PTG.

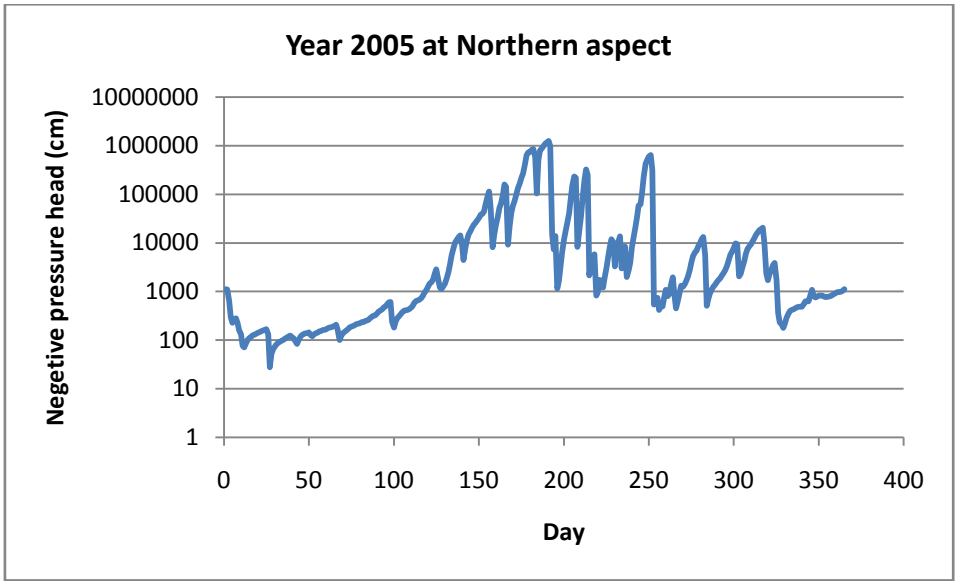

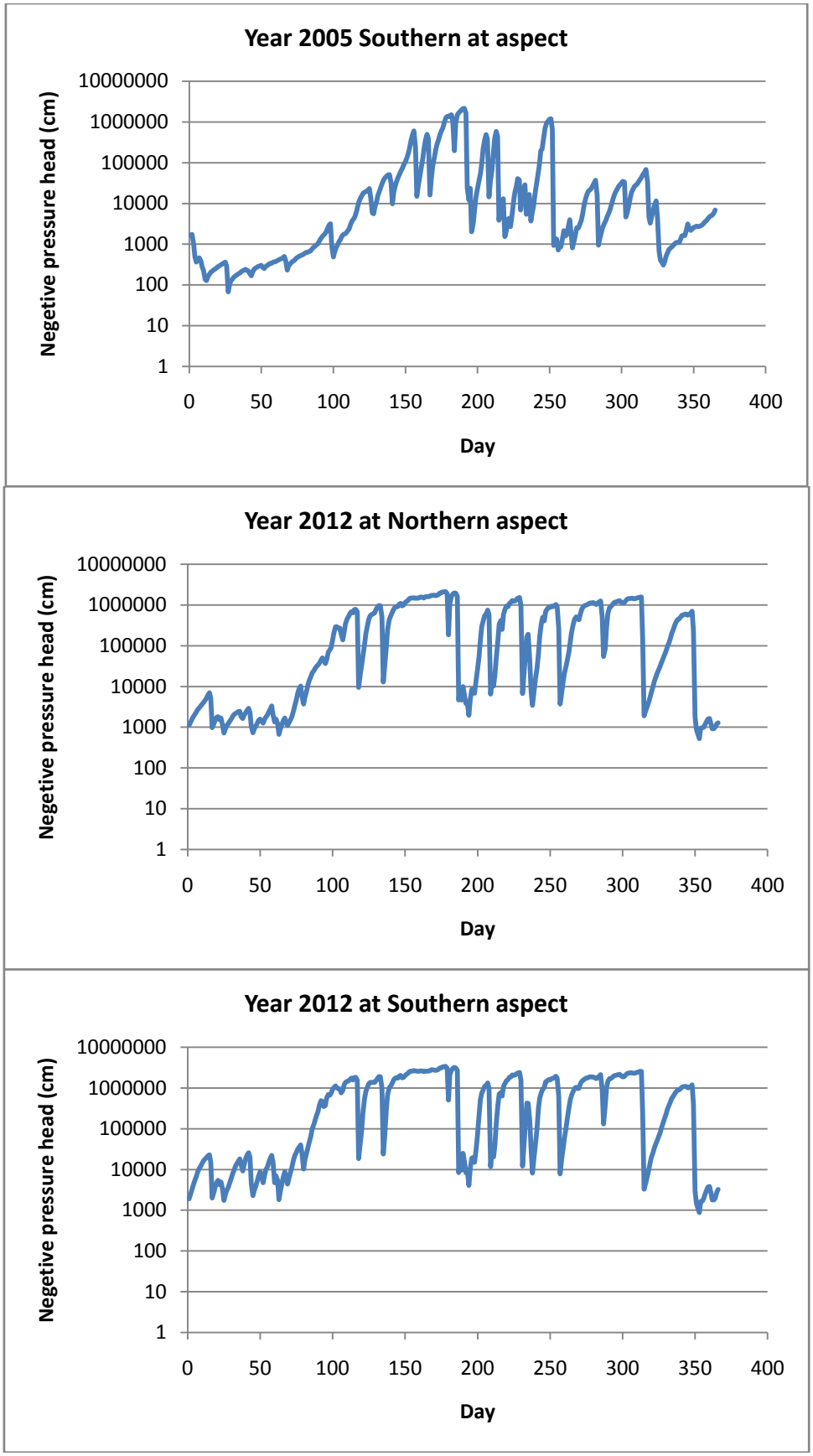

Fig. 18: Matric potential at 2 cm depth from surface for different aspects and climate conditions

The variation of soil matric potential for different aspects is due to the fact that Southern aspect gets more incoming solar radiation than the Northern aspect. Figure 19 shows the incoming solar radiation at Northern and Southern aspects for the climate conditions of year 2005 and 2012. Higher solar radiation increases the potential evapotranspiration from the soil surface. A study by Gutierrez et al., (2013) shows that north facing slopes have higher moisture holding capacity than the south facing slopes as a result of differing solar radiation.

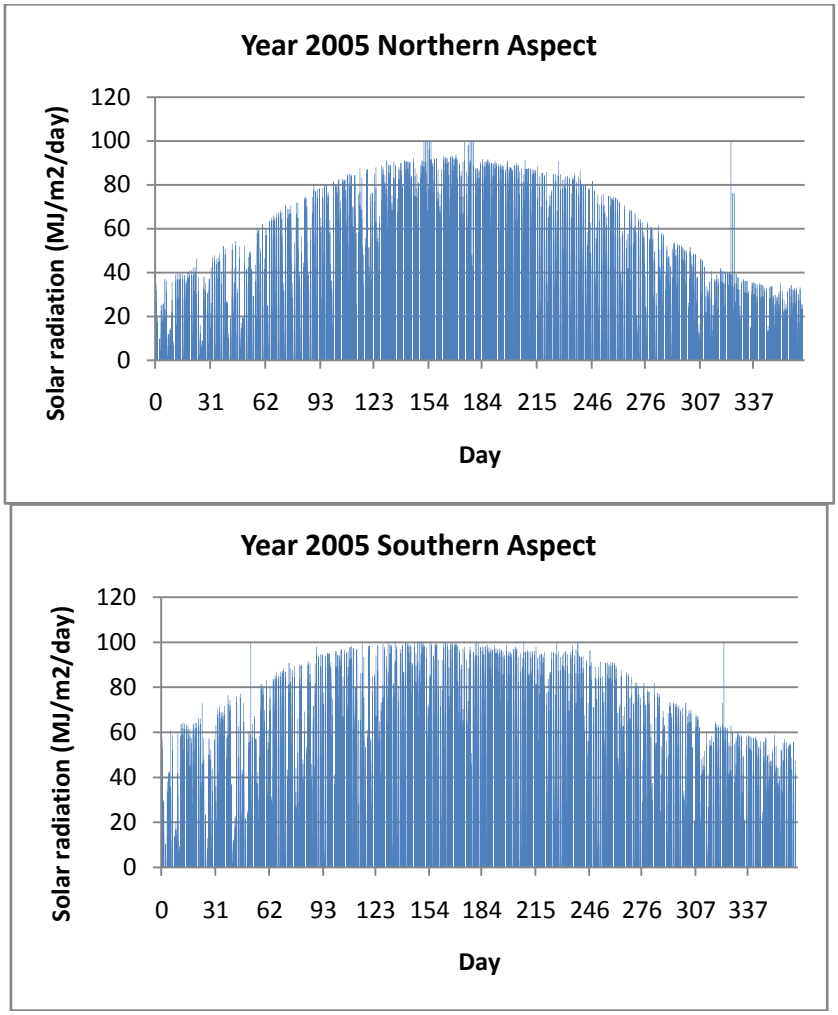

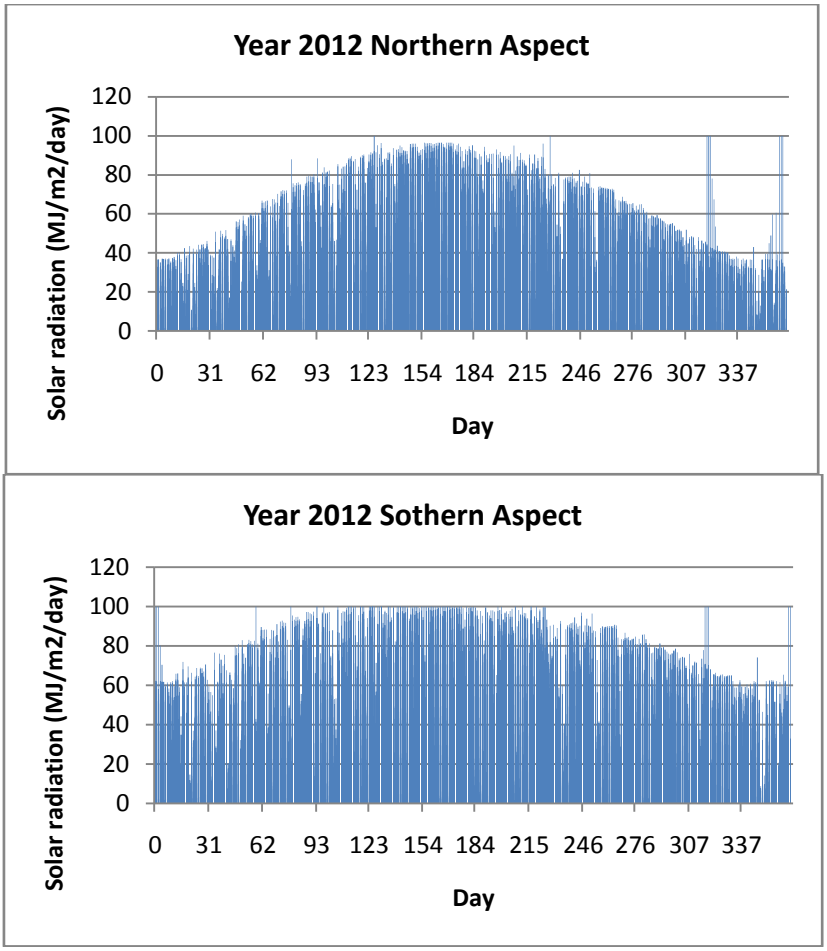

Fig. 19: Incoming solar radiation at Northern and Southern aspects for the climate conditions of year 2005 and 2012

The variation of temperature at 2 cm depth for different aspects is not significant. We used common air temperature as boundary conditions for simulation of subsurface soil temperature for north and south aspects. This accounts for the very similar subsurface temperatures for both aspects in same climate conditions. We compared the temperature difference for two different climate conditions. Figure 20 shows the daily maximum and minimum temperature for year 2005 and 2012 at the depth of 2 cm from surface. The plots show that for both years the temperature goes below 0° C during the months of January, February, March and December. Temperature lower than the 0° C stops the germination process and reduces the PTG value.

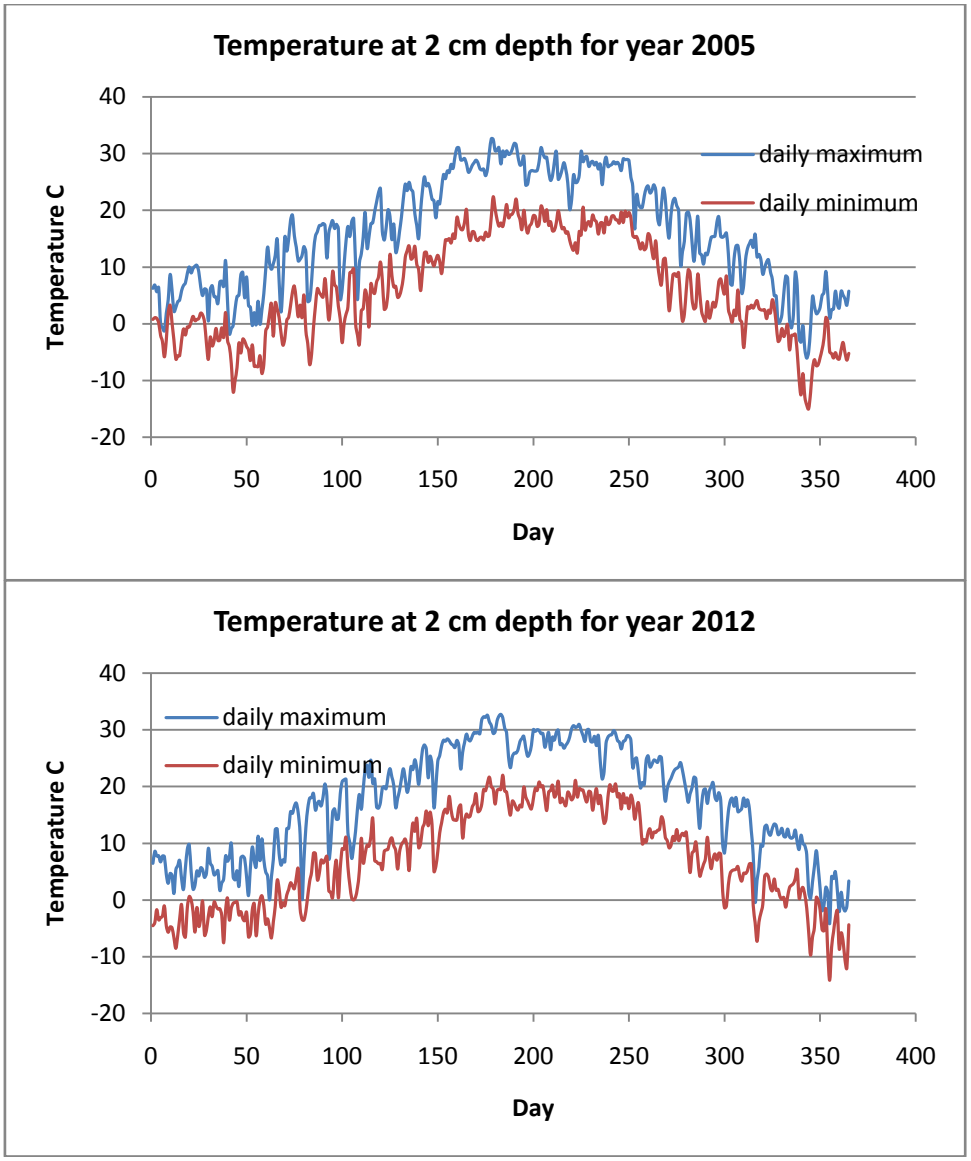

Fig. 20: Temperature of soil at 2 cm depth for two different climate conditions.

9.2 Plant Survival

If the matric potential of soil water goes below the wilting point then the plants are no longer able to extract water from soil. The ability of existing plants to survive at different climate conditions and slope aspects were determined by comparing the soil matric potential with wilting point at different times of the year. The wilting point for blue grama grass is -90000 cm where the wilting point of cheatgrass is -9100 cm. Observation nodes were set at 5, 10, 20 and 40 cm depth from soil surface to see the variation of soil water potential. Blue grama grass has the root length of 40 cm where the cheatgrass has root length of 30 cm. Figure 21 shows the soil water potential for different climate conditions and aspects for blue grama grass and cheatgrass. The solid black lines in Fig. 21 represent the wilting points for corresponding plants.

The results show that for blue grama grass in the Northern aspect of year 2005, the root zone stays above wilting point (in terms of negative pressure head). For the Southern aspect the 5 cm depth zone crosses the wilting point at the beginning of July only for couple of days. So the wet climate condition similar to 2005 provides favorable condition for root water uptake by blue grama grass throughout the year in all aspects. In case of cheatgrass the root zone from 10 cm depth and below stays above wilting point throughout its growing season in the Northern aspect. At the Southern aspect the matric potential at 5 cm depth stays below wilting point most of the days from beginning of May. For root zones below 5 cm depth the matric potential stays above wilting point. At the Southern aspect with climate condition similar to 2005 the cheatgrass is expected to survive during its growing season.

We observed the matric potential at different depths for the dry climate condition similar to 2012. Most of the root zone of blue grama grass at the Northern aspect stays above wilting point. The root zone at 5 cm depth crosses the wilting point during the months of May, June and October. At the Southern aspect the matric potential drops below the wilting point for whole root zone of blue grama grass during the month of July. Matric potential available for root water uptake drops below the wilting point in most of the days from August to November in 2012. The condition remains favorable for root water uptake by blue grama only at 10 cm depth during that period. At the Northen aspect of 2012 climate condition the root zone above 20 cm depth goes below the wilting point from May for cheatgrass. Water potential at 20 cm depth stays below wilting point for growth period of cheatgrass. At the Southern aspect of climate condition similar to 2012 provides a harsh condition for survival of cheatgrass. The whole root zone goes below the wilting point from the middle of April.

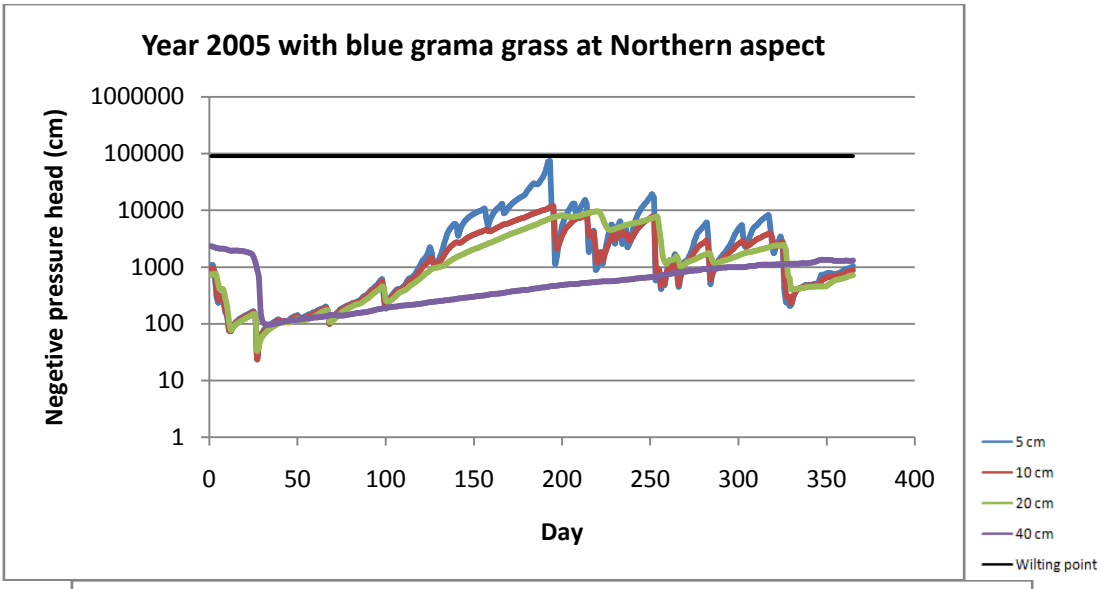
Year 2005 with blue grama grass at Northern aspect
Negetive pressure head (cm)
1000000
100000
10000
1000
100
10
1
0
50
100
150
200
250
300
350
400
Day
5 cm
10 cm
20 cm
40 cm
Wilting point

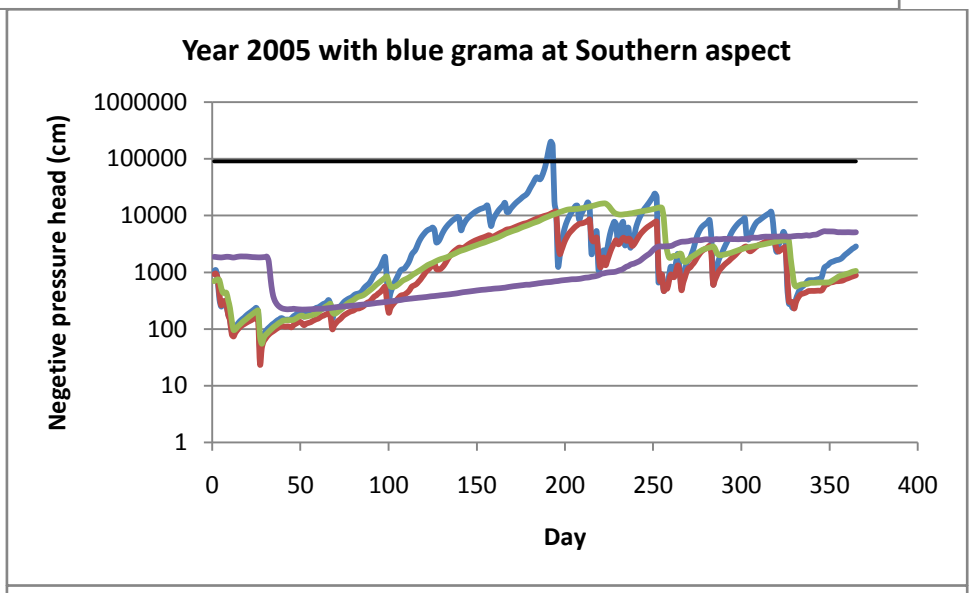
Year 2005 with blue grama at Southern aspect
Negetive pressure head (cm)
1000000
100000
10000
1000
100
10
1
0
50
100
150
200
250
300
350
400
Day

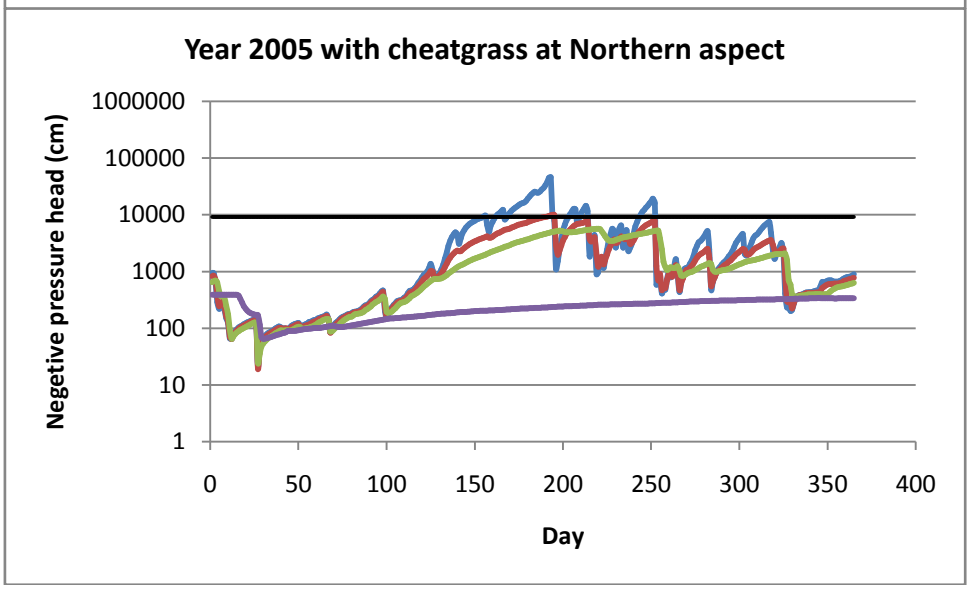
Year 2005 with cheatgrass at Northern aspect
Negetive pressure head (cm)
1000000
100000
10000
1000
100
10
1
0
50
100
150
200
250
300
350
400
Day

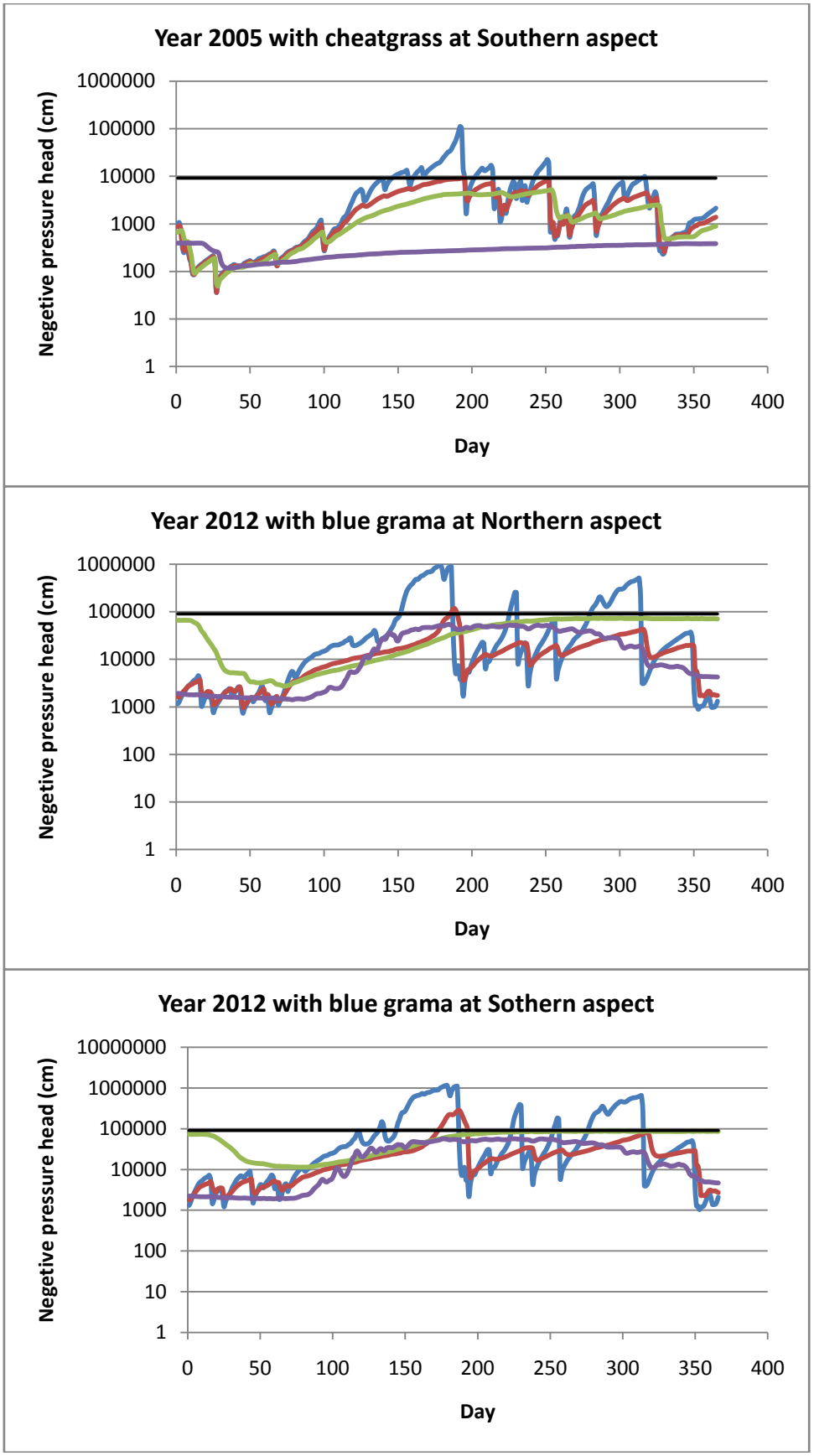
Year 2005 with cheatgrass at Southern aspect
Negetive pressure head (cm)
1000000
100000
10000
1000
100
10
1
0
50
100
150
200
250
300
350
400
Day
Year 2012 with blue grama at Northern aspect
Negetive pressure head (cm)
1000000
100000
10000
1000
100
10
1
0
50
100
150
200
250
300
350
400
Day
Year 2012 with blue grama at Sothern aspect
Negetive pressure head (cm)
10000000
1000000
100000
10000
1000
100
10
1
0
50
100
150
200
250
300
350
400
Day

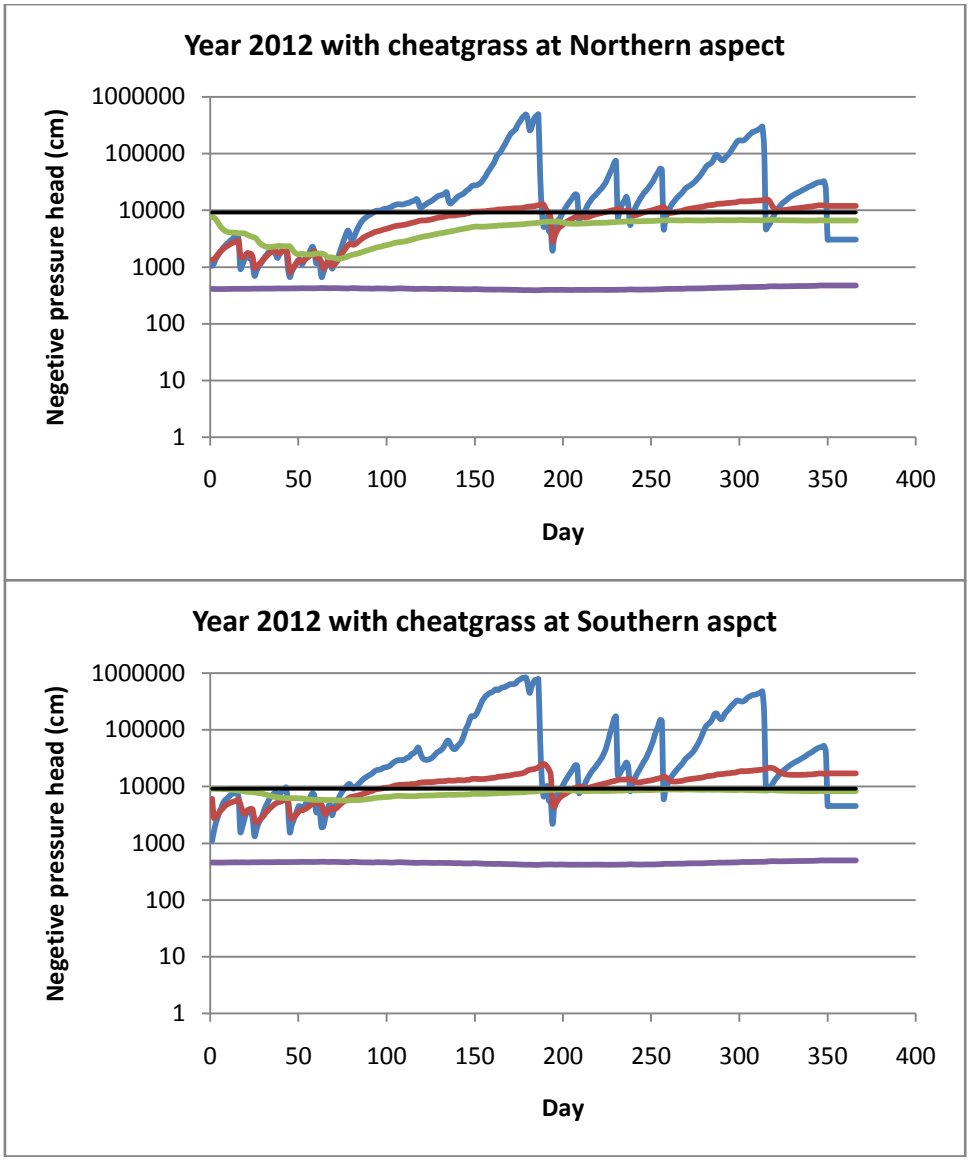

Fig. 21: Matric potential at different depths for different aspects and climate conditions

10 CONCLUSIONS

The results from laboratory and field experiments indicate variability of soil hydraulic properties at different depths. The physical properties of topdressing soil determined from different locations and depths shows the uniformity in composition and soil texture. However, the density measurements by laboratory and field experiments at different depths show the variation in density in topdressing for different layers. The variation in density of topdressing accounts for the variation in the observed soil hydraulic properties. The loose soils at the near surface have an enhanced hydraulic

conductivity and consequently allow water to move in and move out more quickly from that region.

The existence of different soil layers needs to be recognized for appropriate measurement of soil hydraulic properties by both laboratory experiments and field tests. In-situ density measurements of the field soil can be used to compare density values of undisturbed samples and field soil. In case of determining soil hydraulic properties from tension infiltrometer data, tests should be conducted at different depths.

The numerical model to predict the near surface soil water balance is sensitive to soil hydraulic properties used as input to the model. Variation in hydraulic properties for the topdressing soil needs to be considered for accurate prediction of soil water balance by numerical simulation. Uniform soil layer condition at the topdressing will predict higher water storage within the near surface compared to the model that explicitly accounts for the layering.

For the purpose of investigating the link between the near surface water balance and plant germination, germination potentials were evaluated for bottlebrush squirreltail and cheatgrass for different climates and slope aspects. Bottlebrush squirreltail has more favorable condition for germination during wet climate conditions than dry climate conditions for all aspects. During dry climate conditions based on historical data, cheatgrass has the higher potential of germination while the condition remains less favorable for germination of bottlebrush squirreltail.

The germination potentials of cheatgrass and bottlebrush squirreltail on the Northern aspect were somewhat higher than the Southern aspect. Water potentials and temperatures were considered for calculating germination potentials. Simulation results showed that the Northern aspect holds more moisture than the Southern aspect due to less evaporation.

While the numerical model reasonably reproduced measured water content values, it failed to capture the expected variations in sub-surface soil temperatures for different aspects. This shortcoming may be a result of assigning a single air temperature boundary condition independent of aspect. This result may account for the less than expected variability in germination potentials for opposing aspects.

The potential of invasion by cheatgrass is higher at the Northern aspect during dry climate conditions. Here the invasion by cheatgrass is studied by evaluating the germination potential and survivability of bottlebrush squirreltail. We only considered a single native species (bottlebrush squirreltail) because of the availability of germination parameters for this species. There are two reasons that account for invasion by cheatgrass. First, the cheatgrass has favorable conditions to germinate and survive on the Northern aspect during dry climate conditions similar to 2012. Second, the conditions are less favorable for germination of bottlebrush squirreltail than cheatgrass in dry climate conditions. Cheatgrass can germinate and become established quickly by utilizing the soil moisture available. Failure to utilize the soil moisture resources by native species leaves the system vulnerable to establishment of invasive cheatgrass species. To avoid invasion, seeding work needs to be carried out with appropriate selection of species which can germinate and grow before the germination period of cheatgrass.

The results of plant survival study suggest that wet climate conditions provide favorable conditions on both Northern and Southern aspects for C_3 plants similar to blue grama grass. However, for dry climate conditions, some portions of the root zones go below wilting point especially on Southern aspects. During dry climate conditions similar to year 2012, soil water potentials stay above wilting point only within depths of 10 cm form the surface for the months of July and August. The study reveals that the method of placement of topdressing and watershed design followed in geomorphic reclamation provide favorable conditions for vegetation similar to C_3 plants during wet climates. The conditions become less favorable on the Southern aspect compared to the Northern aspect during dry climate conditions.

Further improvement to the numerical model can include mixed canopy of vegetation to better fit the simulation to observed soil water content. More continuous measurements of soil water contents at different depths would aid in evaluating the numerical model. Predictive results on seed germination and plant survival should be evaluated with field measurement and observation of vegetation cover. Vegetation studies for long periods of time will strengthen the prediction of plant germination and survival based on numerical model results.

REFERENCES

Ankeny, M. D., Ahmed, M., Kaspar, T. C., Horton, R., 1991. Simple field method for determining unsaturated hydraulic conductivity. Soil Science Society of America Journal, 55,467-470.

Bauer, M. C., Meyer, S. E., Allen, P. S., 1998. A simulation model to predict seed dormancy loss in the field for *Bromus tectorum* L. Journal of Experimental Botany, Vol.49, No. 32, pp. 1235-1244.

Bodhinayake, W., Si, B. C., Noborio, K., 2004. Determination of hydraulic properties in sloping landscape from tension and double-ring infiltrometer. Vadose Zone Journal, 3:964-970.

Bolsenga, H. J., 1967. Daily sums of global radiation for cloudless sky. *Res. Rep.* 160. Pp. 124. US Army Cold Reg. Res. And Eng. Lab., Hanover, N. H., 1964.

Bradford, K. J., 2002. Application of hydrothermal time to quantifying and modeling seed germination and dormancy. Weed Science, vol. 50, no. 2, pp. 248-260.

Bugosh, N., 2009. A summary of some land surface and water quality monitoring results for constructed GeoFluv landforms, presented at the 2009 National Meeting of the American Society of Mining and Reclamation, Billings, MT, May 30-June 5, 2009.

Burnett, B. N., Meyer, G. A., McFadden, L. D., 2008. Aspect-related microclimatic influences on slope forms and processes, northern Arizona. Journal of Geophysical Research, vol. 113, F03002.

Campbell, G. S., Norman, J. H., (2000). An introduction to Environmental Physics. 2nd Edition.

Chung S.-O., and R. Horton, 1987. Soil heat and water flow with a partial surface mulch, Water Resource research, 23(12), 2175-2186.

Clark, D., 2009. Geomorphic reclamation in New Mexico: A regulator's perspective. Proceedings of Geomorphic Reclamation and Natural Stream Design at Coal Mines: A Technical Interactive Forum. Bristol, VA, April 28-30, 2009.

Das, B. M., 2010. Principles of geotechnical engineer, 7th edition, 2010.

Dingman, L. S., 2000. Physical Hydrology, 365 pp, 2nd edition, Prentice Hall.

Ducas, L. P., Leffler, A. J., Ryel, R. J., 2010. Associations of near-surface soil moisture and annual plant community dynamics. Proceedings of Threat to Shrubland Ecosystem Integrity, Logan, UT, May 18-20, 2010.

Dwyer, S., 2003. Water balance measurement and computer simulations of landfill covers. Ph.D thesis submitted at University of New Mexico.

Eagleson, P. S., 1978. Climate, soil, and vegetation: Introduction to water balance. Water Resource Research, 14(5), 705-712.

Eckels, R., Bugosh, N., 2010. Natural approach to mined land rehabilitation. Proceedings of Facing the Challenges- Building the Capacity, Sydney, Australia, 11-16 April, 2010.

Feddes, R. A., Kowalik, P. J., Zaradny, H., 1978. Simulation of field water use and crop yield. John Wiley & Sons, New York, NY, 1978.

Finch-Savage, W. E., 2004. The use of population-based threshold models to describe and predict the effects of seedbed environment on germination and seedling emergence or crops. Handbook of Seed Physiology Application to Agriculture, chapter 2, page 51-96.

Fischer, J. M., 1992. Sediment properties and water movement through shallow unsaturated alluvium at an arid site for disposal of low-level radioactive waste near Beatty, Nye county, Nevada. Water Resour. Invest. Rep. 92-4032. USGS, Denver, CO.

Furbank, R. T., Taylor, W. C., 1995. Regulation of photosynthesis in C3 and C4 plants: A molecular approach, The Plant Cell Vol. 7 (1995): 797-807.

Galnor, T., Calabrese, J., Downey, S., 2009. Integrating natural processes with drainage reclamation design in Montana. Proceedings of Geomorphic Reclamation and Natural Stream Design at Coal Mines: A Technical Interactive Forum. Bristol, VA, April 28-30, 2009.

Garcia, C. A., Andraski, B. J., Stonestorm, D. A., Cooper, C. A., Simunek, J., Wheatcraft, S. W., 2011. Interacting vegetative and thermal contributions to water movement in desert soil, Vadose Zone Journal, 10: 552-564.

Gardiner, D. T., Miller, R. W., 2008. Soils in our environment, Pearson Prentice Hall publication, 11th edition, 2008.

Geroy, I. J., Gribb, M. M., Marshall, H. P., Chandler, D. G., Benner, S. G., McNamara, J. P., 2011. Aspect influences on soil water retention and storage. Hydrological Processes, 25, 3836-3842.

Gutierrez-Jurado, H. A., Vivoni, E. R., Cikoski, C., Harrison, J. B. J., Bras, R. L., Istanbulloglu, E., 2013. On the observed ecohydrologic dynamics of a semiarid basin with aspect-delimited ecosystems. Water Resource Research, Vol. 49, pages 8263-8284.

Hussen, A. A., Warrick, A. W., 1995. Tension infiltrometers for the measurement of vadose zone hydraulic properties. Handbook of Vadose Zone Characterization and Monitoring, Ch 13, page 189-201.

Iqbal, M., 1983. An introduction to solar radiation. Academic Press, Canada, 1983.

Indorante, S. J., Jansen, I. J., Boast, C. W., 1981. Surface mining and reclamation: Initial changes in soil character. Journal of Soil and Water Conservation 36(6): 347:351.

Jackson, R. B., Canadell, J., Ehleringer, J. R., Mooney, H. A., Sala, O. E., Schulze, E. D., 1996. A glibal analysis of root distributions for terrestrial biomes. Oecoloia 108(3): 389-411.

Jury, W. A., Horton, R., 2004. Soil Physics, sixth edition, John Wiley and Sons Inc.

Meyer, N. A., 2012. Simulating the accumulation of calcite in soils using the soil hydraulic model HYDRUS-1D. Master's thesis submitted to University of Texas at Austin.

Meyer, S. E., Debaene-Gill, S. B., Allen, P. S., 2000. Using Hydrothermal time concepts to model seed germination response to temperature, dormancy loss, and

priming effects in *Elymus elymoides*. Seed Science Research, vol. 10, issue 3, pp. 213-223.

Milczarek, M. A., Van Zyl, D., Peng, S., Rice, R. C., 2006. Saturated and unsaturated hydraulic properties characterization at mine facilities, are we doing it right? Presented at 7th International Conference on Acid Rock Drainage, St. Louis, Missouri, March 26-29.

New Mexico Mining and Mineral division, 2014.
http://www.emnrd.state.nm.us/MMD/gismapminedata.html

Kemp, P. R., Reynolds, J. F., Pachepsky, Y., Chen, J. L., 1997. A comparative modeling study of soil water dynamics in a desert ecosystem. Water Resource Research, Vol. 33, no. 1, pages 73-90.

La Plata Mine Permit, 2001. Reclamation plan: general requirements subpart 906, BHP Billiton, NM.

Lascano, R. J., 1991. Review of models for predicting soil water balance. Proceedings of the Niamey Workshop, Soil Water Balance in the Sudano-Sahelian Zone, 1991.

Revfeim, K. J. A., (1978). A simple procedure for estimating global daily radiation on any surface. Journal of applied meteorology, 17, 1126–1131.

Roundy, B. A., Hardegree, S. P., Chambers, J. C., Whittaker, A., 2007. Prediction of cheatgrass field germination potential using wet thermal accumulation. Rangeland Ecology and Management 60:613-623.

Reynolds, W. D., Zebchuk, W. D., 1996. Use of contact material in tension infiltrometer measurements. Soil Technology. 9, 141-159.

Reynolds, W. D., 2006. Tension infiltrometer measurements: implications of pressure head offset due to contact sand. Vadose Zone Journal 5:1287-1292.

Simunek, J., van Ganuchten, M. Th., 1996. Estimating unsaturated soil hydraulic properties from tension-disc infiltrometer data by numerical inversion. Water Resource Research, 32, 2683-2696.

Simunek, J., Sejna, M., Saito, H., Sakai, van Ganuchten, M. Th., 2013. The HYDRUS-1D software package for simulating the movement of water, heat, and multiple solutes in variably saturated media, version 4.16. Department of Environmental Science, University of California, Riverside.

Tian, Y. Q., Davis-Colley, R. J.,Gong, P., Thorrold, B. W., 2001. Estimating solar radiation on slopes of arbitrary aspect. Agriculture and Forest Meteorology, vol. 109, no. 1, pages 67-74.

van Ganuchten, M. Th., Leij, F. J., Yates, S. R., Williams, J. R., 1997. RETC code for quantifying the hydraulic functions of unsaturated soils. U. S. Salinity Laboratory, USDA, ARS. Riverside, California.

van Ganuchten, M. Th., 1980. A closed from equation for predicting the hydraulic conductivity of unsaturated soils. Soil Science Society of America Journal, 44: 892-898.

APPENDIX A: Field Test Results

TDR calibration

Weight of bucket g=	278.16
Height of bucket cm=	30
Diameter of bucket cm=	15.4

weight of bucket with soil g	height of soil from top cm	TDR long %	TDR short %	GWC %	volume of soil cm3	density of soil g/cc	dry density gm/cc	calculated VWC %
7362.3	3.67	8.07	8.20	3.82	4901.13	1.45	1.39	5.31
7378.2	3.75	23.70	21.55	8.70	4886.42	1.45	1.34	11.63
6765.4	4.14	32.45	26.60	12.40	4813.81	1.35	1.20	14.86
7122.9	4.00	56.47	48.55	18.83	4840.44	1.41	1.19	22.04

TDR long %	TDR short %	actual VWC%
8.07	8.20	5.31
23.70	21.55	11.63
32.45	26.60	14.86
56.47	48.55	22.04

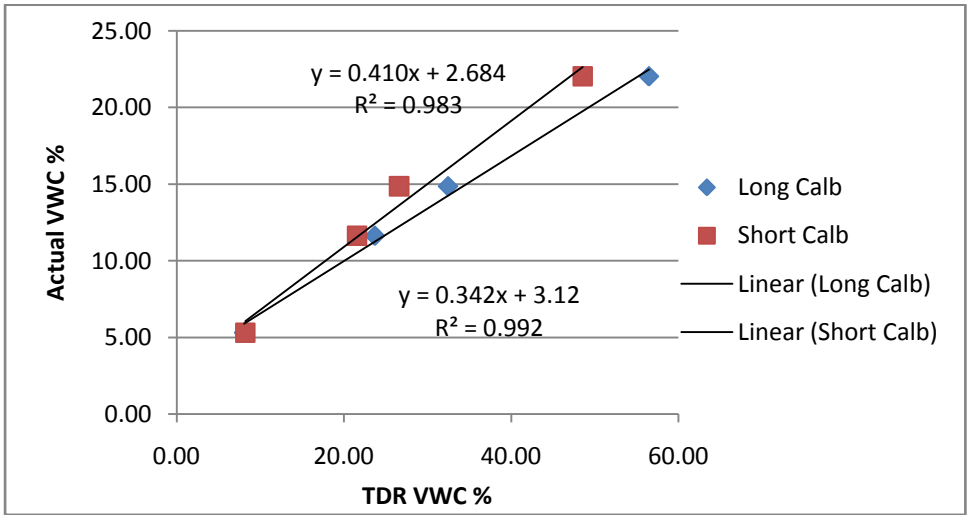

Calibration equation for TDR long

$y = 0.342x + 3.12$

Calibration equation for TDR short

$y = 0.41x + 2.684$

TDR Measurements: Well-vegetated site

Measurement date: 8/6/2012

Site	TDR short %	Calibrated TDR short %	TDR long %	Calibrated TDR long %
W11	3.60	4.16	4.50	4.66
W12	6.60	5.39	9.30	6.30
W13	4.60	4.57	10.40	6.68
W21	4.60	4.57	8.70	6.10
W22	3.60	4.16	16.20	8.66
W23	4.10	4.37	9.50	6.37
W31	5.60	4.98	11.20	6.95
W32	6.10	5.19	10.10	6.57
W33	2.70	3.79	14.30	8.01
W41	3.60	4.16	8.20	5.92
W42	6.60	5.39	9.80	6.47
W43	5.10	4.78	6.20	5.24

Measurement date: 9/27/2012

Site	TDR short %	Calibrated TDR short %	TDR long %	Calibrated TDR long %
W11	5.00	4.73	13.70	7.81
W12	6.30	5.27	15.90	8.56
W13	4.90	4.69	16.80	8.87
W21	4.90	4.69	15.80	8.52
W22	4.80	4.65	16.50	8.76
W23	11.40	7.36	18.60	9.48
W31	6.20	5.23	17.20	9.00
W32	5.10	4.78	11.20	6.95
W33	4.80	4.65	8.30	5.96
W41	5.60	4.98	18.40	9.41
W42	6.20	5.23	25.60	11.88
W43	5.90	5.10	12.20	7.29

Measurement date: 11/28/2012

Site	TDR short %	Calibrated TDR short %	TDR long %	Calibrated TDR long %
W11	10.00	6.78	10.40	6.68
W12	6.60	5.39	17.90	9.24
W13	6.60	5.39	12.60	7.43
W21	9.50	6.58	20.10	9.99
W22	8.50	6.17	24.30	11.43
W23	4.60	4.57	10.10	6.57
W31	9.00	6.37	23.20	11.05
W32	10.00	6.78	7.00	5.51
W33	6.60	5.39	7.60	5.72
W41	8.50	6.17	11.80	7.16
W42	8.10	6.01	8.40	5.99
W43	6.10	5.19	11.50	7.05

Measurement date: 4/19/2013

Site	TDR short %	Calibrated TDR short %	TDR long %	Calibrated TDR long %
W11	31.60	15.64	49.50	20.05
W12	17.40	9.82	32.20	14.13
W13	20.30	11.01	38.40	16.25
W21	14.90	8.79	36.20	15.50
W22	18.40	10.23	30.40	13.52
W23	15.40	9.00	34.50	14.92
W31	27.70	14.04	46.80	19.13
W32	18.40	10.23	30.90	13.69
W33	20.30	11.01	28.70	12.94
W41	17.90	10.02	41.20	17.21
W42	34.10	16.67	52.90	21.21
W43	36.00	17.44	43.90	18.13

Measurement date: 7/11/2013

Site	TDR short %	Calibrated TDR short %	TDR long %	Calibrated TDR long %
W11	3.60	4.16	12.00	7.22
W12	4.60	4.57	10.40	6.68
W13	6.10	5.19	11.20	6.95
W21	7.10	5.60	15.10	8.28
W22	5.10	4.78	11.20	6.95
W23	4.10	4.37	8.70	6.10
W31	7.10	5.60	26.50	12.18
W32	5.10	4.78	13.20	7.63
W33	7.10	5.60	14.30	8.01
W41	4.10	4.37	15.90	8.56
W42	4.60	4.57	9.50	6.37
W43	3.60	4.16	12.60	7.43

Measurement date: 10/25/2013

Site	TDR short %	Calibrated TDR short %	TDR long %	Calibrated TDR long %
W11	31.10	15.44	43.40	17.96
W12	13.00	8.01	45.70	18.75
W13	24.70	12.81	31.80	14.00
W21	45.90	21.50	37.60	15.98
W22	18.40	10.23	17.60	9.14
W23	13.00	8.01	16.80	8.87
W31	30.10	15.03	56.80	22.55
W32	9.00	6.37	27.60	12.56
W33	13.90	8.38	36.50	15.60
W41	15.40	9.00	26.20	12.08
W42	20.80	11.21	20.90	10.27
W43	18.90	10.43	45.10	18.54

Measurement date: 3/31/2014

Site	TDR short %	Calibrated TDR short %	TDR long %	Calibrated TDR long %
W11	19.30	10.60	30.90	13.69
W12	20.30	11.01	34.30	14.85
W13	15.40	9.00	34.90	15.06
W21	12.20	7.69	28.20	12.76
W22	15.40	9.00	29.30	13.14
W23	14.40	8.59	25.70	11.91
W31	21.30	11.42	46.80	19.13
W32	20.50	11.09	31.50	13.89
W33	24.90	12.89	45.40	18.65
W41	23.90	12.48	31.10	13.76
W42	14.60	8.67	27.00	12.35
W43	10.50	6.99	29.40	13.17

TDR measurements: Moderately-vegetated site

Measurement date: 9/27/2012

Site	TDR short %	Calibrated TDR short %	TDR long %	Calibrated TDR long %
M11	5.60	4.98	12.30	7.33
M12	8.00	5.96	35.10	15.12
M13	6.10	5.19	16.80	8.87
M21	6.10	5.19	15.70	8.49
M22	4.60	4.57	15.70	8.49
M23	5.60	4.98	13.70	7.81
M31	10.60	7.03	19.50	9.79
M32	11.00	7.19	10.40	6.68
M33	4.60	4.57	6.20	5.24
M41	5.60	4.98	24.50	11.50
M42	8.50	6.17	12.00	7.22
M43	5.60	4.98	13.40	7.70

Measurement date: 11/28/2012

Site	TDR short %	Calibrated TDR short %	TDR long %	Calibrated TDR long %
M11	5.60	4.98	3.20	4.21
M12	6.60	5.39	7.30	5.62
M13	8.10	6.01	7.30	5.62
M21	6.60	5.39	8.70	6.10
M22	8.10	6.01	9.00	6.20
M23	5.10	4.78	5.70	5.07
M31	7.10	5.60	10.90	6.85
M32	8.10	6.01	10.90	6.85
M33	9.50	6.58	9.30	6.30
M41	6.60	5.39	11.20	6.95
M42	7.60	5.80	5.90	5.14
M43	10.50	6.99	26.20	12.08

Measurement date: 4/19/2013

Site	TDR short %	Calibrated TDR short %	TDR long %	Calibrated TDR long %
M11	19.80	10.80	37.90	16.08
M12	20.80	11.21	40.90	17.11
M13	23.70	12.40	58.70	23.20
M21	34.10	16.67	58.40	23.09
M22	27.20	13.84	57.00	22.61
M23	33.10	16.26	60.90	23.95
M31	29.20	14.66	57.30	22.72
M32	20.30	11.01	57.90	22.92
M33	44.40	20.89	61.80	24.26
M41	24.70	12.81	47.30	19.30
M42	28.20	14.25	40.90	17.11
M43	26.20	13.43	46.50	19.02

Measurement date: 7/11/2013

Site	TDR short %	Calibrated TDR short %	TDR long %	Calibrated TDR long %
M11	7.60	5.80	15.10	8.28
M12	5.60	4.98	11.20	6.95
M13	6.60	5.39	8.70	6.10
M21	7.60	5.80	17.90	9.24
M22	8.50	6.17	27.30	12.46
M23	8.10	6.01	20.10	9.99
M31	4.60	4.57	17.60	9.14
M32	6.60	5.39	11.20	6.95
M33	5.60	4.98	21.20	10.37
M41	9.00	6.37	22.00	10.64
M42	6.10	5.19	9.80	6.47
M43	8.10	6.01	18.70	9.52

Measurement date: 10/25/2013

Site	TDR short %	Calibrated TDR short %	TDR long %	Calibrated TDR long %
M11	19.30	10.60	43.70	18.07
M12	26.70	13.63	28.40	12.83
M13	18.90	10.43	35.90	15.40
M21	20.30	11.01	27.90	12.66
M22	27.70	14.04	55.10	21.96
M23	32.60	16.05	48.70	19.78
M31	21.30	11.42	31.20	13.79
M32	19.30	10.60	39.00	16.46
M33	12.00	7.60	17.60	9.14
M41	35.50	17.24	40.40	16.94
M42	18.90	10.43	39.80	16.73
M43	38.00	18.26	45.10	18.54

Measurement date: 3/31/2014

Site	TDR short %	Calibrated TDR short %	TDR long %	Calibrated TDR long %
M11	8.20	6.05	24.00	11.33
M12	17.40	9.82	32.90	14.37
M13	11.50	7.40	48.30	19.64
M21	25.70	13.22	42.70	17.72
M22	30.30	15.11	42.90	17.79
M23	23.80	12.44	42.60	17.69
M31	13.00	8.01	43.80	18.10
M32	17.60	9.90	36.50	15.60
M33	27.00	13.75	42.30	17.59
M41	20.30	11.01	41.20	17.21
M42	19.80	10.80	41.80	17.42
M43	30.20	15.07	53.70	21.49

Sand cone density measurement

Calibration of sand cone apparatus

Test no	Mass of sand before test (g)	Mass of sand after test (g)	Mass of sand required to fill (g)	Avg mass of sand to fill the cone and base plate (g)
1	4139.5	2343.9	1795.6	
2	3778.6	1979.2	1799.4	1797.3
3	3990.1	2193.2	1796.9	

Calibration for density of sand

Weight of container (g)	volume of container (in3)	volume of container (cc)
771.54	89.72754	1470.371

Test no	Weight of container with sand (g)	Weight of sand (g)	Density of sand (g/cc)	Avg bulk density of sand (g/cc)
1	3262.13	2490.59	1.693852	
2	3236.52	2464.98	1.676434	1.688744
3	3265.21	2493.67	1.695946	

APPENDIX B: Laboratory Test Results

Specific gravity test results

Well-vegetated site				Moderately-vegetated site			
Sample ID	Specific gravity	Sample ID	Specific gravity	Sample ID	Specific gravity	Sample ID	Specific gravity
11-T	2.670	11-B	2.661	11-T	2.688	11-B	2.658
12-T	2.679	12-B	2.584	12-T	2.711	12-B	2.671
13-T	2.678	13-B	2.662	13-T	2.684	13-B	2.654
21-T	2.680	21-B	2.645	21-T	2.674	21-B	2.665
22-T	2.683	22-B	2.671	22-T	2.674	22-B	2.678
23-T	2.670	23-B	2.659	23-T	2.667	23-B	2.676
31-T	2.672	31-B	2.680	31-T	2.674	31-B	2.685
32-T	2.679	32-B	2.656	32-T	2.671	32-B	2.657
33-T	2.697	33-B	2.691	33-T	2.675	33-B	2.700
41-T	2.660	41-B	2.664	41-T	2.670	41-B	2.646
42-T	2.671	42-B	2.673	42-T	2.658	42-B	2.680
43-T	2.667	43-B	2.652	43-T	2.682	43-B	2.697

Organic content test results

Well-vegetated site				Moderately-vegetated site			
Sample ID	Organic content %	Sample ID	Organic content %	Sample ID	Organic content %	Sample ID	Organic content %
11-T	6.79	11-B	4.95	11-T	4.37	11-B	4.95
12-T	8.52	12-B	7.75	12-T	4.20	12-B	7.75
13-T	5.39	13-B	4.18	13-T	4.37	13-B	4.18
21-T	5.05	21-B	5.81	21-T	4.18	21-B	5.81
22-T	5.37	22-B	5.62	22-T	4.64	22-B	5.62
23-T	5.22	23-B	3.89	23-T	4.92	23-B	3.89
31-T	5.53	31-B	5.06	31-T	4.58	31-B	3.32
32-T	5.77	32-B	5.21	32-T	4.62	32-B	3.68
33-T	4.31	33-B	4.00	33-T	4.25	33-B	2.74
41-T	6.01	41-B	5.08	41-T	4.82	41-B	1.04
42-T	5.00	42-B	4.84	42-T	4.94	42-B	1.67
43-T	5.12	43-B	5.48	43-T	4.92	43-B	1.14

Sieve analysis and hydrometer test results: Well-vegetated top samples

11-T		12-T		13-T		21-T		22-T		23-T	
Size (mm)	% finer	Size (mm)	% finer	Size (mm)	% finer	Size (mm)	% finer	Size (mm)	% finer	Size (mm)	% finer
19	100.0	19	97.1	19	100.0	19	100.0	19	100.0	19	97.9
9.5	98.7	9.5	92.4	9.5	97.3	9.5	95.8	9.5	95.5	9.5	95.4
4.75	96.1	4.75	87.0	4.75	94.1	4.75	90.7	4.75	90.7	4.75	91.1
2	92.7	2	81.0	2	90.7	2	85.7	2	86.1	2	86.7
0.84	89.5	0.84	76.2	0.84	87.9	0.84	80.8	0.84	82.7	0.84	82.9
0.6	87.6	0.6	74.1	0.6	86.4	0.6	78.0	0.6	80.9	0.6	80.6
0.425	85.6	0.425	72.1	0.425	84.9	0.425	75.4	0.425	79.1	0.425	78.2
0.25	81.1	0.25	68.1	0.25	81.5	0.25	70.0	0.25	75.0	0.25	73.0
0.15	72.7	0.15	61.8	0.15	75.1	0.15	60.2	0.15	66.4	0.15	62.7
0.106	64.9	0.106	55.1	0.106	68.5	0.106	51.6	0.106	58.8	0.106	54.1
0.075	59.1	0.075	50.9	0.075	63.0	0.075	45.9	0.075	53.1	0.075	48.0
0.0319	43.5	0.0325	40.1	0.0319	42.6	0.0321	35.1	0.0319	33.3	0.0326	31.4
0.0228	40.5	0.0232	38.1	0.0227	40.6	0.0229	33.1	0.0227	31.3	0.0232	29.4
0.0162	39.1	0.0164	37.9	0.0162	38.6	0.0163	31.1	0.0162	27.7	0.0165	27.9
0.0116	36.2	0.0117	36.0	0.0116	35.8	0.0117	25.2	0.0116	25.4	0.0118	25.5
0.0086	32.6	0.0086	34.2	0.0083	35.4	0.0086	23.8	0.0085	25.2	0.0086	23.5
0.0061	32.4	0.0061	32.1	0.0060	33.9	0.0061	21.5	0.0060	23.0	0.0062	21.3
0.0043	28.6	0.0043	31.3	0.0043	31.7	0.0044	19.3	0.0043	19.4	0.0044	17.9
0.0031	26.7	0.0031	28.3	0.0031	29.1	0.0031	17.1	0.0031	17.2	0.0031	16.1
0.0020	22.8	0.0020	24.6	0.0019	25.7	0.0018	13.2	0.0018	13.9	0.0018	13.1
0.0014	19.1	0.0014	20.5	0.0014	21.8	0.0014	10.0	0.0014	11.5	0.0014	9.9
0.0011	16.5	0.0011	18.7	0.0011	19.1	0.0011	7.2	0.0011	9.2	0.0011	7.6
0.0008	14.6	0.0008	16.8	0.0008	16.8	0.0008	5.5	0.0008	7.3	0.0008	6.0

31-T		32-T		33-T		41-T		42-T		43-T	
Size (mm)	% finer	Size (mm)	% finer	Size (mm)	% finer	Size (mm)	% finer	Size (mm)	% finer	Size (mm)	% finer
19	100.0	19	100.0	19	100.0	19	100.0	19	100.0	19	100.0
9.5	97.2	9.5	98.7	9.5	100.0	9.5	95.4	9.5	98.8	9.5	94.8
4.75	93.7	4.75	92.9	4.75	99.7	4.75	91.2	4.75	95.6	4.75	90.5
2	90.2	2	88.6	2	99.6	2	87.0	2	91.6	2	86.3
0.84	87.2	0.84	85.3	0.84	99.3	0.84	83.0	0.84	88.1	0.84	82.9
0.6	85.6	0.6	83.5	0.6	98.9	0.6	80.9	0.6	86.0	0.6	80.9
0.425	84.0	0.425	81.7	0.425	98.2	0.425	78.8	0.425	83.9	0.425	78.9
0.25	80.4	0.25	77.9	0.25	95.9	0.25	74.4	0.25	79.3	0.25	74.7
0.15	73.6	0.15	70.8	0.15	92.0	0.15	66.3	0.15	70.8	0.15	66.6
0.106	66.6	0.106	63.9	0.106	87.8	0.106	58.8	0.106	62.7	0.106	58.8
0.075	60.8	0.075	58.7	0.075	83.2	0.075	53.5	0.075	56.7	0.075	53.6
0.0313	39.3	0.0311	59.5	0.0306	55.3	0.0317	46.4	0.0315	47.7	0.0323	40.4
0.0224	36.5	0.0221	57.6	0.0219	51.4	0.0226	44.4	0.0226	42.9	0.0230	38.4
0.0159	34.7	0.0158	55.6	0.0157	47.5	0.0151	42.5	0.0152	40.7	0.0164	36.5
0.0114	31.8	0.0112	53.8	0.0113	42.1	0.0114	40.5	0.0115	38.7	0.0116	35.1
0.0084	28.4	0.0083	51.7	0.0082	39.4	0.0082	36.5	0.0082	35.1	0.0084	33.9
0.0060	25.6	0.0048	49.7	0.0060	35.9	0.0059	35.0	0.0059	33.4	0.0061	32.5
0.0043	23.0	0.0037	47.6	0.0043	32.6	0.0043	32.4	0.0043	31.2	0.0043	30.1
0.0031	19.9	0.0028	45.8	0.0031	30.1	0.0031	29.0	0.0031	29.0	0.0030	28.6
0.0018	17.1	0.0018	41.7	0.0020	25.9	0.0021	25.0	0.0021	26.5	0.0021	26.3
0.0014	14.1	0.0012	38.3	0.0014	22.5	0.0014	21.5	0.0014	21.8	0.0014	21.1
0.0011	11.6	0.0011	36.3	0.0011	20.3	0.0011	18.7	0.0011	19.2	0.0011	20.0
0.0008	9.3	0.0008	33.2	0.0008	18.2	0.0008	16.6	0.0008	16.9	0.0008	18.1

Sieve analysis and hydrometer test results: Well-vegetated bottom samples

11-B		12-B		13-B		21-B		22-B		23-B	
Size (mm)	% finer	Size (mm)	% finer	Size (mm)	% finer	Size (mm)	% finer	Size (mm)	% finer	Size (mm)	% finer
19	100.0	19	96.7	19	97.9	19	100.0	19	100.0	19	100.0
9.5	99.6	9.5	89.8	9.5	92.9	9.5	95.8	9.5	97.3	9.5	98.0
4.75	97.2	4.75	82.0	4.75	89.3	4.75	92.3	4.75	93.5	4.75	93.3
2	93.2	2	72.7	2	84.6	2	87.1	2	89.1	2	88.6
0.84	89.7	0.84	65.4	0.84	80.9	0.84	82.3	0.84	85.3	0.84	84.3
0.6	88.1	0.6	62.8	0.6	79.0	0.6	79.9	0.6	83.2	0.6	81.9
0.425	86.5	0.425	60.9	0.425	76.9	0.425	77.5	0.425	81.0	0.425	79.4
0.25	82.8	0.25	57.9	0.25	72.6	0.25	73.0	0.25	76.5	0.25	74.4
0.15	75.1	0.15	53.3	0.15	63.6	0.15	64.1	0.15	67.1	0.15	64.2
0.106	66.8	0.106	49.2	0.106	56.4	0.106	56.6	0.106	58.8	0.106	55.5
0.075	60.5	0.075	46.4	0.075	51.4	0.075	51.6	0.075	53.5	0.075	49.6
0.0309	50.8	0.032	45.2	0.033	29.7	0.033	28.5	0.031	43.8	0.032	40.3
0.0223	45.0	0.023	39.4	0.023	25.8	0.024	24.1	0.022	41.8	0.023	38.3
0.0159	43.1	0.016	35.0	0.017	24.2	0.017	22.7	0.016	38.2	0.016	36.4
0.0113	41.1	0.012	31.2	0.012	22.2	0.012	20.9	0.011	36.3	0.011	34.6
0.0083	39.2	0.008	28.6	0.008	20.3	0.008	18.9	0.008	34.3	0.008	32.6
0.0060	35.9	0.006	23.0	0.006	18.1	0.006	16.6	0.006	31.9	0.006	29.9
0.0042	33.4	0.004	18.6	0.004	15.2	0.005	12.8	0.004	29.8	0.004	27.5
0.0030	31.8	0.003	15.4	0.003	12.8	0.003	11.2	0.003	27.6	0.003	25.1
0.0022	30.5	0.002	12.6	0.002	11.8	0.002	10.2	0.002	26.0	0.002	24.3
0.0013	24.9	0.001	6.9	0.001	5.9	0.001	5.0	0.001	20.3	0.001	18.8
0.0011	23.3	0.001	4.8	0.001	5.1	0.001	3.0	0.001	19.8	0.001	18.1
0.0008	20.9	0.0009	2.9	0.0009	2.9	0.0009	1.1	0.0009	16.0	0.0009	16.4

31-B		32-B		33-B		41-B		42-B		43-B	
Size (mm)	% finer	Size (mm)	% finer	Size (mm)	% finer	Size (mm)	% finer	Size (mm)	% finer	Size (mm)	% finer
19	100.0	19	100.0	19	100.0	19	100.0	19	100.0	19	98.8
9.5	96.7	9.5	98.6	9.5	100.0	9.5	97.6	9.5	99.5	9.5	97.2
4.75	93.0	4.75	95.3	4.75	100.0	4.75	93.7	4.75	96.4	4.75	94.1
2	88.8	2	91.1	2	99.9	2	89.9	2	92.6	2	89.4
0.84	85.5	0.84	88.0	0.84	99.6	0.84	86.2	0.84	89.3	0.84	85.7
0.6	83.8	0.6	86.6	0.6	99.2	0.6	84.1	0.6	87.5	0.6	83.7
0.425	82.1	0.425	85.0	0.425	98.5	0.425	81.9	0.425	85.5	0.425	81.7
0.25	78.5	0.25	81.8	0.25	95.9	0.25	77.6	0.25	81.4	0.25	77.6
0.15	71.2	0.15	74.8	0.15	91.4	0.15	69.0	0.15	73.0	0.15	68.8
0.106	64.3	0.106	68.4	0.106	86.8	0.106	61.4	0.106	65.3	0.106	61.1
0.075	58.4	0.075	62.9	0.075	81.7	0.075	55.6	0.075	59.3	0.075	55.4
0.0320	39.5	0.0323	40.1	0.0303	51.7	0.0327	36.4	0.0314	45.9	0.0319	44.8
0.0228	37.6	0.0231	36.7	0.0219	46.6	0.0233	34.1	0.0224	43.9	0.0229	40.8
0.0164	33.4	0.0166	33.0	0.0158	41.9	0.0166	32.3	0.0150	42.1	0.0153	39.2
0.0116	31.6	0.0118	30.5	0.0113	38.2	0.0118	30.5	0.0114	40.2	0.0116	36.6
0.0086	28.4	0.0087	26.3	0.0082	34.4	0.0085	28.9	0.0081	38.2	0.0083	33.4
0.0061	27.4	0.0062	24.6	0.0060	30.4	0.0062	24.6	0.0059	35.8	0.0060	30.8
0.0044	23.5	0.0044	24.2	0.0043	25.9	0.0044	22.6	0.0042	33.7	0.0044	28.6
0.0031	21.2	0.0031	20.8	0.0031	23.1	0.0031	20.8	0.0030	30.9	0.0031	26.8
0.0023	19.5	0.0023	19.3	0.0023	21.2	0.0023	18.6	0.0022	29.7	0.0022	24.6
0.0013	13.5	0.0013	15.7	0.0013	16.1	0.0013	13.3	0.0013	24.0	0.0013	19.4
0.0011	11.8	0.0011	12.4	0.0011	15.1	0.0011	11.9	0.0011	22.5	0.0011	18.9
0.0009	10.7	0.0009	10.1	0.0009	12.6	0.0009	9.8	0.0009	19.0	0.0009	17.0

Sieve analysis and hydrometer test results: Moderately-vegetated top samples

11-T		12-T		13-T		21-T		22-T		23-T	
Size (mm)	% finer	Size (mm)	% finer	Size (mm)	% finer	Size (mm)	% finer	Size (mm)	% finer	Size (mm)	% finer
19	100.0	19	100.0	19	96.9	19	100.0	19	100.0	19	100.0
9.5	96.6	9.5	97.3	9.5	96.6	9.5	99.6	9.5	99.0	9.5	98.8
4.75	94.5	4.75	95.6	4.75	95.2	4.75	97.8	4.75	97.5	4.75	96.6
2	92.3	2	93.1	2	93.3	2	95.8	2	95.5	2	94.7
0.84	90.6	0.84	91.5	0.84	91.4	0.84	94.1	0.84	93.8	0.84	93.3
0.6	89.8	0.6	90.6	0.6	90.3	0.6	93.3	0.6	92.8	0.6	92.6
0.425	89.0	0.425	89.7	0.425	89.2	0.425	92.6	0.425	91.9	0.425	91.9
0.25	87.2	0.25	87.8	0.25	86.9	0.25	90.9	0.25	89.9	0.25	90.1
0.15	82.1	0.15	82.5	0.15	81.5	0.15	85.5	0.15	84.9	0.15	85.1
0.106	74.8	0.106	75.4	0.106	74.5	0.106	78.0	0.106	77.7	0.106	78.2
0.075	68.5	0.075	69.3	0.075	68.4	0.075	71.5	0.075	71.3	0.075	72.4
0.0310	42.4	0.0309	47.0	0.0306	46.3	0.0321	40.6	0.0317	36.2	0.0326	36.6
0.0224	36.5	0.0220	45.1	0.0218	44.4	0.0230	36.6	0.0228	32.5	0.0232	34.2
0.0160	32.9	0.0157	43.1	0.0156	41.4	0.0164	34.6	0.0162	30.0	0.0165	32.8
0.0114	30.5	0.0112	41.2	0.0111	39.0	0.0117	32.6	0.0116	26.3	0.0117	31.2
0.0084	27.1	0.0083	37.5	0.0082	35.8	0.0086	30.9	0.0085	24.4	0.0086	29.2
0.0060	24.6	0.0059	34.2	0.0059	33.3	0.0061	27.1	0.0061	20.8	0.0062	26.3
0.0043	20.6	0.0042	31.3	0.0042	30.5	0.0044	25.1	0.0044	18.5	0.0044	24.3
0.0031	18.3	0.0030	29.6	0.0030	28.4	0.0031	24.3	0.0031	16.1	0.0031	22.7
0.0022	14.5	0.0021	27.7	0.0021	25.4	0.0021	23.0	0.0022	14.1	0.0021	21.2
0.0014	10.6	0.0012	21.1	0.0013	21.2	0.0012	18.0	0.0014	10.6	0.0012	16.4
0.0011	7.4	0.0011	20.1	0.0011	19.3	0.0011	16.8	0.0011	8.6	0.0011	14.6
0.0008	4.4	0.0008	17.2	0.0008	16.7	0.0008	13.4	0.0009	5.3	0.0008	12.2

31-T		32-T		33-T		41-T		42-T		43-T	
Size (mm)	% finer	Size (mm)	% finer	Size (mm)	% finer	Size (mm)	% finer	Size (mm)	% finer	Size (mm)	% finer
19	100.0	19	97.2	19	100.0	19	100.0	19	100.0	19	100.0
9.5	99.5	9.5	96.6	9.5	98.8	9.5	99.0	9.5	97.3	9.5	96.9
4.75	97.1	4.75	94.6	4.75	95.9	4.75	97.0	4.75	94.5	4.75	95.4
2	95.1	2	92.9	2	93.8	2	95.4	2	91.3	2	94.1
0.84	93.1	0.84	91.5	0.84	92.2	0.84	94.0	0.84	89.1	0.84	93.0
0.6	92.1	0.6	90.6	0.6	91.3	0.6	93.2	0.6	88.1	0.6	92.3
0.425	91.0	0.425	89.8	0.425	90.4	0.425	92.4	0.425	87.1	0.425	91.6
0.25	88.8	0.25	87.9	0.25	88.5	0.25	90.3	0.25	84.8	0.25	89.9
0.15	83.2	0.15	82.7	0.15	83.7	0.15	83.8	0.15	77.6	0.15	85.9
0.106	75.4	0.106	75.6	0.106	77.3	0.106	75.1	0.106	67.5	0.106	80.5
0.075	68.7	0.075	69.5	0.075	71.3	0.075	68.8	0.075	62.4	0.075	75.3
0.0308	45.3	0.032	44.1	0.0316	37.8	0.0319	42.1	0.0321	49.7	0.0315	52.1
0.0222	40.3	0.023	42.1	0.0226	33.9	0.0227	40.1	0.0229	47.5	0.0227	46.2
0.0159	36.4	0.016	38.4	0.0161	32.3	0.0162	38.2	0.0162	47.3	0.0161	46.2
0.0114	32.8	0.012	36.4	0.0114	31.8	0.0116	33.8	0.0116	43.5	0.0116	41.2
0.0083	32.0	0.008	33.5	0.0084	30.0	0.0085	31.8	0.0085	42.3	0.0085	38.8
0.0059	30.2	0.006	30.7	0.0060	27.1	0.0061	29.2	0.0061	39.5	0.0061	35.1
0.0043	26.3	0.004	28.4	0.0043	24.5	0.0043	26.4	0.0043	37.1	0.0044	30.9
0.0030	23.8	0.003	26.6	0.0031	22.1	0.0031	25.3	0.0031	35.3	0.0031	28.3
0.0022	20.2	0.002	24.9	0.0022	18.2	0.0022	22.5	0.0022	31.0	0.0022	24.2
0.0014	17.8	0.001	19.0	0.0014	13.9	0.0013	16.8	0.0014	28.4	0.0014	19.3
0.0011	14.3	0.001	17.0	0.0011	11.2	0.0011	16.4	0.0011	25.4	0.0011	16.1
0.0008	12.3	0.001	14.7	0.0008	8.0	0.0008	13.0	0.0009	23.6	0.0009	12.1

Sieve analysis and hydrometer test results: Moderately-vegetated bottom samples

11-B		12-B		13-B		21-B		22-B		23-B	
Size (mm)	% finer	Size (mm)	% finer	Size (mm)	% finer	Size (mm)	% finer	Size (mm)	% finer	Size (mm)	% finer
19	100.0	19	100.0	19	100.0	19	100.0	19	100.0	19	100.0
9.5	99.3	9.5	99.7	9.5	99.4	9.5	98.3	9.5	98.7	9.5	99.5
4.75	97.8	4.75	97.9	4.75	97.6	4.75	96.7	4.75	97.2	4.75	96.6
2	95.4	2	96.2	2	95.6	2	94.4	2	95.2	2	93.3
0.84	93.7	0.84	94.7	0.84	93.9	0.84	92.4	0.84	93.7	0.84	90.9
0.6	92.9	0.6	93.8	0.6	93.0	0.6	91.4	0.6	92.8	0.6	89.9
0.425	92.1	0.425	93.0	0.425	92.2	0.425	90.5	0.425	92.0	0.425	89.0
0.25	90.4	0.25	91.0	0.25	90.3	0.25	88.6	0.25	90.2	0.25	87.1
0.15	85.6	0.15	85.8	0.15	84.9	0.15	83.0	0.15	85.5	0.15	81.9
0.106	78.4	0.106	78.5	0.106	77.5	0.106	75.2	0.106	78.6	0.106	74.7
0.075	72.3	0.075	71.9	0.075	70.9	0.075	68.7	0.075	72.5	0.075	68.6
0.0313	48.3	0.0316	44.7	0.0320	42.3	0.0323	38.8	0.0313	46.2	0.0318	42.6
0.0223	46.3	0.0225	42.7	0.0228	40.3	0.0229	37.8	0.0225	42.3	0.0227	39.3
0.0160	42.3	0.0161	39.4	0.0161	40.3	0.0163	35.8	0.0160	40.3	0.0161	38.3
0.0113	41.3	0.0115	37.4	0.0115	38.4	0.0117	33.2	0.0114	37.5	0.0115	36.5
0.0083	40.4	0.0084	35.0	0.0085	35.8	0.0086	30.8	0.0084	36.1	0.0085	32.7
0.0059	36.8	0.0060	33.0	0.0060	32.8	0.0061	28.5	0.0060	32.1	0.0061	29.3
0.0043	32.6	0.0043	29.0	0.0043	30.0	0.0044	24.9	0.0043	29.2	0.0043	26.8
0.0030	30.6	0.0031	27.0	0.0031	28.2	0.0031	23.1	0.0031	26.8	0.0031	24.4
0.0021	28.9	0.0021	24.7	0.0021	24.5	0.0022	21.0	0.0021	24.7	0.0022	22.5
0.0013	24.1	0.0013	21.0	0.0013	20.7	0.0013	16.8	0.0013	19.3	0.0013	17.3
0.0011	22.5	0.0011	19.6	0.0011	20.0	0.0011	15.0	0.0011	17.7	0.0011	16.5
0.0009	19.0	0.0009	16.6	0.0009	16.4	0.0009	13.0	0.0009	15.9	0.0009	13.2

31-B		32-B		33-B		41-B		42-B		43-B	
Size (mm)	% finer	Size (mm)	% finer	Size (mm)	% finer	Size (mm)	% finer	Size (mm)	% finer	Size (mm)	% finer
19	100.0	19	100.0	19	100.0	19	100.0	19	100.0	19	100.0
9.5	99.0	9.5	99.8	9.5	99.7	9.5	98.7	9.5	99.5	9.5	99.6
4.75	97.1	4.75	98.1	4.75	97.1	4.75	97.7	4.75	96.7	4.75	98.0
2	95.1	2	96.5	2	95.5	2	95.7	2	93.2	2	96.6
0.84	93.4	0.84	95.0	0.84	93.8	0.84	94.0	0.84	90.5	0.84	95.5
0.6	92.4	0.6	94.2	0.6	92.9	0.6	93.1	0.6	89.3	0.6	95.0
0.425	91.5	0.425	93.4	0.425	92.1	0.425	92.2	0.425	88.2	0.425	94.4
0.25	89.6	0.25	91.7	0.25	90.3	0.25	90.2	0.25	86.0	0.25	93.2
0.15	84.3	0.15	86.6	0.15	85.6	0.15	84.6	0.15	79.9	0.15	89.7
0.106	76.9	0.106	79.3	0.106	79.1	0.106	77.2	0.106	71.8	0.106	84.4
0.075	70.2	0.075	73.0	0.075	73.1	0.075	71.0	0.075	65.8	0.075	79.3
0.0317	41.8	0.0310	50.7	0.0313	44.0	0.0318	45.0	0.0309	58.8	0.0301	63.7
0.0228	36.9	0.0223	46.8	0.0223	42.0	0.0228	41.6	0.0220	56.9	0.0216	59.8
0.0162	35.9	0.0159	44.8	0.0159	40.0	0.0161	41.0	0.0157	55.3	0.0154	57.6
0.0115	33.9	0.0113	43.2	0.0114	36.5	0.0116	37.4	0.0112	52.3	0.0110	53.8
0.0085	31.0	0.0083	40.8	0.0083	35.1	0.0085	35.2	0.0082	50.7	0.0081	51.9
0.0061	27.8	0.0060	36.8	0.0060	32.3	0.0061	32.6	0.0059	49.1	0.0058	48.3
0.0043	25.7	0.0042	34.8	0.0042	30.4	0.0043	29.6	0.0042	44.9	0.0041	45.9
0.0031	24.1	0.0030	32.4	0.0030	26.2	0.0031	27.0	0.0030	42.6	0.0030	43.4
0.0022	22.0	0.0021	30.1	0.0022	24.3	0.0022	24.9	0.0022	39.4	0.0022	41.8
0.0013	16.6	0.0013	25.3	0.0013	19.6	0.0013	20.7	0.0013	33.4	0.0012	35.9
0.0011	16.0	0.0011	24.6	0.0011	16.6	0.0011	18.5	0.0011	32.7	0.0011	34.4
0.0009	12.4	0.0009	20.4	0.0009	14.1	0.0009	16.7	0.0008	29.5	0.0008	32.1

USDA classification for well-vegetated samples

Sample ID	11T	12T	13T	21T	22T	23T	31T	32T	33T	41T	42T	43T
Sand %	46.06	48.77	43.77	55.66	52.38	56.17	46.78	38.49	29.72	45.98	45.41	49.02
Silt %	31.28	26.54	29.77	30.34	32.52	29.99	35.48	28.78	44.18	29.31	28.38	25.49
Clay %	22.65	24.69	26.46	14.00	15.10	13.84	17.74	32.73	26.10	24.71	26.20	25.49
USDA classification	Sandy Clay Loam	Sandy Clay Loam	Loam	Sandy Clay Loam	Sandy Clay Loam	Sandy Clay Loam	Sandy Clay	Clay Loam	Loam	Sandy Clay Loam	Sandy Clay Loam	Sandy Clay Loam

Sample ID	11B	12B	13B	21B	22B	23B	31B	32B	33B	41B	42B	43B
Sand %	42.06	44.98	55.67	57.52	48.37	52.03	48.20	45.12	31.93	51.06	44.92	46.31
Silt %	27.90	44.02	33.69	33.30	26.94	24.27	33.78	36.22	48.05	31.15	25.92	30.20
Clay %	30.04	11.00	10.64	9.18	23.57	23.70	18.02	18.66	20.02	17.80	29.16	23.49
USDA classification	Clay Loam	Loam	Sandy Loam	Sandy Loam	Loam	Sandy Clay Loam	Loam	Loam	Loam	Loam	Clay Loam	Loam

USDA classification for moderately-vegetated samples

Sample ID	11T	12T	13T	21T	22T	23T	31T	32T	33T	41T	42T	43T
Sand %	41.50	37.70	38.91	42.59	43.46	44.03	40.06	39.72	42.43	42.35	40.85	33.05
Silt %	44.96	34.37	36.44	34.45	42.93	34.85	39.96	35.52	40.51	35.64	28.48	43.57
Clay %	13.54	27.93	24.65	22.96	13.61	21.12	19.98	24.76	17.06	22.01	30.67	23.38
USDA classification	Loam	Clay Loam	Clay Loam	Loam	Loam	Loam	Loam	Loam	Loam	Loam	Clay Loam	Loam

Sample ID	11B	12B	13B	21B	22B	23B	31B	32B	33B	41B	42B	43B
Sand %	37.11	39.71	41.42	44.92	38.03	42.12	42.17	35.75	39.27	40.44	35.62	26.50
Silt %	33.54	35.34	34.52	34.96	37.82	36.44	36.80	34.20	36.65	35.53	25.75	32.09
Clay %	29.35	24.95	24.06	20.13	24.16	21.44	21.03	30.05	24.08	24.03	38.63	41.41
USDA classification	Clay Loam	Loam	Loam	Loam	Loam	Loam	Loam	Clay Loam	Loam	Loam	Clay Loam	Clay

Hanging column, pressure plate and dew potentiometer test results

Sample ID: W11 T

Mass of mesh +rings (g)	Cross sectional area of tube (cm2)	Average sample height (cm)	Dry weight of sample+ tube+ mesh+ rings (g)	Mass of tube (g)	Dry mass of sample (g)	Dry density of sample (g/cc)
47.680	17.193	4.365	176.820	11.854	117.286	1.568

Suction (cm)	Mass of sample+ tube+ mesh+ rings (g)	Gravimetric water content %	Volumetric water content %	Volumetric water content
0	207.960	26.550	41.637	0.416
10	207.350	26.030	40.822	0.408
20	206.720	25.493	39.979	0.400
50	206.480	25.289	39.658	0.397
100	205.820	24.726	38.776	0.388
150	205.000	24.027	37.680	0.377
500	200.960	20.582	32.278	0.323
1000	199.720	19.525	30.620	0.306
3000	199.030	18.937	29.697	0.297
22699.23		10.781	16.907	0.169
273377.7		5.205	8.162	0.082

Sample ID: W21 T

Mass of mesh +rings (g)	Cross sectional area of tube (cm2)	Average sample height (cm)	Dry mass of sample+ tube+ mesh+ rings (g)	Mass of tube (g)	Dry mass of sample (g)	Dry density of sample (g/cc)
48.550	17.193	4.965	198.140	13.482	136.108	1.765

Suction (cm)	Mass of sample+ tube+ mesh+ rings (g)	Gravimetric water content %	Volumetric water content %	Volumetric water content
0	231.860	24.774	43.731	0.437
10	231.840	24.760	43.705	0.437
20	231.600	24.583	43.393	0.434
50	231.040	24.172	42.667	0.427
100	229.890	23.327	41.176	0.412
150	229.200	22.820	40.281	0.403
500	223.970	18.978	33.498	0.335
1000	222.690	18.037	31.838	0.318
3000	221.680	17.295	30.528	0.305
11744.38		11.439	20.192	0.202
63163.07		6.690	11.809	0.118
343449.2		4.262	7.524	0.075

Sample ID: W31 T

Mass of mesh +rings (g)	Cross sectional area of tube (cm2)	Average sample height (cm)	Dry mass of sample+ tube+ mesh+ rings (g)	Mass of tube (g)	Dry mass of sample (g)	Dry density of sample (g/cc)
48.560	17.193	4.922	191.980	13.366	130.054	1.482

Suction (cm)	Mass of sample+ tube+ mesh+ rings (g)	Gravimetric water content %	Volumetric water content %	Volumetric water content
0	228.000	27.696	41.043	0.410
10	228.410	28.011	41.510	0.415
20	228.350	27.965	41.442	0.414
50	228.040	27.727	41.089	0.411
100	227.600	27.389	40.587	0.406
150	227.150	27.043	40.075	0.401
500	221.130	22.414	33.215	0.332
1000	219.770	21.368	31.665	0.317
3000	219.210	20.937	31.027	0.310
26844.31		11.149	16.522	0.165
261534.6		5.846	8.664	0.087

Sample ID: W41 T

Mass of mesh +rings (g)	Cross sectional area of tube (cm2)	Average sample height (cm)	Dry mass of sample+ tube+ mesh+ rings (g)	Mass of tube (g)	Dry mass of sample (g)	Dry density of sample (g/cc)
47.380	17.193	4.540	180.870	12.329	121.161	1.629

Suction (cm)	Mass of sample+ tube+ mesh+ rings (g)	Gravimetric water content %	Volumetric water content %	Volumetric water content
0	212.050	25.734	41.912	
10	212.390	26.015	42.369	0.424
20	212.070	25.751	41.938	0.419
50	211.500	25.280	41.172	0.412
100	210.050	24.084	39.223	0.392
150	209.230	23.407	38.121	0.381
500	205.720	20.510	33.403	0.334
1000	204.400	19.420	31.629	0.316
3000	203.790	18.917	30.809	0.308
37305.69		8.099	13.190	0.132
332593.1		4.578	7.455	0.075

Sample ID: M11 T

Mass of mesh +rings (g)	Cross sectional area of tube (cm2)	Average sample height (cm)	Dry mass of sample+ tube+ mesh+ rings (g)	Mass of tube (g)	Dry mass of sample (g)	Dry density of sample (g/cc)
47.470	17.193	5.033	194.100	13.669	132.961	1.599

Suction (cm)	Mass of sample+ tube+ mesh+ rings (g)	Gravimetric water content %	Volumetric water content %	Volumetric water content
0	231.680	28.264	45.181	
10	232.230	28.677	45.842	0.458
20	232.030	28.527	45.601	0.456
50	231.590	28.196	45.072	0.451
100	231.100	27.828	44.483	0.445
150	229.360	26.519	42.391	0.424
500	224.080	22.548	36.043	0.360
1000	220.910	20.164	32.232	0.322
3000	217.080	17.283	27.628	0.276
12237.85		14.520	23.211	0.232
82802.84		9.210	14.722	0.147
355292.3		6.350	10.151	0.102

Sample ID: M21 T

Mass of mesh +rings (g)	Cross sectional area of tube (cm2)	Average sample height (cm)	Dry mass of sample+ tube+ mesh+ rings (g)	Mass of tube (g)	Dry mass of sample (g)	Dry density of sample (g/cc)
48.440	17.193	4.965	197.340	13.482	135.418	1.626

Suction (cm)	Mass of sample+ tube+ mesh+ rings (g)	Gravimetric water content %	Volumetric water content %	Volumetric water content
0	233.030	26.355	42.859	
10	232.890	26.252	42.691	0.427
20	232.750	26.149	42.523	0.425
50	232.280	25.802	41.959	0.420
100	231.900	25.521	41.502	0.415
150	231.440	25.181	40.950	0.409
500	225.800	21.016	34.177	0.342
1000	222.330	18.454	30.010	0.300
3000	219.120	16.084	26.155	0.262
70268.92		8.178	13.299	0.133
130273.8		6.642	10.801	0.108

Sample ID: M31 T

Mass of mesh +rings (g)	Cross sectional area of tube (cm2)	Average sample height (cm)	Dry mass of sample+ tube+ mesh+ rings (g)	Mass of tube (g)	Dry mass of sample (g)	Dry density of sample (g/cc)
49.250	17.193	4.792	196.120	13.014	133.856	1.629

Suction (cm)	Mass of sample+ tube+ mesh+ rings (g)	Gravimetric water content %	Volumetric water content %	Volumetric water content
0	228.880	24.474	39.873	
10	228.550	24.228	39.471	0.395
20	228.200	23.966	39.045	0.390
50	227.210	23.226	37.840	0.378
100	227.010	23.077	37.597	0.376
150	225.900	22.248	36.246	0.362
500	222.680	19.842	32.326	0.323
1000	219.980	17.825	29.040	0.290
3000	217.240	15.778	25.705	0.257
47471		8.118	13.226	0.132
620774.6		4.000	6.517	0.065

Sample ID: M31 B

Mass of mesh +rings (g)	Cross sectional area of tube (cm2)	Average sample height (cm)	Dry mass of sample+ tube+ mesh+ rings (g)	Mass of tube (g)	Dry mass of sample (g)	Dry density of sample (g/cc)
47.670	17.193	4.456	180.960	12.102	121.188	1.600

Suction (cm)	Mass of sample+ tube+ mesh+ rings (g)	Gravimetric water content %	Volumetric water content %	Volumetric water content
0	212.720	26.207	41.927	
10	212.320	25.877	41.399	0.414
20	213.290	26.677	42.680	0.427
50	213.060	26.488	42.376	0.424
100	212.660	26.158	41.848	0.418
150	211.090	24.862	39.775	0.398
500	205.350	20.126	32.198	0.322
1000	203.800	18.847	30.152	0.302
3000	203.700	18.764	30.020	0.300
34344.92		9.322	14.914	0.149
161855.4		6.564	10.501	0.105
310880.7		5.405	8.647	0.086

Sample ID: M42 T

Mass of mesh +rings (g)	Cross sectional area of tube (cm2)	Average sample height (cm)	Dry mass of sample+ tube+ mesh+ rings (g)	Mass of tube (g)	Dry mass of sample (g)	Dry density of sample (g/cc)
44.260	17.193	4.189	164.970	11.376	109.334	1.498

Suction (cm)	Mass of sample+ tube+ mesh+ rings (g)	Gravimetric water content %	Volumetric water content %	Volumetric water content
0	197.600	29.844	44.715	
10	197.270	29.542	44.263	0.443
20	197.120	29.405	44.058	0.441
50	196.340	28.692	42.989	0.430
100	195.440	27.869	41.755	0.418
150	194.270	26.799	40.152	0.402
500	189.220	22.180	33.232	0.332
1000	187.620	20.716	31.039	0.310
3000	187.220	20.350	30.491	0.305
40365.15		8.642	12.948	0.129
219096.9		6.173	9.249	0.092
664199.2		4.115	6.165	0.062

Sample ID: Spoil 1

Mass of mesh +rings (g)	Cross sectional area of tube (cm2)	Average sample height (cm)	Dry mass of sample+ tube+ mesh+ rings (g)	Mass of tube (g)	Dry mass of sample (g)	Dry density of sample (g/cc)
48.020	17.193	4.333	166.990	11.767	107.203	1.400

Suction (cm)	Mass of sample+ tube+ mesh+ rings (g)	Gravimetric water content %	Volumetric water content %	Volumetric water content
0	198.730	29.607	41.449	
10	197.430	28.395	39.751	0.398
20	197.020	28.012	39.216	0.392
50	195.730	26.809	37.531	0.375
100	194.260	25.438	35.612	0.356
150	192.890	24.160	33.822	0.338
500	187.920	19.524	27.332	0.273
1000	187.070	18.731	26.222	0.262
3000	186.490	18.190	25.465	0.255
16679		11.618	16.265	0.163
39871.69		9.848	13.787	0.138
168763.8		6.987	9.781	0.098

Sample ID: Spoil 2

Mass of mesh +rings (g)	Cross sectional area of tube (cm2)	Average sample height (cm)	Dry mass of sample+ tube+ mesh+ rings (g)	Mass of tube (g)	Dry mass of sample (g)	Dry density of sample (g/cc)
49.820	17.193	4.221	157.020	11.462	95.738	1.311

Suction (cm)	Mass of sample+ tube+ mesh+ rings (g)	Gravimetric water content %	Volumetric water content %	Volumetric water content
0	191.360	35.869	47.030	
10	189.240	33.654	44.126	0.441
20	188.890	33.289	43.647	0.436
50	187.470	31.805	41.702	0.417
100	185.500	29.748	39.004	0.390
150	184.310	28.505	37.374	0.374
500	178.310	22.238	29.157	0.292
1000	177.400	21.287	27.911	0.279
3000	177.130	21.005	27.541	0.275
16679		11.618	15.233	0.152
39871.69		9.848	12.912	0.129
168763.8		6.987	9.161	0.092

CEC test results

Sample ID	Clay content (%) (based on USDA classification)	CEC (meq/100 g soil)
N12 T	11	41.3
N33 T	22	39.6
N21 T	35	44.6
N41 T	43	39.2
W23 T	12	20.1
W12 T	20	25.9
W42 T	24	29.4
W32 T	29	26.8
M22 T	13	25.4
M31 T	19	24.5
M13 T	23	25.5
M42 T	28	24.5